USGS
science for a changing world

Carpinteria Coastal Processes Study, 2005-2007; Final Report

By Patrick L. Barnard, David L. Revell, Jodi L. Eshleman, and Neomi Mustain

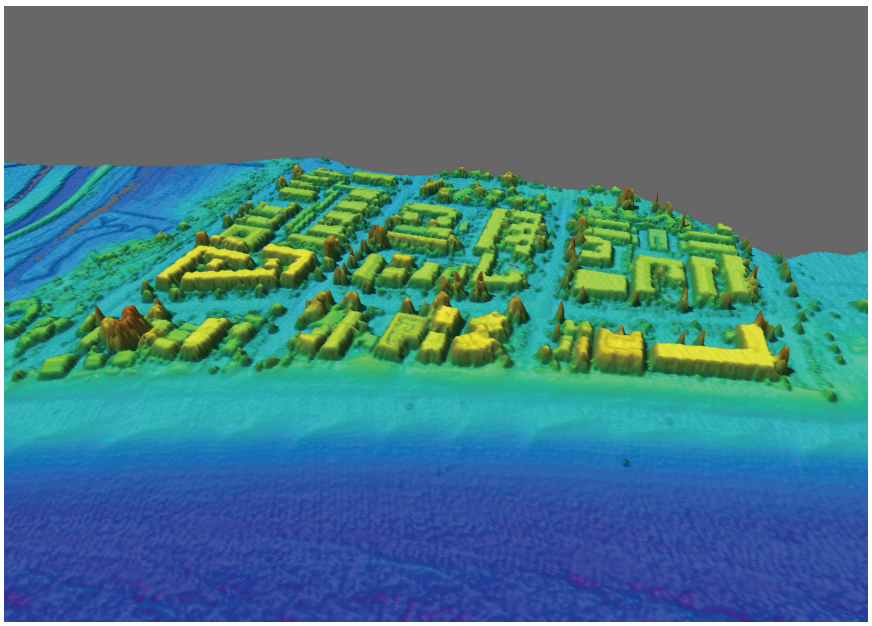

Open-File Report 2007-1412

2008

U.S. Department of the Interior
U.S. Geological Survey

U.S. Department of the Interior
Dirk Kempthorne, Secretary

U.S. Geological Survey
Mark D. Myers, Director

U.S. Geological Survey, Reston, Virginia 2007

For product and ordering information:
World Wide Web: http://www.usgs.gov/pubprod
Telephone: 1-888-ASK-USGS

For more information on the USGS—the Federal source for science about the Earth, its natural and living resources, natural hazards, and the environment:
World Wide Web: http://www.usgs.gov
Telephone: 1-888-ASK-USGS

Suggested citation:
Barnard, P.L., Revell, D.L., Eshleman, J.L., and Mustain, N., 2008, Carpinteria Coastal Processes Study, 2005-2007; Final Report: U.S. Geological Survey, Open-File Report 2007-1412, 129 p. [http://pubs.usgs.gov/of/2007/1412].

Contents

Figures

Carpinteria Coastal Processes Study: Final Report

By Patrick L. Barnard[1], David Revell[2], Jodi Eshleman[3], and Neomi Mustain[4]

Executive Summary of Major Findings

Chapter 2 - Historical Changes

- The beach at Beacon#10 (Linden Avenue) has flattened over the last 18 years (1987 – 2005), with the MSL shoreline maintaining its position while the MLLW shoreline accreted by ~15 m.
- Historic subaerial beach volumes declined by more than 175,000 m^3 following the erosion caused by the construction of the Santa Barbara Harbor.
- Beach widths along the City of Carpinteria beach have been relatively stable over time ranging from 25 m to 60 m with no single event correlating to minimum or maximum beach widths.
- Beach width and shoreline change analyses show that there is a long-term trend of beach erosion in the west and accretion in the eastern part of study area.
- The El Niño pattern of beach impacts is to preferentially erode the beaches in the west and accrete the beaches in the east. Differences between the 1982-83 and 1997-98 events show that the erosion hotspot in 1982-83 migrated east onto the City of Carpinteria Beach during the 1997-98 El Niño. The construction of the revetment along Sandyland Cove following the 1982-83 El Niño event may have caused this migration.
- Correlation analyses of the sand volumes dredged from the Santa Barbara Harbor and the sand volume found on the beach at Carpinteria suggest a four year travel time for sediment to reach downdrift Carpinteria beach.
- The consistent pattern among the El Niño beach response, the 138-year long-term shoreline change rates, and the 77-year long-term beach width changes provide evidence that El Niños play a major role in shaping the coastline of Carpinteria.
- Over the last 75 years the there has been a trend of nearshore sediment loss and mild offshore gain, with the most substantial loss offshore of Sand Point.

Chapter 3 – Recent Morphologic Changes

- The Carpinteria shoreline responds in the typical seasonal pattern, with accretion in the summer and erosion in the winter of ~60,000 m^3 of sediment.

[1] Coastal and Marine Geology Team, Santa Cruz, CA, pbarnard@usgs.gov
[2] UC Santa Cruz, Institute of Marine Sciences, *drevell@es.ucsc.edu*
[3] Coastal and Marine Geology Team, Santa Cruz, CA
[4] UC Santa Cruz, Institute of Marine Sciences

- Seasonal beach width changes show relatively uniform erosion across the Carpinteria shoreline of around 20 m during the winter surveys and a near mirror image of accretion during the summer recovery period
- The City of Carpinteria Beach is more variable than the rest of the beach, with up to 50 m^3/m of seasonal volume change, as opposed to a mean seasonal maximum change of 23 m^3/m for the rest of the study area.
- Winter erosion peaks adjacent to the east end revetment on the City of Carpinteria beach, which is reflected in the analysis of shoreline position, beach width, volume change and profile change.
- Seasonal change exceeds the observed short-term annual signal.
- Significant seasonal changes in nearshore profiles are restricted to depths < 5 m, and are reflected by patterns of accretion in spring surveys and erosion in fall surveys. The beach shows the mirror opposite pattern.

Chapter 4- Sediment Analysis

- Mean grain size for the Carpinteria shoreline averages 0.28 mm, but increases and is more variable alongshore in the winter.
- Locally, grain size can vary by a factor of two seasonally.
- Grain size peaks (coarser sediments) are co-located with the erosion hotspot immediately downdrift of the revetment at Ash Avenue.
- Together with previously collected cores, this current analysis confirms that coarser sediments suitable for beach nourishment do not exist in large quantities along the previously identified potential borrow areas offshore of Carpinteria.

Chapter 5- High Resolution Nearshore Mapping

- Sand dominates the substrate in water depths < 20 m, where clearly visible wave-induced ripples are present
- The only prominent hard bottom area mapped in the nearshore is the extension of Rincon Point., which is dominated by boulders and large rocks. Additional information on the reef complex off of Sand Point will be available in 2008.

Chapter 6- Wave and current analysis

- Tidal current magnitudes were mild and rarely exceeded 20 cm/s.
- Measured currents were not strong enough to suspend sediment based on the threshold current velocity and closest measured sediment grain size.
- Current profiles show stratification throughout the water column with strong surface currents decaying with depth, especially on the ebbing tide of the spring tidal cycle.
- Current directions are oriented northeast to southwest, with a principal axis that is skewed slightly south of onshore.
- Wave heights never exceed 2 m in the summer and rarely do in the winter at inshore locations. Average values are less than one meter.
- Wave directions are generally slightly south of onshore at Rincon, with waves refracting more in the winter as a result of lower frequency energy.

Chapter 1- Introduction

Project Summary

The United States Geological Survey (USGS), in collaboration with the University of California, Santa Cruz (UCSC), conducted a two-year study of the beach and nearshore coastal processes for the City of Carpinteria and adjacent beaches. The work was performed in response to and worked directly with the United States Army Corps of Engineers (USACE) Project Management Plan (PMP) for the City of Carpinteria:

- *Carpinteria Shoreline, Santa Barbara County, California PMP* (June 2003)

www.spl.usace.army.mil/cms/index.php?option=com_content&task=view&id=487&Itemid=31

The City of Carpinteria has experienced significant erosion and storm damage over the last decade (Figure 1.1). A USACE reconnaissance survey has shown shoreline retreat rates that approach 2 m/yr in some locations. The goals of this project are to analyze historical trends/changes in the beach and nearshore environment, document local wave and tidal currents, and assess current beach and nearshore conditions in terms of grain size, beach size and shape, seasonal changes, and nearshore bathymetry. In summary, this work serves to quantify sediment sources, transport and sinks throughout the study area to support USACE and the City of Carpinteria coastal management activities.

Objectives

The objectives of this report are the following:

- Provide a thorough summary of the data collection efforts conducted as part of the USGS/UCSC Carpinteria Coastal Processes Study, initiated in October 2005.
- Present key findings, particularly as they may relate to pending management decisions.
- Discuss the implications of analyzed field data on coastal processes.

Study Area

Carpinteria is a sandy beach in the Santa Barbara littoral cell, a 150 km length of California coastline that extends from Point Conception to Point Mugu (Figure 1.2). It is also part of the broader Santa Barbara Sandshed (detailed below). The study area extends 10 km alongshore from Loon Point southeast to Rincon Point. However, the focus area of this study includes just the City of Carpinteria beach, a 400 m long section between Ash Avenue and Linden Avenue in the center of the broader study area (Figure 1.3). The Carpinteria shoreline analysis that was conducted extends from Sand Point in the west to the Asphaltum outcrop in the east (Figure 1.2).

The Santa Barbara Sandshed (watershed + littoral cell) (Revell and others, 2007) extends 245 km from the Santa Maria River in the north, around Point Conception, where the north-south trending U.S. West Coast takes an abrupt turn to a west-east trending shoreline orientation into the Southern California Bight. The sand found on these beaches moves along the coast of southern Santa Barbara and Ventura Counties to the Point Mugu submarine canyon in the south.

The Santa Barbara Sandshed consists of a relatively complex coastline with a variety of rocky outcrops, offshore reefs, and relatively narrow beaches. The beaches receive the majority of their sand inputs from four major rivers: the Santa Maria, Santa Ynez, Ventura, and Santa Clara, which drain the sedimentary rocks of the Transverse Range, along with numerous small coastal drainages that pulse sediment during episodic rain events (Inman and Jenkins, 1999).

Point Conception in the northwest and the Channel Islands to the south, create a narrow swell window that shelters much of the south facing coast of Santa Barbara County from extreme wave events (Figure 1.2). The Mediterranean climate of southern California results in mild annual temperatures and low precipitation punctuated by episodic and often extreme events, frequently associated with El Niños. Winds and wave heights vary seasonally but focusing of waves into the Santa Barbara Channel drive an almost unidirectional longshore sediment transport from west to east in which beaches narrow during the winter and spring (November to April), and widen during the summer and fall (May to October). Longshore transport rates for the study area are approximated by the 70-yr Santa Barbara Harbor dredge record which shows a mean annual rate of ~230,000 m^3 of sand removed per year (Figure 1.4; Patsch and Griggs, 2007). Variability in the dredge volumes stem from sediment supply, navigational depth requirements, and funding. The southern coast of Santa Barbara and Ventura counties are composed mostly of bluff-backed beaches perched on bedrock shore platforms. Along this coast are a few dune-backed beaches that have formed near ephemeral creeks and sloughs, typically controlled by the complex faulting in the Western Transverse Ranges.

This northern end of this sandshed has been characterized as the last remaining stretch of relatively undeveloped coast in southern California. However, this does not imply that it is without anthropogenic influence. Physical alterations to the Santa Barbara coastline began with the completion of the Southern Pacific Railroad in 1901. Physical alterations to the Santa Barbara Sandshed began with dam construction on major rivers: the Santa Ynez River in 1920, the Santa Clara River in 1948, and on the Ventura River in 1955 (Patsch, 2005). In 1927, construction began on the Santa Barbara Harbor and began to impound sand resulting in an erosion wave that propagated downcoast caused by the disruption of longshore transport (Wiegel, 2002). This erosion wave substantially impacted the dune system at Sandyland and the beaches of Carpinteria in the late 1930s. The effects of dam impoundment and shore protection structures on sand delivery to the coast have been quantified in the Santa Barbara littoral cell and show an approximately 40% reduction in sand supplied to the sandshed by the major rivers and bluff erosion, although the great majority of the sand reduction is from stream impoundment (Runyan and Griggs, 2003; Willis and Griggs, 2003). It was predicted that this reduction would correspond with a decline of sand volume dredged at the harbors in the cell. Using dredge records as a proxy for littoral drift, Patsch and Griggs (2007) determined an average longshore transport of sand at Santa Barbara Harbor since 1933 (~230,000 m^3/year), and the Ventura Harbor since 1964 (~550,000 m^3/yr) with no sign of reductions in dredge volumes.

Report Outline

This report is set up to provide a broad summary of each major data collection effort in Carpinteria from 2005-2007 (Fig. 1.5):

- Chapter 2- Historical Changes
- Chapter 3- Recent Morphologic Changes
- Chapter 4- Sediment Analysis
- Chapter 5- High Resolution Nearshore Mapping

- Chapter 6- Wave and current analysis

Project Support and Collaboration

The Carpinteria Coastal Processes Study was funded by the City of Carpinteria, through a grant from the California Department of Boating Waterways. This project also benefited greatly from internal support at the USGS as well as interactions with a number of other agencies and groups. A list of the primary collaborators is outlined below:

- USGS Support:
  - California Urban Oceans Project (Homa Lee)
  - Seafloor Mapping Project (Guy Cochrane)
  - Coastal Evolution: Process-based, Multi-scale Modeling Project (Dan Hanes)
  - Delft Hydraulics Cooperative (Edwin Elias)

- Government Agencies:
  - U.S. Army Corps of Engineers, Los Angeles District (Heather Schlosser, Arthur Shak, Jane Grandon)
  - City of Carpinteria (Matt Roberts)
  - California Department of Boating and Waterways (Kim Sterrett)
  - Beach Erosion Authority for Clean Oceans and Nourishment (BEACON: Gerald Comati and Jim Bailard)

Recent Publications/Reports

Barnard, P.L., 2006. Interim Progress Report to BEACON- Santa Barbara and Ventura Counties Coastal Processes Study, 14 pp.

Cochrane, G.R., Golden, N.E., Dartnell, P., Schroeder, D.M., and Finlayson, D.P., 2007. Seafloor Mapping and Benthic Habitat GIS for Southern California, Volume III. U.S. Geological Survey Open-File Report 2007-1271. Available online at http://pubs.usgs.gov/of/2007/1271/

Mustain, Neomi, 2007. Grain size distribution of beach and nearshore sediments of the Santa Barbara Littoral Cell: Implications for Beach Nourishment. MS Thesis in Earth Sciences, University of California, Santa Cruz. 107 pp.

Mustain, N., Griggs, G. and Barnard, P.L., 2007. A rapid compatibility analysis of potential offshore sand sources for beaches of the Santa Barbara littoral cell. In: Kraus, N.C., Rosati, J.D. (eds.), Coastal Sediments '07, Proceedings of the 6th International Symposium on Coastal Engineering and Science of Coastal Sediment Processes, American Society of Civil Engineers, New Orleans, LA, Volume 3, p. 2501-2514

Revell, David, 2007. Evaluation of Long-Term and storm event changes to the beaches of the Santa Barbara Sandshed. Ph.D. dissertation in Earth Sciences, University of California, Santa Cruz. 148 pp.

Revell, D.L. and Griggs, G.B., 2007. Regional shoreline and beach changes in the Santa Barbara sandshed. In: Kraus, N.C., Rosati, J.D. (eds.), Coastal Sediments '07, Proceedings of the 6th

International Symposium on Coastal Engineering and Science of Coastal Sediment Processes, American Society of Civil Engineers, New Orleans, LA, Volume 3, 14 pp.

References

Inman, D.L. and Jenkins, S.A., 1999. Climate Change and the Episodicity of Sediment Flux of Small California Rivers. Journal of Geology, vol. 107, p. 251-270.

Patsch, K., 2005. Littoral Cells of California. PhD Dissertation, University of California, Santa Cruz Earth Science Department.

Patsch, K. and Griggs, G.B., 2007. Development of Sand Budgets for California's Major Littoral Cells. Report to California Department of Boating and Waterways. Coastal Sediment Management Work Group. http://dbw.ca.gov/CSMW/PDF/Sand_Budgets_Major_Littoral_Cells.pdf

Revell, D.L., Marra, J.J., and Griggs, G.B., 2007. Sandshed Management. Journal of Coastal Research – Proceedings of ICS2007. Gold Coast, Australia, Special Issue 50, p. 93-98.

Runyan, K.B., and Griggs, G.B., 2003. The effects of armoring seacliffs on the natural sand supply to the beaches of California. Journal of Coastal Research v. 19, no. 2, p. 336-347.

Weigel, R. L., 2002. Seawalls, seacliffs, beachrock: What beach effects? Part 2. Shore and Beach, v. 70, no. 2, p. 13-22.

Willis, C.W. and Griggs, G.B., 2003. Reductions in fluvial sediment discharge by coastal dams in California and implications for beach sustainability. Journal of Geology, v. 111, p. 167-182.

Figure 1.1. Winter storm waves at Carpinteria (photo courtesy of Matt Roberts).

Figure 1.2. Map of the study area included in the Carpinteria Coastal Processes Study, and the focus site. Yellow bathymetric contours are expressed in meters.

Figure 1.3. Oblique aerial view (top) of the City of Carpinteria with a close-up (bottom) of the beach in front of Ash Avenue, the rock revetment protecting Sandyland Cove, and the Carpinteria Salt Marsh (photo courtesy of California Coastal Records).

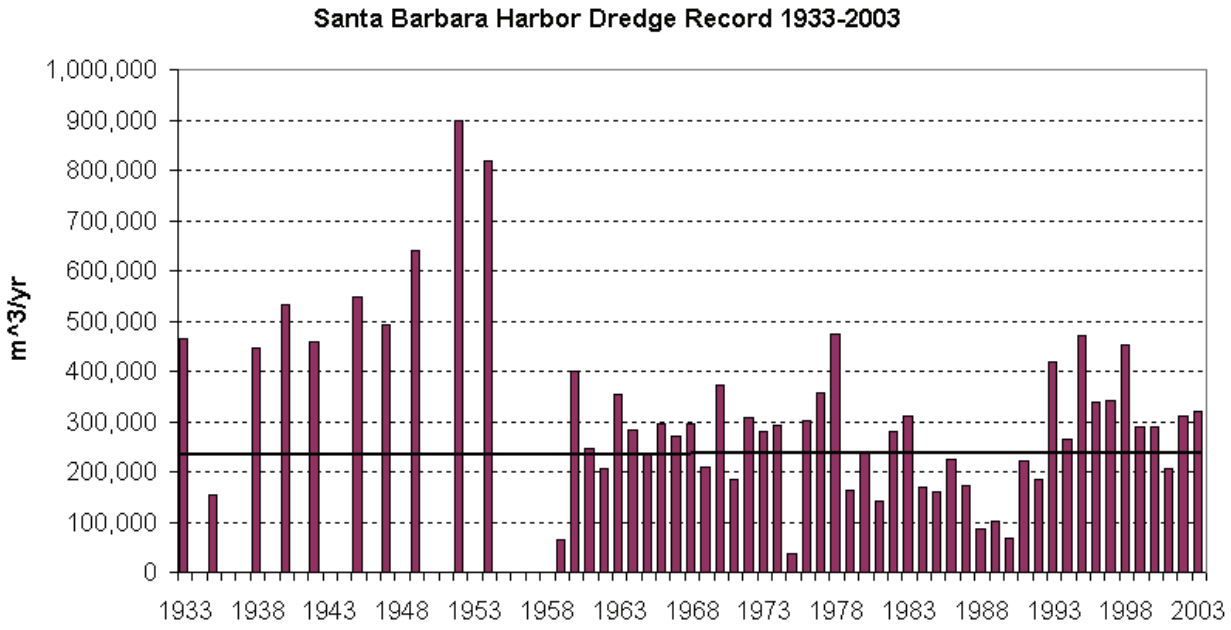

Figure 1.4. Santa Barbara Harbor dredge records for the last 70 years (1933-2003) from Patsch and Griggs (2007), with original data supplied by USACE. The solid black line represents the long- term mean of 230,000 m^3/yr.

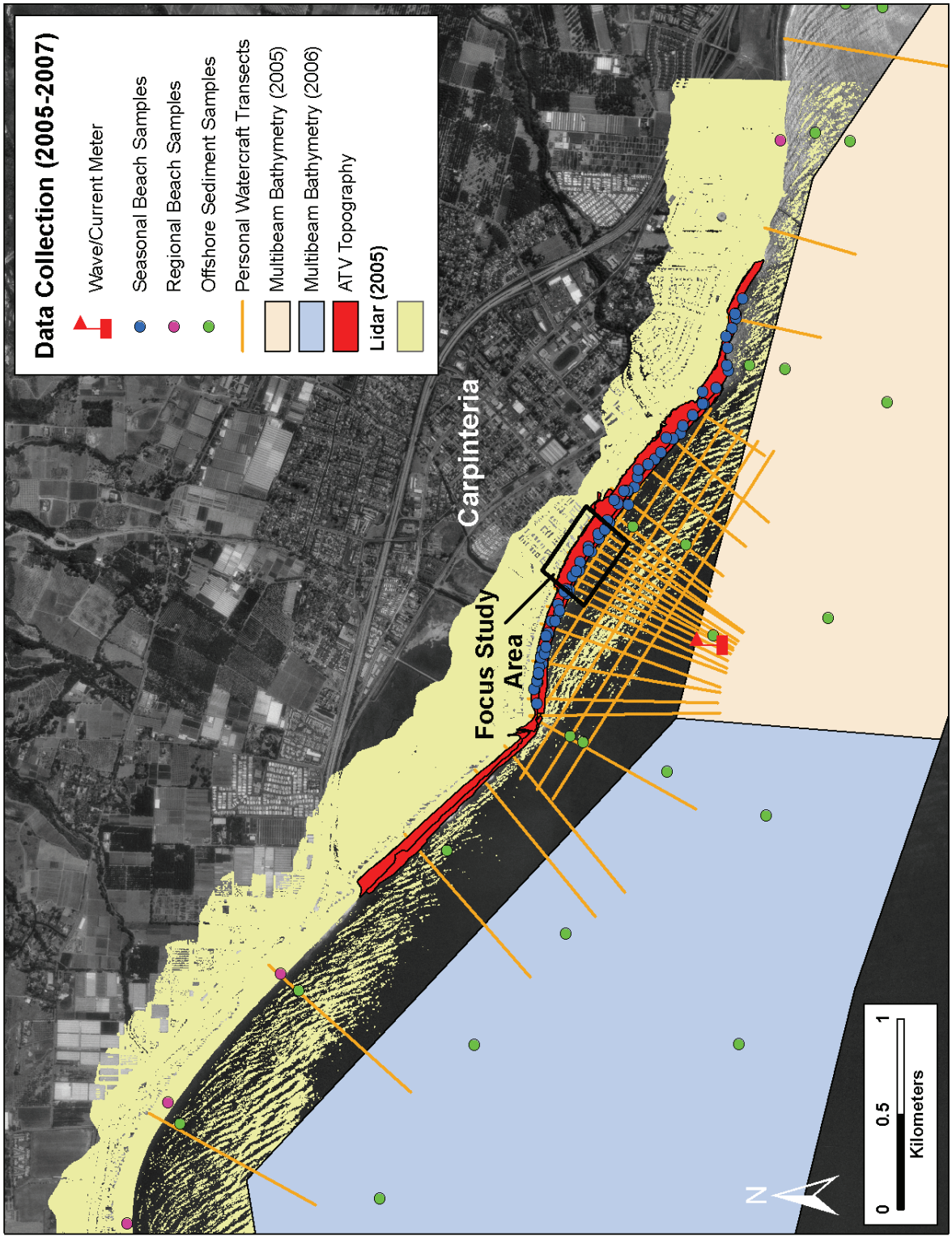

Figure 1.5. Summary of data collection locations during the two-year study.

Chapter 2- Historical Changes

By David L. Revell and Patrick L. Barnard

Introduction

Carpinteria Beach is a 1.5 km long south facing stretch of coast in Santa Barbara County, California. It can be broken into three parts based on jurisdictional boundaries. At the west end is Sandyland Cove, the central portion is the City of Carpinteria, and at the east end is the Carpinteria State Beach (Figure 1.2). This shoreline segment is continuous with the influence of regional coastal processes and human alterations affecting this coastline (Table 2.1). Breakwater construction at the Santa Barbara Harbor began in 1927 and was completed by 1930 during which almost 2 million cubic meters of sand were impounded updrift of the Santa Barbara Harbor. This sand impoundment led to a well documented erosion wave that migrated downcoast at ~1.7 km/yr (~1 mi/yr) leading to the erosion of the historic dune field at Sandyland and the beach at Carpinteria in the late 1930s (e.g. Bailard, 1982; Komar, 1998; Weigel, 2002 and references within) (Figure 2.1). While the reporting of this erosion wave and its impacts are not new, the application of beach width methods, coupled with shoreline change analyses to study this erosion event provides new information on the response of the beach and shoreline at a variety of temporal scales from long-term (1869 to present) to seasonal (e.g. El Niño storm events).

Methods

The historic shoreline and beach width changes were documented using a combination of historic beach profiles, historic topographic maps, aerial photography, and Lidar and Global Positioning System (GPS) survey techniques. Many investigators have utilized various shoreline reference features to examine changes to beaches (e.g. Crowell and Leatherman, 1999; Boak and Turner, 2005). More recent advances in remote sensing of topographic data (e.g. light detection and ranging (Lidar)) and Real-Time Kinematic (RTK) GPS beach surveying have increased the ability to accurately measure changes at a regional spatial scale. All of the analyses have been completed for the shoreline segment from Sand Point at the west end near the mouth of the Carpinteria Salt Marsh to the Asphaltum Outcrop at the east end of the Carpinteria State Beach (Figure 1.2). In the middle of this shoreline segment is the City of Carpinteria Beach focus area (~400 m long). All analyses were completed for the entire shoreline segment because there are no subcells or compartments separating the different shoreline segments. In several of the analyses the City of Carpinteria Beach is separated to highlight the City's relative contribution to the overall shoreline segment.

Historic Beach Profiles

Historic beach profiles have been collected by BEACON quasi-periodically every 5 years with irregular seasonal sampling beginning in 1987 up to 2003 (Figure 2.2). In general these profiles extend from a backshore benchmark to the offshore beyond the depth of closure. For comparison with the historic shoreline change analyses, only the subaerial (dry sand) portion of the profile was analyzed. These historic beach profiles were analyzed to examine beach slopes, shoreline position change, and beach volumes above Mean Sea Level (MSL) (0.83m above the North America Vertical Datum of 1988 (NAVD88)). From BEACON profile #10 (BCN10 in

Figure 2.2) along Linden Avenue in Carpinteria, historic foreshore beach slopes were calculated. Beach slopes ranged from 1:23 to 1:10 (.036 to .10 tanβ). The average summer beach slope extracted from the historic BEACON profiles and Lidar data sets and used throughout the various change analyses after consultation with Army Corp of Engineers Staff was 1:17 (0.058 tanβ) (Art Shak and Jane Grandon, personal communication, 8/21/2006). Analyses of BEACON profile #10 examined changes in shoreline position at MSL and Mean Lower Low Water (MLLW: -0.027 m NAVD88). Additional analyses compared beach volume and shoreline position. Beach volume was calculated by integrating the volume of sand under the profile above an elevation plane drawn at MSL and MLLW. Additionally, a corresponding beach profile was extracted from the 2005 Lidar data set and included in the analyses. Relative changes were calculated by subtracting the volume and shoreline positions from the 1987 baseline profile, providing insights into an 18-year profile change analyses.

Historic Air Photos and Topographic Sheets

Historical aerial photographs and topographic sheets provide one of the best data sources for long-term shoreline and beach change investigations. For this study, twelve different sets of vertical air photos were obtained for the period from 1929 to 2003 (Table 2.2). Photographs selected for this study (at scale 1:24,000 or smaller) were taken during the calmer season (summer to fall) to reduce the influence of seasonal variability and to ensure that beaches were near a maximum width. Additionally, the use of historic National Ocean Service (formerly US Coast and Geodetic Survey) T-sheets in 1869 and 1933 that mapped a High Water Line (HWL) shoreline extended the shoreline change analyses to 138 years. These historic T-sheets are generally assumed to be similar to MHW (see further discussion below under errors and uncertainties). To minimize errors, historical imagery and topographic maps were georectified using known coordinates of ground locations obtained through GPS surveys to reduce photo distortions (Table 2.2; Moore, 2000; Hapke and others, 2006; Moore and others, 2006).

For each rectified air photo, two shoreline reference features were digitized - the wet/dry line identified using tonal contrasts, and the back beach or toe of the cliff, revetment, or dune. The beach width is the distance between the wet/dry line and the back beach feature, generally the dry sand (subaerial) portion of the beach at the time of the photo. Given the short-term variability of water levels, corrections to the wet/dry proxy- based shoreline reference features were based on the tide level portion of the total water level model discussed in Ruggiero et al. (2003). Tide level corrections adjusted the wet/dry shorelines to Mean Sea Level (MSL) (0.83m NAVD88) using historic hourly water level data at Santa Barbara harbor available from Station # 9411340 (National Oceanic and Atmospheric Administration, 2007b). These corrections translated the water level at the time of each historic photo onto an average summer beach slope calculated from historic profiles and more recent Lidar data sets. A similar correction was also applied to the historic topographic sheets (T-sheets) that mapped a high water mark, assumed to be a proxy for MHW thus adjusting the T-sheet shoreline to MSL.

The beach slope averages used in the tidal correction were taken only from the historical summer profiles (June to October) and ranged from 0.036 (sand beach) to 0.11 (cobble beach). The specific value of the beach slope used in the tide level correction was based on discussions with the USACE. Due to the typical low energy waves found in the Santa Barbara Channel during the summer and fall, and the lack of directional hindcast wave data for most of the photography, a wave run-up adjustment was not included in the proxy-based shoreline correction.

Shoreline change and beach widths for all imagery were measured along the same 50-meter spaced transects drawn from an offshore baseline using the USGS Digital Shoreline Analysis System (DSAS) (Thieler and others, 2005). All shoreline change rates discussed in this paper were calculated using DSAS version 3.2, which uses an offshore baseline to calculate relative shoreline position and change rates. This study focused on the shoreline change linear regressions rate (LRR) of both the wet/dry MSL shoreline and the back beach shoreline. Using the intersection locations of the shorelines along each transect, a history of shoreline positions relative to the 1869 baseline were calculated to examine the movement of the shoreline over time.

Beach widths were measured for individual years, by setting the back beach reference feature to one year after the date of the wet/dry shoreline so that the end point rate calculation in DSAS actually measured the beach width. Tide corrections were then applied to the beach widths following measurement with DSAS. Beach width changes were calculated by subtracting the older beach widths from the more recent year at each transect. For example, to calculate the long-term changes between 1929 and 2006, the 1929 beach width (e.g. 30m) was subtracted from the 2006 beach width (e.g. 20 m) so that any negative change would indicate beach narrowing (e.g. 20 m -30 m= -10 m).

Beach width measurements and the average beach slopes used in the tide level corrections were multiplied to calculate sand volumes above MSL per transect (m^3/m). Transect volumes were then multiplied by the 50 m transect spacing and summed alongshore to provide a total volume for a length of shoreline. A sensitivity analysis examined the difference in beach volumes calculated using the range of beach slopes. The use of maximum and minimum (1:10 and 1:23) beach slopes in the volume calculation led to maximum differences on wide beaches up to +/- 23 m^3/m. The use of the mean 1:17 beach slope however can be expected to further reduce the volume errors.

LIDAR and GPS surveys

More recent applications of high accuracy, topographic Lidar data coupled with historic air photo analyses enables rapid assessment of long stretches of coastline and provides additional information on beach volumes and regional shoreline changes caused by extreme storm events (Revell and others, 2002; Sallenger and others, 2003). To understand the changes caused by the 1997-98 El Niño event, NOAA, NASA, and the USGS partnered to conduct pre- and post- storm Lidar surveys in October 1997 and April 1998 throughout the US Pacific Coast (Sallenger and others, 1999).

An additional Lidar data set was collected in October of 2005 by the University of Texas in collaboration with the USGS, UCSC, and BEACON, and has been included in these analyses. Topographic data sets were also collected seasonally by the USGS/UCSC Cooperative using Differential GPS (DGPS) and RTK-GPS surveys conducted using all terrain vehicles on the sub-aerial beach and sounding data collected with the Coastal Profiling System (CPS) to measure the changes in nearshore bathymetry. For more detailed discussion of the Lidar and GPS survey Methods and results, please see Chapter 3.

All of the Lidar data sets were clipped to the study area along the entire Carpinteria coastline. These Lidar data sets were processed to extract a MSL contour. The back beach reference feature was hand digitized using visual cues in cross-shore profiles, slope breaks, and hillshade layers. These two reference features were included in the beach width change analyses, and the 1997 and 2005 MSL contours were included in the shoreline change analyses. Subaerial beach volumes (above MSL 0.83m) were calculated and reported. Changes between the various

data sets were calculated by differencing the grids showing the spatial extent of the changes between time periods.

Uncertainties and Errors

The use of air photos for accurate shoreline change assessments requires an understanding of potential error sources. Errors inherent in air photo interpretation can be broken down into 1) source error, 2) interpretation error, and 3) short-term natural variability errors (Morton and Speed, 1998). Source error results from photo distortion, scale, and scanning errors (Moore, 2000). Interpretation errors come from difficulty in locating shoreline reference features. Short-term variability errors arise from seasonal changes in beach profile and variations in water levels and wave run-up elevations that change the location of the shoreline reference features (Morton and Speed, 1998; Ruggiero and others, 2003). The use of historic T-sheets also introduces another level of uncertainty. Recent studies have shown that there is a systematic offset of MHW seaward when compared to HWL derived shorelines (Ruggiero and others, 2003; Hapke and others, 2006; Moore and others, 2006). This offset varies depending on beach morphology, especially slope, but is tied primarily to water levels which are comprised of both tide level and wave–run-up components (Ruggiero and others, 2003; Moore and others, 2006).

Error estimates for the identification and absolute spatial location of the shoreline reference features associated with shoreline change analysis are, +/- 9.7m, and +/- 9.3 m for the early 1929 and 1938 photography, respectively based on a quadrature, or sum of the squares method (Hapke and others, 2006). More recent photography scanned at a higher resolution provides lower spatial errors on the order of +/- 7m (Table 2.2). Errors reported in Table 2.2 are an average root mean square (RMS) error of all photos used in the flight line and relate to the spatial accuracies associated with the reference features.

To reduce the errors associated with the use of historic T-sheets, given the lack of availability of historic wave data, an elevation correction of 0.46 m was applied to adjust the HWL to MHW based on estimates of average horizontal offsets found along Texas and Maryland coasts with similar beach slopes (Morton and Speed, 1998, Hapke and others, 2006). Additionally, another vertical offset of 0.45 m was applied to adjust the MHW shoreline to MSL based on the tidal records available from Santa Barbara Harbor. The overall horizontal offset after these vertical adjustments applied to the HWL T-sheet shoreline was 15.8 m seaward.

Unlike the shoreline change analysis that depends on different images and T-sheets, the errors in beach width measurements are spatially independent because both reference features can be seen in each image. Maximum potential errors to the beach width corrections associated with choosing one tide level and slope for the entire flight is 10.6 m, assuming a spring tide range (2.3 m) and the most dissipative mean slope (.036 tan). The tidal records show, however, that none of the photo flights were taken during the maximum spring tide fluctuations although several flights occurred during spring tides making this most likely an overestimate of the magnitude of beach width error. Beach width errors resulting from the use of a mean summer beach slope for all of the photos were examined by comparing the beach width corrections using the range of historic beach slopes through all seasons. The largest difference in beach width corrections using the minimum versus maximum historic beach slope and the maximum water level adjustment for a given year was 29.2 m. However, because the photos were selected from summer and fall, the use of a mean summer beach slope should reduce the potential errors from the use of a single slope.

Lidar data sets from the 1997-98 flights have been reported to have accuracies on the order of 1 meter in the horizontal, and +/- 15 cm in the vertical (Sallenger and others, 1999;

2003). However, the recent 2005 Lidar flight reports a vertical error of only +/- 7 cm, and in comparison with survey grade control points gathered at the end of Linden and Ash Avenues coincident with the Lidar flight, the mean vertical error of 325 co-located points (within 0.5 m) is only 0.5 cm. Comparison of control points between the 2005 Lidar and the 1997-8 flights reveals a systematic offset of < 4 cm.

Correlation of Dredge Volumes and Beach Volumes

Given the downdrift location of Carpinteria to Santa Barbara Harbor, there is an expected correlation between the volume of sand dredged at the Santa Barbara harbor and the volume of sand found on the beach along the Carpinteria Beach. To examine this relationship, a lagged cross-correlation analyses was conducted between the harbor dredge records (from Patsch and Griggs (2007)) and the summer/fall beach volume data set for the entire Carpinteria coastline from Sand Point to the Asphaltum outcrop. Prior to the analysis, modifications of the two data were necessary. First, the dredge record (Figure 1.4) was interpolated during the early years (1930s to 1960s) during the sporadic dredge operations. The dredge data was smoothed using a moving average between the existing volume records producing a continuous time series of dredging. The summer/fall beach volume record, consisting of 16 records collected from a variety of methods as discussed above, was also smoothed using linear interpolation between existing records to create a continuous time series. The final alteration to the beach volume data set was the assumption that the beach in 1983, following the especially energetic 1982-83 El Niño, was significantly reduced to beach volume levels similar to those following the 1997-98 El Niño (estimated ~80,000 m^3). A lagged cross-correlation was then performed to examine potential transport times between sand dredged from Santa Barbara Harbor and Carpinteria Beach.

Results

Historic Profile Analyses

The historic profiles collected at Linden Ave (BEACON #10) appear relatively stable across the entire profile with some lowering of the profile up to 0.6 m (Figure 2.3). There is also some potential steepening of the upper portion of the nearshore profile between –3 and –8 m MLLW. However these changes may be due to some discrepancies in the tidal epoch used for the 2003 survey, and the unknown accuracies of the historic profile surveys.

Figure 2.4 shows the shoreline position changes and the changes in beach volume calculated above MSL and MLLW along the BEACON #10 Carpinteria Beach profile at Linden Ave. The analysis reveals differences between the response at the MSL and MLLW portions of the beach- the MSL shoreline position (Figure 2.4a left side) has been relatively stable, losing <1 m over the interceding 18 years, while the MLLW shoreline position (Figure 2.4a right side) accreted seaward by ~15 m, indicating a decrease in beach slope or a flattening of the beach slope over that time period. In general, a relationship typically exists between shoreline changes and volume changes causing the shoreline to retreat (accrete) as sand volume is lost (gained) (e.g. Farris and List, 2007). This pattern generally fits in Figure 2.4b although a closer examination between 1992 and 2003 shows that while there is a reduction of sand volumes on both profiles, there is a larger shoreline retreat in 1992 that corresponds to a smaller volume of sand loss. In 2005, the shoreline shows relative retreat (~-1.0 m), but there has been a gain in volume (~2 m^3/m). Figure 2.4c plots the relation between the MLLW shoreline position and sand volumes, showing wider variability than MSL and poorer relation between volume and shoreline

position. In 1988, the volume loss on the subaerial profile was rather large ~-85 m^3/m but only amounted to a ~10 m shoreline retreat. In 1997, however, the MLLW shoreline position accreted seaward by ~4 m despite a slight decrease (~-5 m^3/m) in subaerial sand volume on the profile. In 2005, a volume increase of ~12 m^3/m resulted in an accretion of 15 m.

These profile analyses results indicate that there has been an overall flattening of the beach profile at BEACON #10 since 1987 due to progradation of the MLLW shoreline compared to a relatively stable MSL shoreline position. Some of this may be related to the change in cobble abundance seen on Carpinteria before the energetic 1982-83 and 1997-98 El Niños (Figure 2.5). In light of the high variability of the MLLW portion, further analyses focus on the MSL shoreline as a more representative indicator of overall beach condition.

Historic Volume Changes, Beach and Shoreline Changes

Figure 2.6 shows the time series from 1929-2006 of summer/fall subaerial beach sand volumes, beach area and mean beach width above MSL for the Carpinteria coastline and the contribution of the City of Carpinteria Beach to the total volume. The maximum beach volume along this coastline occurred in 1929 and is estimated to be ~400,000 m^3. Although the Santa Barbara Harbor was impounding sand by 1929, measurements from the 1929 photo at Carpinteria represent pre-harbor conditions, as Carpinteria Beach had not yet been impacted by sediment supply reductions from the harbor construction. The largest reductions in beach volume (~175,000 m^3) followed between 1929 and 1938 as the erosion wave migrated through Carpinteria. Since 1929, the total volume of sand at Carpinteria has never recovered to pre-Harbor conditions (Figure 2.6a). The minimum beach volumes (~93,000 m^3) measured during the study occurred in 1989 following several years after the 1982-83 El Niño. The lack of suitable air photos immediately following the El Niño event prevents any documentation of beach recovery prior to 1989, so in actuality the minimum beach volume was likely lower between 1983 and 1989. After considering the erosion wave that had the greatest impact on the Carpinteria shoreline, it should be noted that the late 1960s and 1970s had the highest beach volumes following this erosion event. Overall there has been a long-term decrease in beach volumes across the Carpinteria coastline.

Historic beach area follows a similar pattern to beach volumes with changes in the more recent trends. Historically, beach areas declined steadily following the erosion wave, reaching lows in beach area and width in 1947 (Figure 2.5b, c). However, recent measurements taken during the DPGS surveys, show that recent beach areas and mean beach widths are closer to the pre harbor conditions (Figure 2.6b, c). The comparison of these three indicators for beach health show that beach volumes have decreased over time while beach widths seem to be recovering in recent times.

The City of Carpinteria shows a slightly different trend in beach volumes and surface area than the overall Carpinteria shoreline. The maximum beach volume found on the City of Carpinteria occurred in 1975 at ~73,000 m^3 with similar volumes found in 2001 (~69,000 m^3). The minimum beach volume and beach area found along the City Beach occurred in 1947 at ~32,000 m^3 (Figure 2.6). During the historical record, the City of Carpinteria Beach has had a more important contribution to the overall sand volumes and beach area found along the entire Carpinteria shoreline (Figure 2.7). Since 1959, the beach fronting the City of Carpinteria has made up between 30% and 50% of the total subaerial sand volume and about 30% of the total beach surface found along this entire stretch of coastline. In 2001 and 2003, the sand volumes found along the City beach contributed nearly 50% of the total sand volume along the entire Carpinteria coastline (Figure 2.7).

Historically, the beach widths in Carpinteria have oscillated over time, ranging from zero to 80 m (Figure 2.6c; Figure 2.8). The average summer/fall beach widths found along the Carpinteria coastline range from ~20 to 60 m. The City of Carpinteria Beach is a relatively stable beach characterized by a wide minimum beach width of ~25 m and a maximum beach width of ~60 m. The minimum and maximum beach widths found at each transect do not fit a temporal pattern; there is no clear relationship between beach width, El Niños and/or the erosion wave. In general, though, the two lowest years occurred in 1947 and 1989 with beach widths between 30 and 35 m (Figure 2.5c). The two maximum beach width periods were pre harbor 1929, and recent beach width measurements from the recent DGPS surveys which show similar magnitudes between 50 and 65 m.

Figure 2.9 shows the beach changes from 1929 to 1938 following the erosion wave. While beach widths were largely eroded in the west (~-125 m), there was also widening of the beach at the east end of the shoreline segment (~50 m; past the creek mouth located at transect 792). The beach has maintained this alignment for the subsequent 67 years (1938-2006), although the center of the beach has widened ~10 meters since the erosion wave for a near zero change in beach width over much of the coastline. Without shore protection structures, the beach width should remain relatively constant migrating inland or seaward depending on the amount of sand in the system (Komar, 1998). This pattern can be examined by looking at the shoreline change of both reference features along the shoreline.

In Figure 2.10 and Figure 2.11, the MSL shoreline change analysis shows a similar pattern of preferential erosion in the west and accretion in the east. The changes in actual shoreline location in 1929 and in 2006 (Figures 2.11-2.12) also show this pattern of erosion in the west and accretion in the east. However, the back beach change rate shown in Figure 2.10 at the west end of the beach (transects 760-770) shows an accretion trend which is related to the construction of the revetment advancing the back beach feature. The back beach shoreline change immediately adjacent to the revetment along the City beach (transects 770-780) follows the MSL shoreline pattern of erosion in the west and accretion in the east.

In analyzing the shoreline change data, it is apparent that the beach behaves differently alongshore. To better examine these changes, shoreline positions were plotted for four locations along the Carpinteria coastline- Sandyland Cove, Ash Avenue, Linden Avenue, and near the asphaltum outcrop at the eastern end of the beach (Figure 2.12). The west end, now armored, has experienced a strong erosion trend following early accretion between 1869 and 1938. This accretion can be explained by the migration of a sandspit at Sand Point onto the beach by 1929. Shoreline position at the Ash Avenue location has been regularly 20-30 m landward of the 1869 shoreline position, while the shorelines at Linden Avenue and the Asphaltum Outcrop, following early erosion in the early 1900s, have experienced steady accretion exhibiting 15-25 m of seaward accretion since 1869. In 1966, the two downdrift locations, Linden Ave and the asphaltum outcrop show the highest change in shoreline position which follows after the removal of the recreational pier.

El Niño Response

El Niño events have significant impacts on the entire US West Coast and has been shown to have significant impacts to several beaches in the Santa Barbara littoral cell (Revell and Griggs, 2006). The Lidar- and air photo-derived beach widths were combined to examine the response and recovery of the beaches at Carpinteria to the large El Niño events of 1982-83 and 1997-98 (Figure 2.13). The 1982-83 El Niño was the largest El Niño on record and had devastating impacts on several beaches near the study area (Revell and Griggs, 2006; Revell,

2007). In Carpinteria, due to the lack of available air photos at the appropriate scale and season, the closest available photo sets bracketing the event were taken in July 1975 and late May 1989 (Figure 2.13a).

Beach width changes analyzed using these photos, reveal a similar pattern of beach erosion in the west and accretion in the east as that shown in the historic shoreline change. These beach changes are characterized by nearly 40 m of narrowing in the west end and ~20 m of beach widening near the east end. By September 1994, the next available photo set, this erosion at the west end had nearly recovered to the 1975 beach width. Following the 1982-83 El Niño, a revetment was constructed from Sand Point upcoast to transect 770 to protect the oceanfront property near the western erosion hotspot seen in Figure 2.12a.

Examination of the Lidar beach widths of October 1997 and April 1998, reveal a similar erosion trend as the 1982-83 El Niño event and to the long-term beach width and shoreline change patterns (Figure 2.13b). Narrowing near the west end of the beach of ~40 m was conversely related to east end widening of ~20 m. The recovery of the beach at the west end erosion hotspot was complete by the time of the subsequent available air photo set in 2001 when the west end beach widths accreted nearly 40 m. The net result of this El Niño event and subsequent recovery by 2001 was that the beach had widened at the east end an additional ~20 m from the 1998 survey. One interesting note is that the location of the maximum erosion shifted to the east approximately 500 m between these two El Niño events with the hotspot shifting from Transect 767 to 777.

Correlation of Dredge Volumes and Beach Volumes

To examine the transport time of sand dredged from the harbor arriving at Carpinteria, a lagged cross correlation analyses on the smoothed Santa Barbara Harbor dredge record and a linearly interpolated summer/fall beach volume data was conducted (Figure 2.13). The results of this analyses show that the maximum correlation coefficient ($r^2 = 0.81$) occurs at 4 years, significant at the 1% confidence level (n=14). In other words, 81% of the variance in beach volumes can be explained by sand volumes dredged from the Santa Barbara Harbor after a four-year travel time (Figure 2.14a). The raw dredge data and the smoothed beach volumes also show a significant correlation with the peak lag at 4 years ($r^2 = 0.68$), significant at the 1% level (n=14) (Figure 2.14b).

Nearshore Bathymetric Change

Historical National Ocean Service (NOS) surveys from 1930/33 and 1978 (National Oceanic and Atmospheric Administration, 2007a) were gridded and compared with the recent USGS high resolution bathymetric survey (Chapter 5) to analyze changes in bathymetry offshore of Carpinteria (Figure 2.15). Due to uncertainties in the vertical accuracy of the historical soundings, volume changes have not been calculated, but there is a general pattern of nearshore sediment loss and offshore gain. Of particular note is the significant erosion pattern offshore of Sand Point from 1933 to 1978 (Figure 2.13a), coincident with significant reductions in longshore sediment transport due to Santa Barbara Harbor construction in 1929, and the subsequent collapse of the Sand Point sand spit. Nearshore sediment loss since 1978 (Figure 2.13b) coincides with several major El Niño seasons in which sediment would have been preferentially removed from the nearshore and deposited offshore.

Discussion

Historic Profile Analyses

The differences in response of the MSL and MLLW shoreline location indicate that over the 18 year time period, the shoreline has flattened its profile while gaining sand on the lower part of the subaerial beach. These figures indicate that while the MSL shoreline position has been relatively stable, the MLLW shoreline is more variable. The net changes over the 18 years of historic beach profiles show that the MLLW zone has accreted sand volume and moved the shoreline position ~15 m seaward. These analyses document an overall flattening of the subaerial beach profile. This may have been a result in the change of composition of the beach, with a loss of cobble-sized material from the beach during the 1997-98 El Niño (Figure 2.5; Matt Roberts, personal communication). Another potential explanation could be the beach berm management practice that the City of Carpinteria performs every fall. Since 1983, the City of Carpinteria has maintained a winter beach berm to protect the oceanfront properties from flooding and erosion (Table 2.1). The impacts of this practice are not well understood, although the net effect of the practice is to artificially move the shoreline position landward in the late fall, and seaward in the spring. This practice may have played a role in artificially distributing sand more seaward and thus lower on the profile than would have naturally occurred.

Historic Volume Changes, Beach and Shoreline Changes

The significant reductions in beach volumes that occurred over the last century have never recovered and are the major cause of Carpinteria shoreline and infrastructure vulnerability. The comparison of beach volume shows a long term response while beach widths appear to be recovering to pre harbor widths and surface area (Figure 2.6). The discrepancy in beach volume changes and beach width accretion further supports a flattening of the beach profile, although the causative mechanism is not identified. It is possible that these changes may also be related to either the loss of cobbles (Figure 2.5), or the berm management practice. The recent DGPS measurements that show a growth in the total surface area (Figure 2.6b) may be a result of several years of relatively low wave energy during the seasonal surveys.

As the beach fronting the City of Carpinteria has become more important to the overall sand volume and beach surface area, the economic importance of this beach as a location for tourists seeking a beach experience has also grown. Since the removal of the recreational pier in 1966, the city beach has maintained a wider average beach width than the rest of the Carpinteria shoreline.

There is significant alongshore variability in beach width, volume, and shoreline response. Much of this variability can be explained by the impacts of anthropogenic alterations to the coastal system.

Beach width typically remains relatively constant (after factoring out seasonal cycles) by migrating inland or seaward depending on the amount of sand in the system (Komar, 1998). If the shoreline is eroding due to sea level rise or some other factor, that same beach width would then be translated inland, but remain relatively constant, assuming a constant sediment supply and no shoreline armoring. Evidence for this is shown in the relatively stable beach widths along the City of Carpinteria beach that are coupled with rather low shoreline change rates.

However, the examination of the shoreline change rates of both the MSL and the back beach reference feature show that this is not the case in front of Sandyland Cove. The accretion "trend" seen in Figure 2.9 is caused by the construction and encroachment of a revetment onto the beach that has artificially advanced the back beach. While the accretion "rate" of the back

beach is not valid after a structure is built, because the backshore is fixed, the accretion in shoreline change rate identifies a human alteration and impact to the beach. This "rate" in front of the structure should be used carefully in any modeling or forecasting of future shorelines, and in any planning related sense because the overall impact of the revetment is to fix the back beach. Placement loss is the loss of beach width caused by the footprint of a structure on the beach. A revetment, as in the case of Sandyland Cove, occupies a much larger footprint than say a seawall due to its engineered slope requirements. As sea level rises, though, and the back beach remains fixed, then an additional consideration of passive erosion or beach drowning occurs. This is something that should be considered in assessing future impacts to the coastline and in examining various erosion mitigation alternatives.

Another human induced alteration was the accumulation of around the historic pier that was constructed pre 1929 and removed in 1965. The shoreline position changes in 1966 (Figure 2.12) show a retreat some 40 m inland evidence which suggests that the fillet beach accumulated around the pier was rapidly eroded during that time period at both Linden Ave and the downdrift tar outcrop.

El Niño Impacts

El Niños have destructive impacts along much of the Santa Barbara littoral cell and form an almost predictable rotation-like pattern of erosion and accretion along the Carpinteria coastline. The erosion of the beach in the west, and the accretion of the beach in the east can be seen in both of the last major El Niños. The difference between these two events, though, is the migration of the erosion hotspot onto the City of Carpinteria beach. This migration follows the construction of the revetment and associated placement loss along the Sandyland cove section. As a result of the structure, the amount of beach width available to respond to the 1997-98 El Niño compared to the 1982-83 event along Sandyland Cove was reduced. The loss of beach width and reduced buffering capacity caused by increased wave reflection may have increased the alongshore transport and sand suspension resulting in a scour trough that most likely has resulted in this migration of the erosion hotspot downdrift onto the City of Carpinteria beach.

Correlation of Dredge Volumes and Beach Volumes

The highly significant correlations between the dredge volumes and beach volumes is somewhat expected given the impacts of sand impoundment and the erosion wave in the 1930's. The four-year lag time between harbor dredging and sand volume changes is relatively consistent with the findings of Bailard (1982) who examined winter beach widths and dredge volumes and found a peak lag at 5 years. Given the highly energetic El Niño winters of 1982-83 and 1997-98, it is likely that this may have increased the longshore transport rate. The peak in the correlation plots are reached at 4 years, but remain positive and significant up to the 10-year lag (Figure 2.13). This could possibly indicate that the sand volumes dredged from the harbor continue to reach Carpinteria for 10 years following dredging. Another plausible explanation is that much of the sand transport is done during a few energetic years interspersed with calmer years leading to an average arrival time of 4 years.

Conclusions

- The beach at Beacon#10 (Linden Avenue) has flattened over the last 18 years (1987 – 2005), with the MSL shoreline maintaining its position while the MLLW shoreline accreted by ~15 m.

- Historic subaerial beach volumes declined by more than 175,000 m^3 following the erosion caused by the construction of the Santa Barbara Harbor.
- Beach widths along the City of Carpinteria beach have been relatively stable over time ranging from 25 m to 60 m with no single event correlating to minimum or maximum beach widths.
- Beach width and shoreline change analyses show that there is a long-term trend of beach erosion in the west and accretion in the eastern part of study area.
- The El Niño pattern of beach impacts is to preferentially erode the beaches in the west and accrete the beaches in the east. Differences between the 1982-83 and 1997-98 events show that the erosion hotspot in 1982-83 migrated east onto the City of Carpinteria Beach during the 1997-98 El Niño. The construction of the revetment along Sandyland Cove following the 1982-83 El Niño event may have caused this migration.
- Correlation analyses of the sand volumes dredged from the Santa Barbara Harbor and the sand volume found on the beach at Carpinteria suggest a four year travel time for sediment to reach downdrift Carpinteria beach.
- The consistent pattern among the El Niño beach response, the 138-year long-term shoreline change rates, and the 77-year long-term beach width changes provide evidence that El Niños play a major role in shaping the coastline of Carpinteria.
- Over the last 75 years the there has been a trend of nearshore sediment loss and mild offshore gain, with the most substantial loss offshore of Sand Point.

References

Bailard, J., and Jenkins, S.A., 1982. City of Carpinteria Beach Erosion and Pier Study. Final Report to the City of Carpinteria. Bailard/Jenkins Consultants, 292 pp.

Boak, E. H. and Turner, I. L., 2005. Shoreline definition and detection: a review. Journal of Coastal Research, v. 21, no. 4, p. 668-703.

Crowell, P.J., and Leatherman, S.P. (editors), 1999. Coastal Erosion Mapping and Management. Journal of Coastal Research, Special Issue 28. Coastal Education & Research Foundation, Inc.

Farris, A.S. and List. J.H., 2007. Shoreline change as a proxy for subaerial beach volume change. Journal of Coastal Research. v. 23, no. 3, p. 740-748.

Hapke, C., Reid, D., Richmond, B., Ruggiero, P., and List, J. (2006). National Assessment of Shoreline Change Part 3: Historical Shoreline Change and Associated Coastal Land Loss Along Sandy Shorelines of the California Coast. USGS Open-File Report 2006-1219, 72 pp.

Komar, P.D., 1998. Beach Processes and Sedimentation. Prentice Hall, Inc., Simon & Schuster, Upper Saddle River, N.J., 544 pp.

Moore, L.J., 2000. Shoreline mapping techniques. Journal of Coastal Research, v. 16, no.1, p. 111-124.

Moore, L.J., Ruggiero, P., and List, J., 2006. Comparing mean high water and high water shorelines: Should proxy datum offsets be incorporated in shoreline change analysis? Journal of Coastal Research, v. 22, no. 4, p. 894-905.

Morton, R.A. and Speed, F.M., 1998. Evaluation of shorelines and legal boundaries controlled by water levels on sandy beaches. Journal of Coastal Research, v. 18, no. 2, p. 329-337.

National Oceanic and Atmospheric Administration (NOAA), 2007a. NOS Hydrographic Survey Viewer, http://map.ngdc.noaa.gov/website/mgg/nos_hydro/viewer.htm

National Oceanic and Atmospheric Administration (NOAA), 2007b. Tides & Currents, Center of Operational Products and Services, http://tidesandcurrents.noaa.gov/

Patsch, K. and G.B. Griggs, 2007. Development of sand budgets for California's major littoral cells. Report to California Department of Boating and Waterways. Coastal Sediment Management Work Group. http://dbw.ca.gov/CSMW/PDF/Sand_Budgets_Major_Littoral_Cells.pdf

Revell, D.L., Komar, P.D., and Sallenger, A.H., 2002. An application of lidar to analyses of El Niño erosion in the Netarts littoral cell. Journal of Coastal Research v. 18, no. 4, p. 792-801.

Revell, D. L., and Griggs, G.B., 2006. Beach width and climate oscillations along Isla Vista, Santa Barbara, California. Shore and Beach v. 74, no. 3, p. 8-16.

Revell, D.L., 2007. Long Term and Storm Event Changes in the Santa Barbara Sandshed. PhD Dissertation. Earth Science Department, University of California, Santa Cruz. March, 148 pp.

Ruggiero, P., Kaminsky, G.M. and Gelfenbaum, G., 2003. Linking proxy-based and datum-based shorelines on a high energy coastline: implications for shoreline change analyses. Journal of Coastal Research, v. 38, no. 3, p. 57-82.

Sallenger A.H., Krabill, W., Brock, J., Swift, R., Jansen, M., Manizade, S., Richmond, B., Hampton, M. and Eslinger, D., 1999. Airborne laser study quantifies El Niño induced coastal change. EOS, American Geophysical Union, v. 80, p. 92-93.

Sallenger A.H., Krabill, W., Swift, R., Brock, J., List, J., Jansen, M., Holman, R.A., Manizade, S., Sontag, S., Meredith, A., Morgan, K.,. Yunkel, J.K., Frederick, E.B. and Stockdon, H.F., 2003. Evaluation of airborne topographic Lidar for quantifying beach changes. Journal of Coastal Research, v. 19, no. 1, p. 125-133.

Thieler, E.R., Himmelstoss, E.A., Zichichi, J.L. and Miller, T.L., 2005. Digital Shoreline Analysis System (DSAS) version 3.0: An ArcGIS extension for calculating shoreline change: U.S. Geological Survey Open-File Report 2005-1304.

Wiegel, R. L., 2002. Seawalls, seacliffs, beachrock: What beach effects? Part 2. Shore and Beach, v. 70, no. 2, p. 13-22.

Table 2.1. Environmental history of significant events to the Carpinteria shoreline compiled from Bailard (1982), Revell (2007), and historical air photo analyses.

Date	Event
1869 - 1902	Sandspit at Sand Point
Mar. 1905	Large Storm Event 20' at 14 sec from 240 degrees
Feb. 2, 3 1915	Large Storm Event 14-18' at 10-11 sec from 240-270 degrees
Pre -1929	Recreational Pier built east of Carpinteria Creek
1927 -1930	Santa Barbara Harbor built - sand impoundment begins
1935	Dredging begins …offshore East Beach in 20 feet still there
1936	Dredging begins …onto East Beach
1937	Harbor fillet beach full
Sept. 1939	Large hurricane event 18' at 13 sec from 170 degrees
1959	Rip rap seen in air photos at Sandyland
1954-1960	Accumulation at Santa Barbara Harbor to accrete Sandspit
1965	Recreational Pier removed
1969	Rip rap seen in air photos at mouth of Carpinteria Slough and armoring begins East toward City Beach
Oct. 1979	Rip rap seen in oblique air photos with armoring halfway to City Beach
1982-83	Large El Niño extreme southerly displacement of waves
Dec-83	Beach berm construction begins due to erosion at City Beach
Pre- Sept. 1985	Armor constructed east to current configuration just west of Ash Avenue. Lawsuit ensues due to placement of revetment onto public beach. Settled out of court and the revetment remains in the active intertidal zone during the winter season.
1996	City stops collecting pre- and post-berm building beach profiles
1997-98	Large El Niño February 1998 monthly average of 13' waves at 277 degrees

Table 2.2. Specifications of aerial photography. *Spatial errors are an average error for the entire flightline. Sources –University of California, Santa Barbara Map and Imagery Library; California Coastal Commission, USGS- United States Geological Survey, and Pacific Western Aerial Surveys.

Year	Date	Scale	Spatial Error (m)*
1929	NA	15840	9.7
1938	NA	24000	9.3
1943	9/22/1943	20000	9.1
1947	8-/20 and 8/21/1947	24000	9.3
1959	11/23/1959	15600	8.4
1966	9/23/1966	12000	8.4
1969	10/30/1969	12000	8.3
1975	7/29/1975	24000	7.2
1989	5/22 and 5/23/1989	24000	6.4
1994	9/9/1994	24000	5.0
2001	9/25/2001	12000	6.3
2003	6/25/2003	6000	5.4

Figure 2.1. Photo taken 1936 after the erosion wave had passed Fernald Point en route to Carpinteria. Santa Barbara Harbor visible in the distance, note the extent of cross-shore groins in place to retain sand and slow erosion (photo courtesy of the Spence Collection – UCLA).

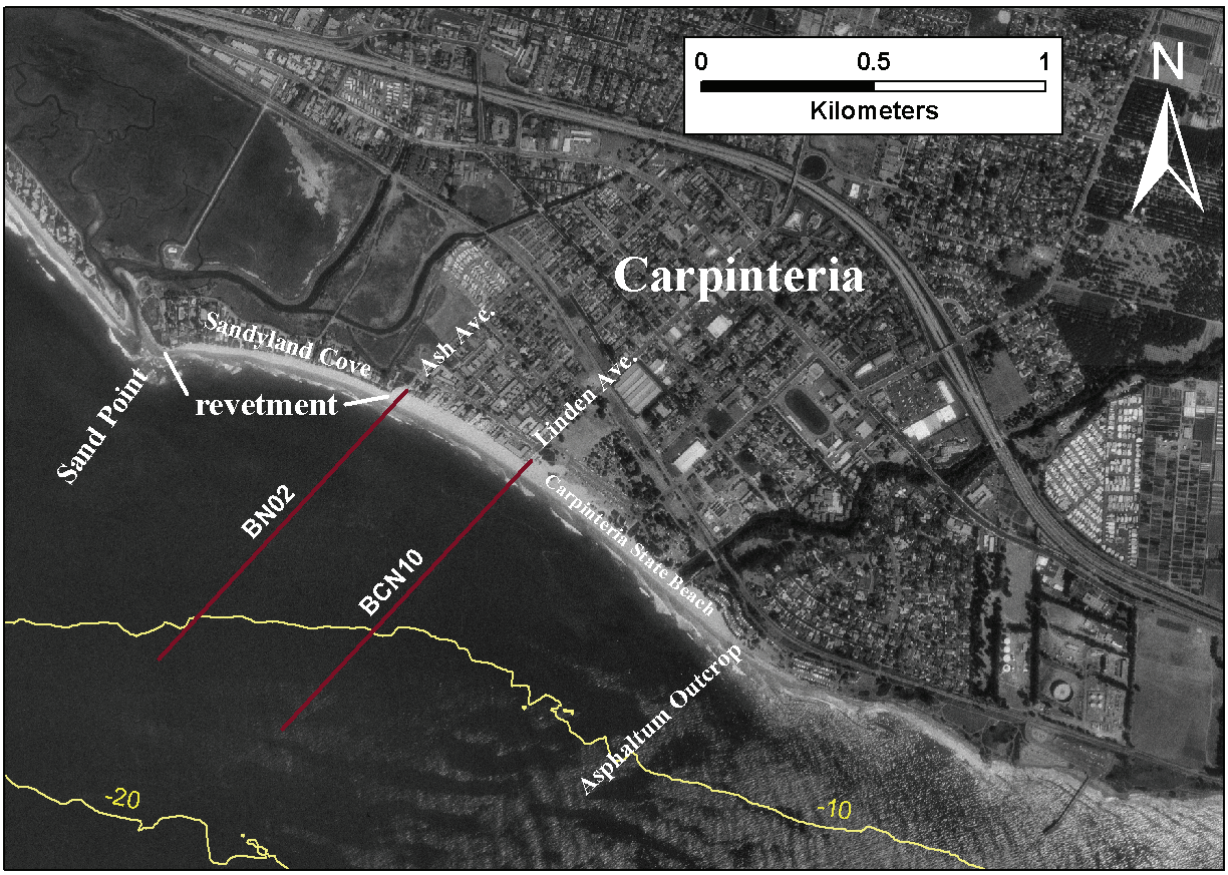

Figure 2.2. Aerial photo of the Carpinteria study area showing the locations of the two historical BEACON profiles, BCN10 and BN02. Yellow bathymetric contours are expressed in meters.

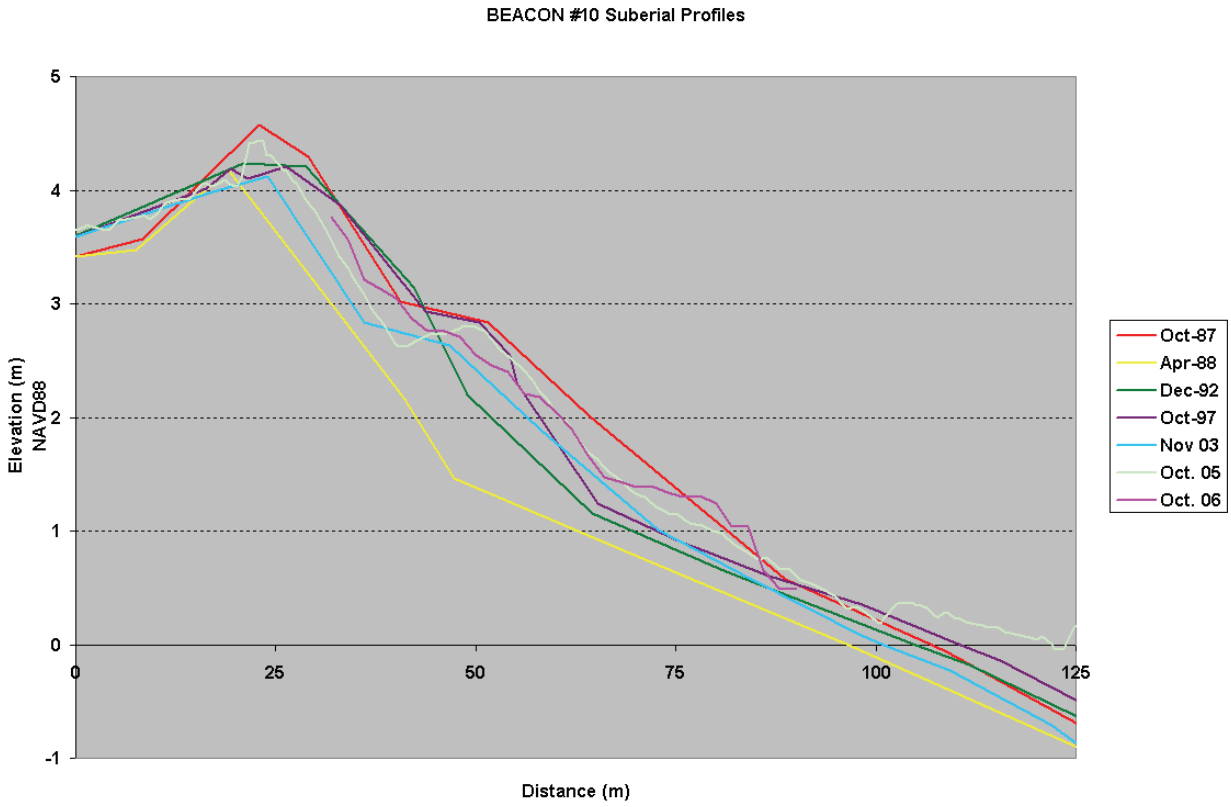

Figure 2.3. Historic profiles taken at Linden Ave (BCN 10). See Figure 2.2. for profile location.

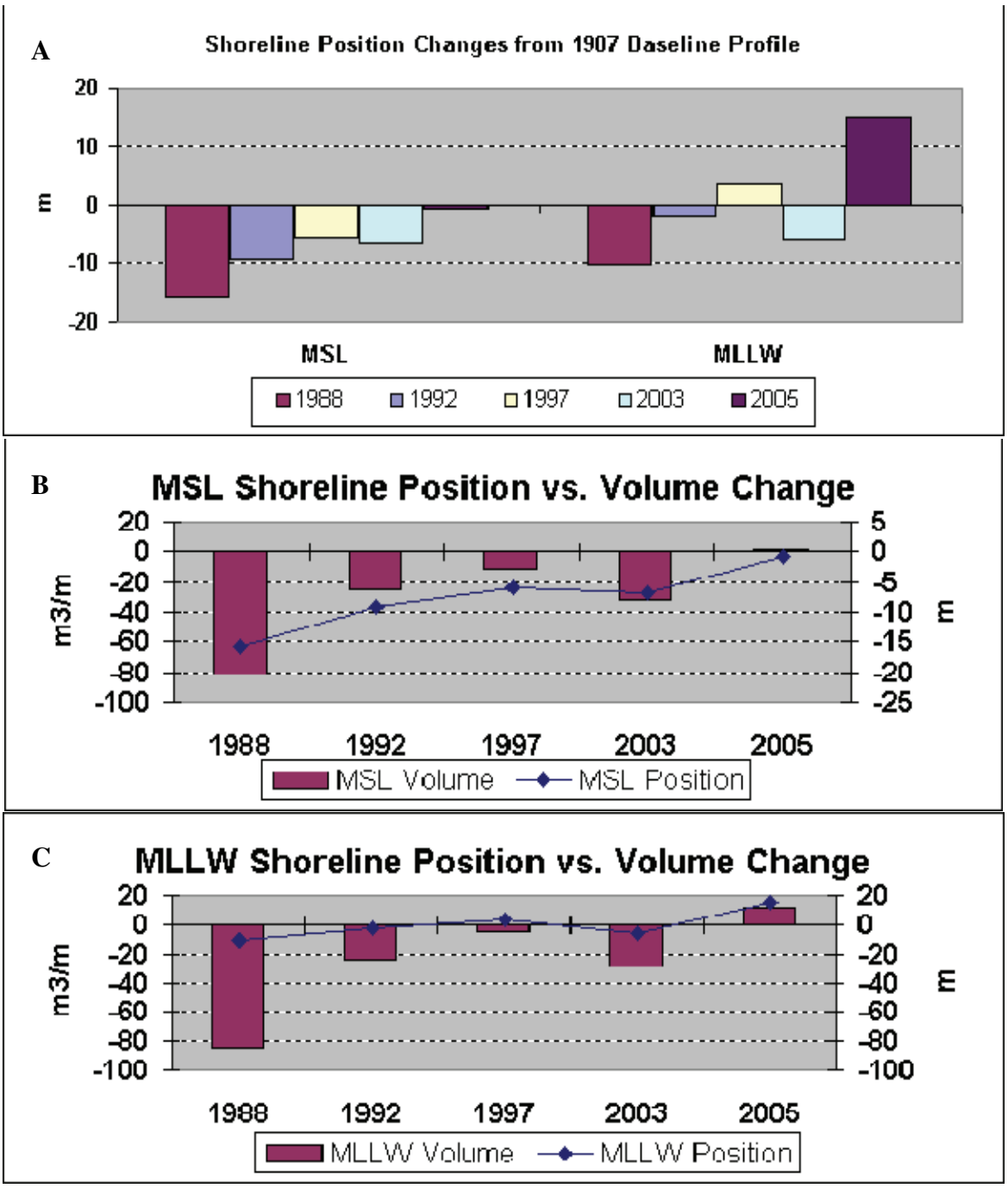

Figure 2.4. A) Shoreline Changes of MSL (0.83 m above MLLW) and MLLW extracted from BEACON profile #10, Carpinteria. B) Shoreline position changes versus volume changes relative to 1987 baseline profile at MSL. C) Shoreline position changes versus volume changes relative to 1987 baseline profile at MLLW. Beach volume estimates are for the City of Carpinteria Beach.

Figure 2.5. Beach cobble on the winter beach– A) 1978 and B) Winter 2006 – City of Carpinteria Beach Ash Avenue looking west, updrift toward Sand Point (photo courtesy of Matt Roberts). Note the revetment in the 2006 photo.

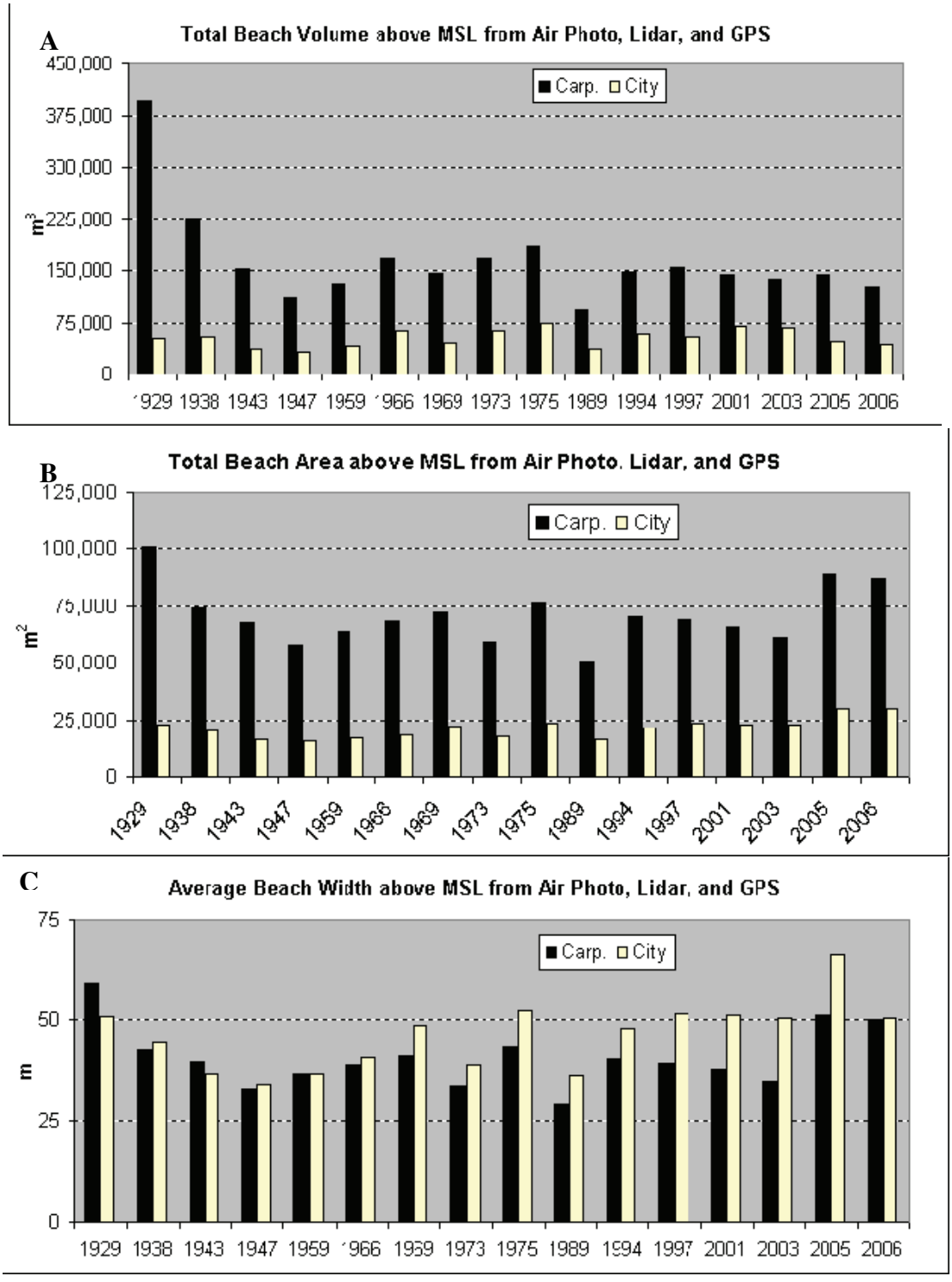

Figure 2.6. A) Total beach volumes, B.) total beach area, and C) average beach widths (above MSL) from 1929-2007, 1929-1994, 2001, and 2003 from aerial photography; 1997,1998, and 2005 from Lidar; 2006 – 2007 from GPS surveys.

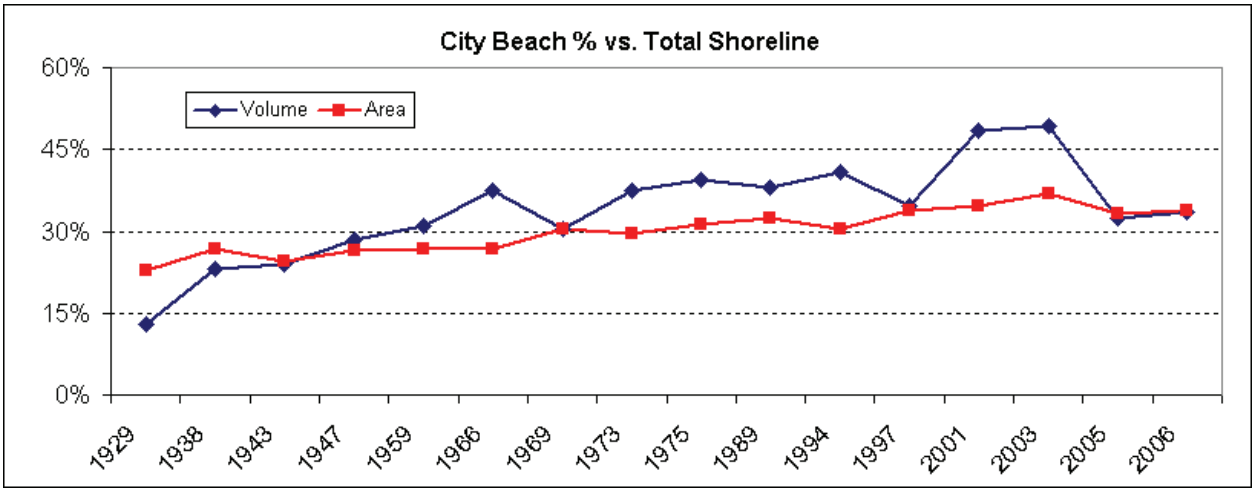

Figure 2.7. City beach volumes and beach area as percentage of Carpinteria coastline west from the Carpinteria Salt Marsh inlet to asphaltum outcrop near lifeguard station in the east.

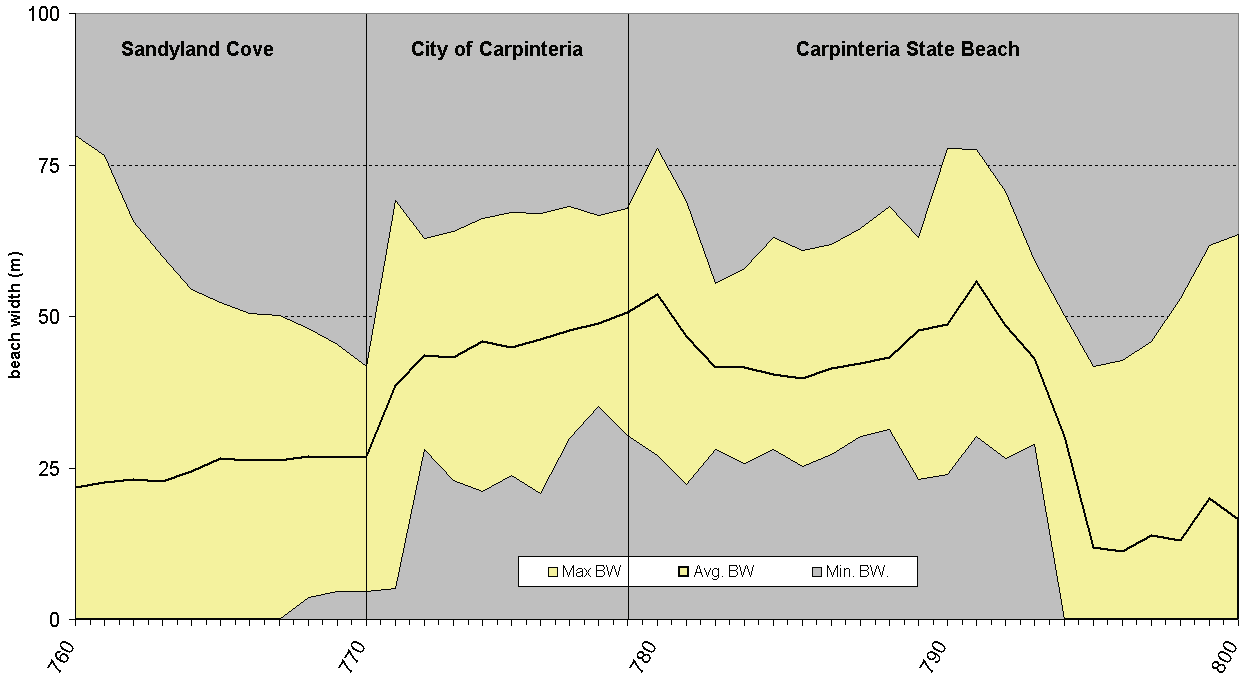

Figure 2.8. Beach width variability along Carpinteria. City Beach is located between transects 771 and 779. The west end is the Carpinteria Salt Marsh tidal inlet, and the east end is the tar outcrop.

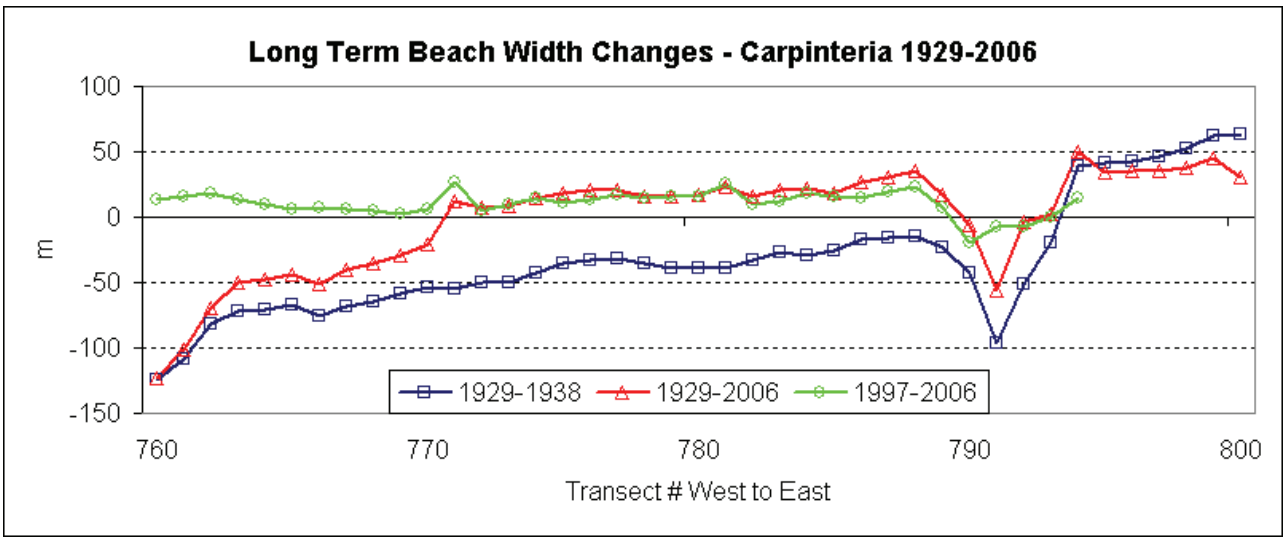

Figure 2.9. Beach width changes from 1929 baseline. Shown are the long-term changes from 1929 to 2006, the changes immediately following the arrival of the erosion wave between 1929 and1938, and the recent changes from 1997 to 2006. Note that the City of Carpinteria focus site is found between transects 771 and 779, and that Carpinteria Creek outlets between transects 791-793.

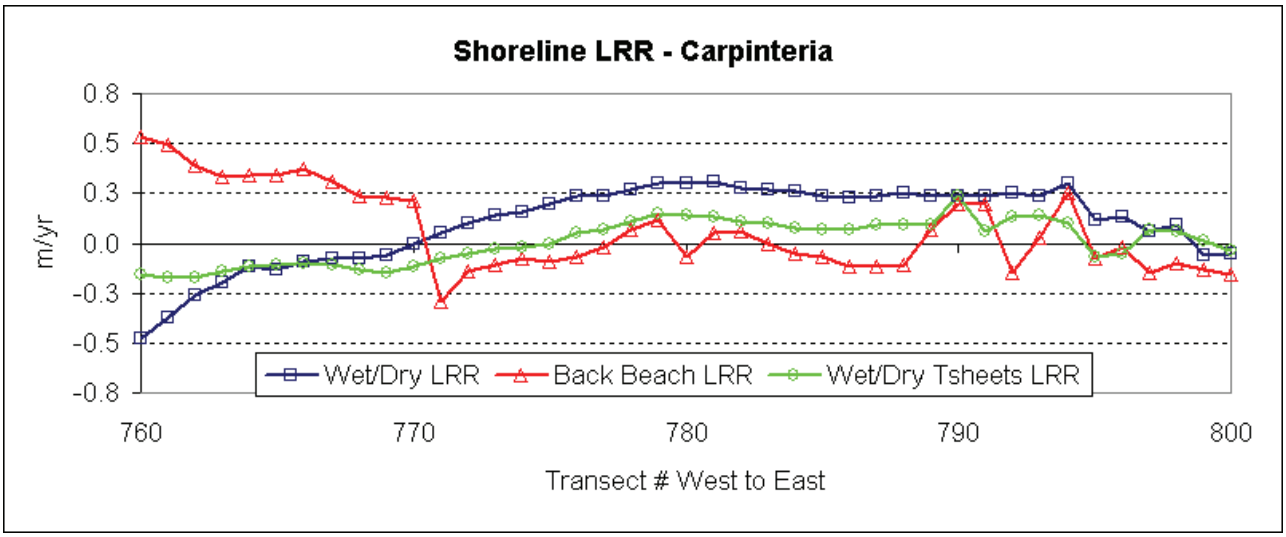

Figure 2.10. Shoreline change linear regression rates of the various shoreline reference features. The red line is the back beach, the blue line is the MSL wet/dry adjusted line from air photos, and the green line is the shoreline change rates derived by including the historic NOS T-sheets as well as air photo and Lidar derived shorelines. Note that the City of Carpinteria focus site is found between transects 771 and 779.

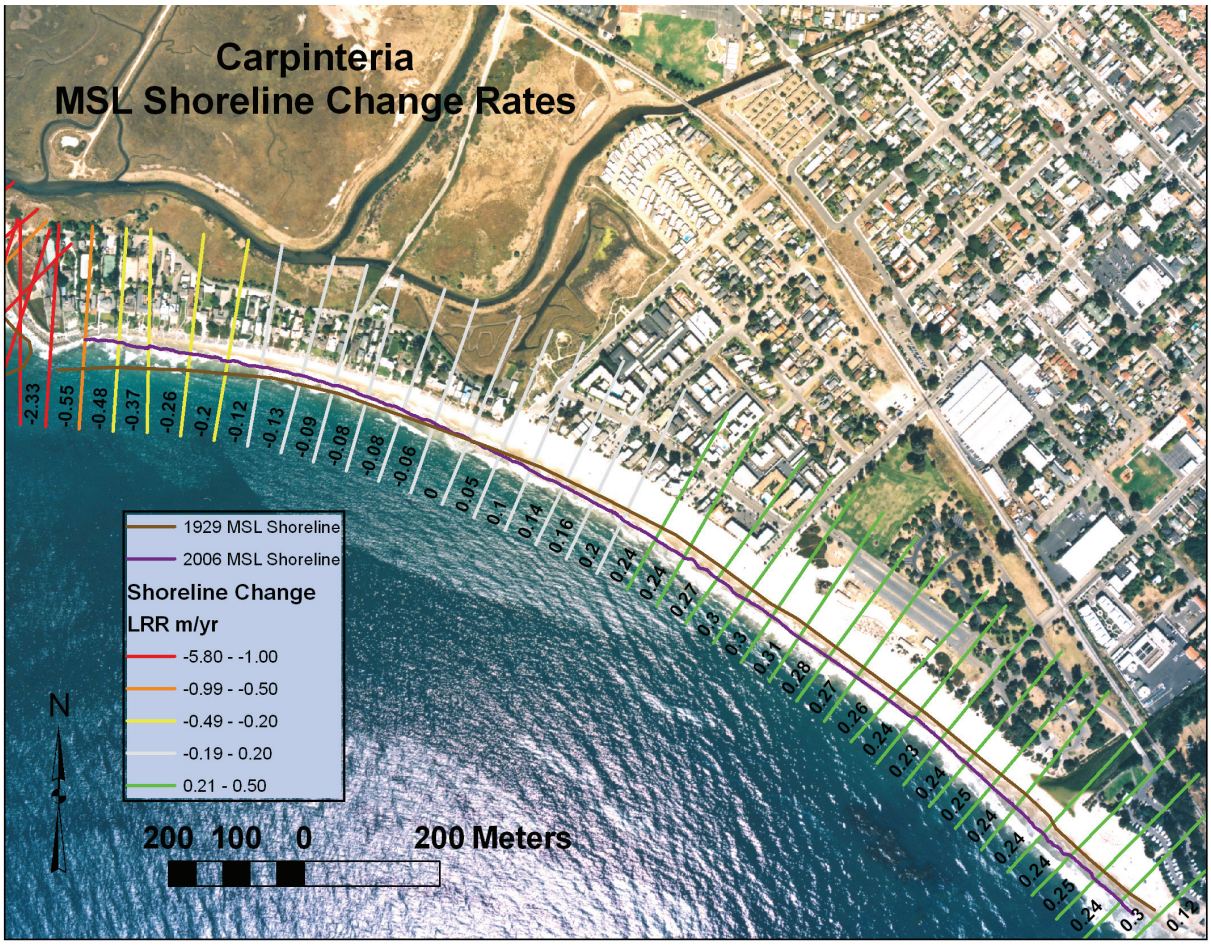

Figure 2.11. Carpinteria shoreline changes. 1929 (brown) and 2006 (purple) MSL shorelines show erosion in the west end and accretion in the east end. Transects used throughout the analyses are color coded to show magnitudes of change rates with the calculated rates at each transects shown.

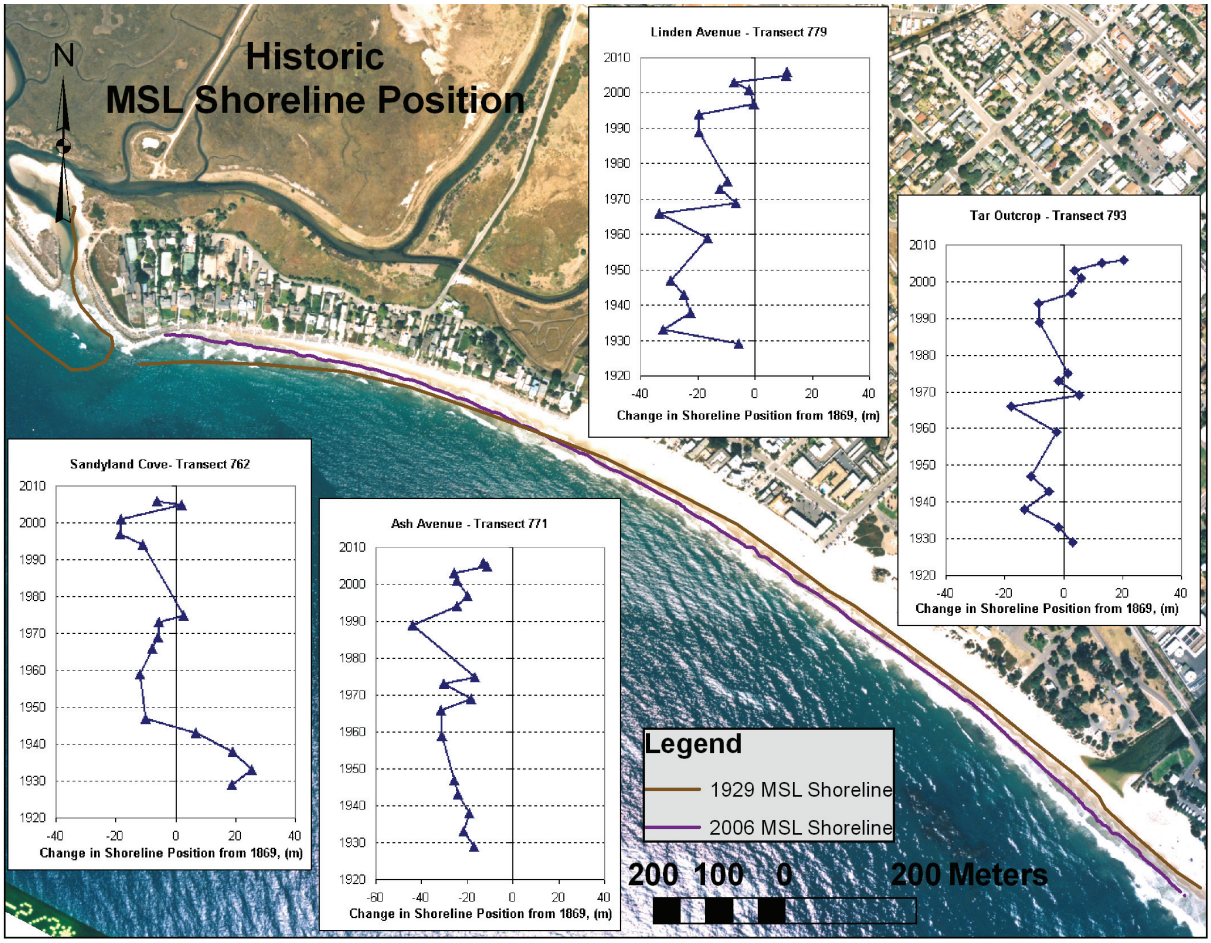

Figure 2.12. Changes in MSL shoreline position relative to the 1869 shoreline at four locations along Carpinteria.

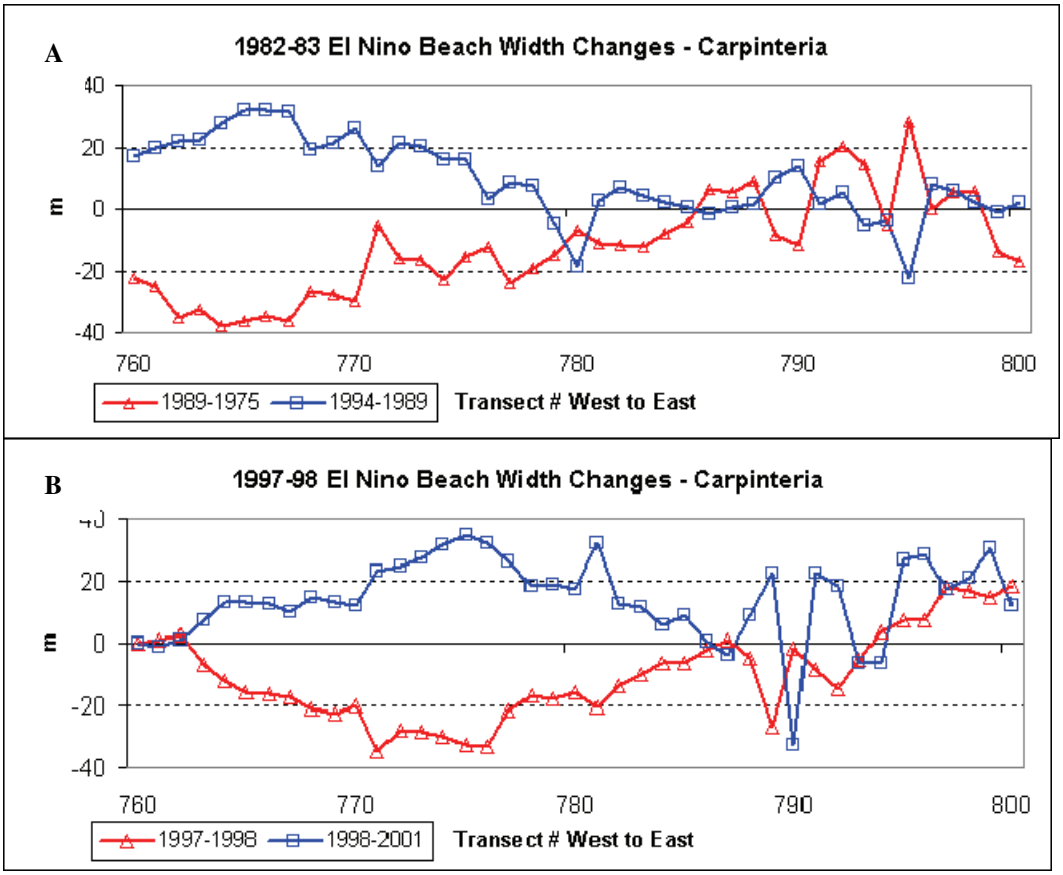

Figure 2.13. Beach width changes and recovery following the A) 1982-83 and B) 1997-98 El Niños. Note that the City of Carpinteria focus area is between transects 771 and 779.

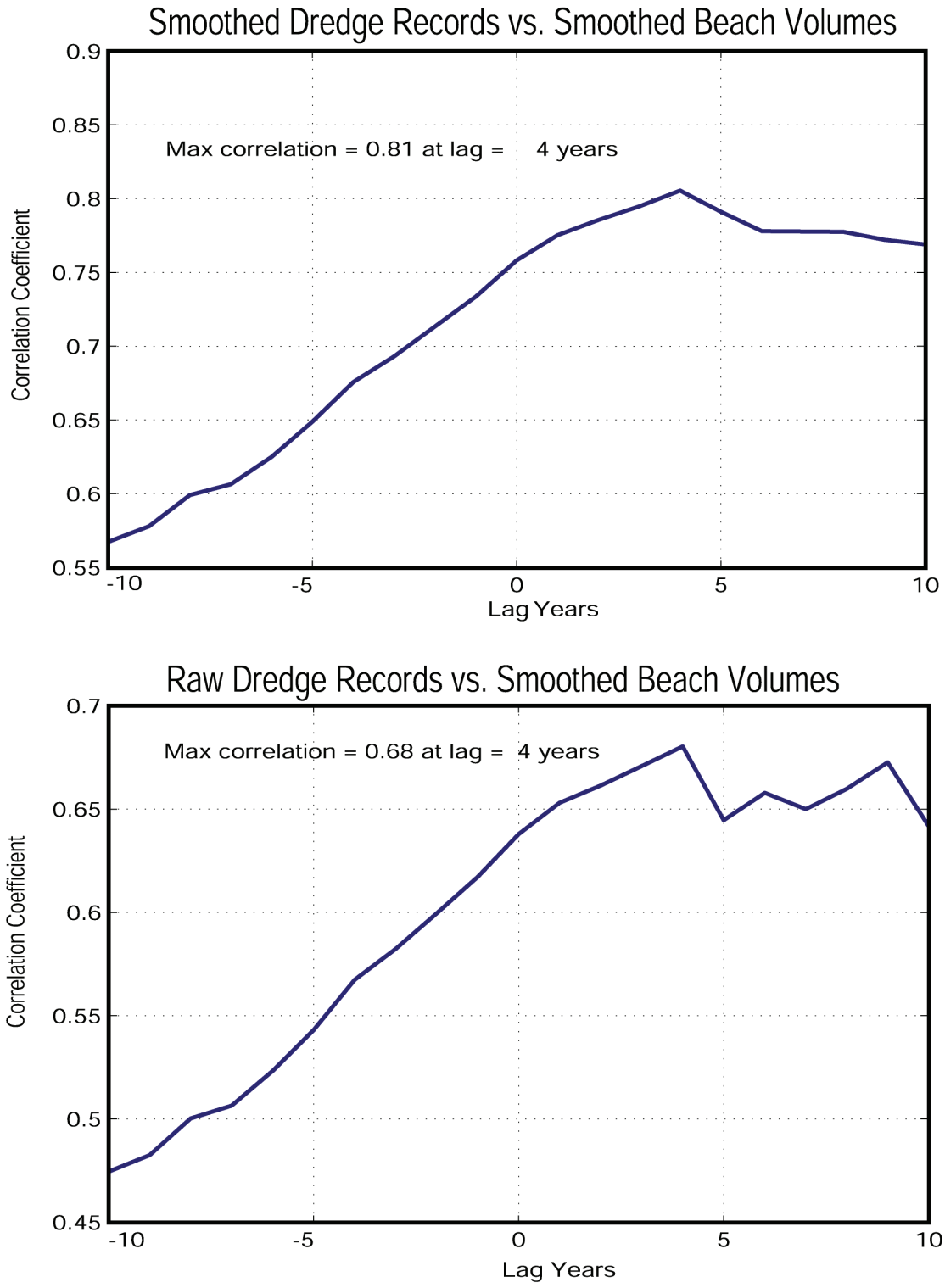

Figure 2.14. Lag correlation analysis of Carpinteria beach volume changes and dredge records. A) Smoothed dredge records vs. smoothed beach volumes. B) Raw dredge records vs. smoothed beach volumes. In both cases maximum correlation occurs at the 4 year lag.

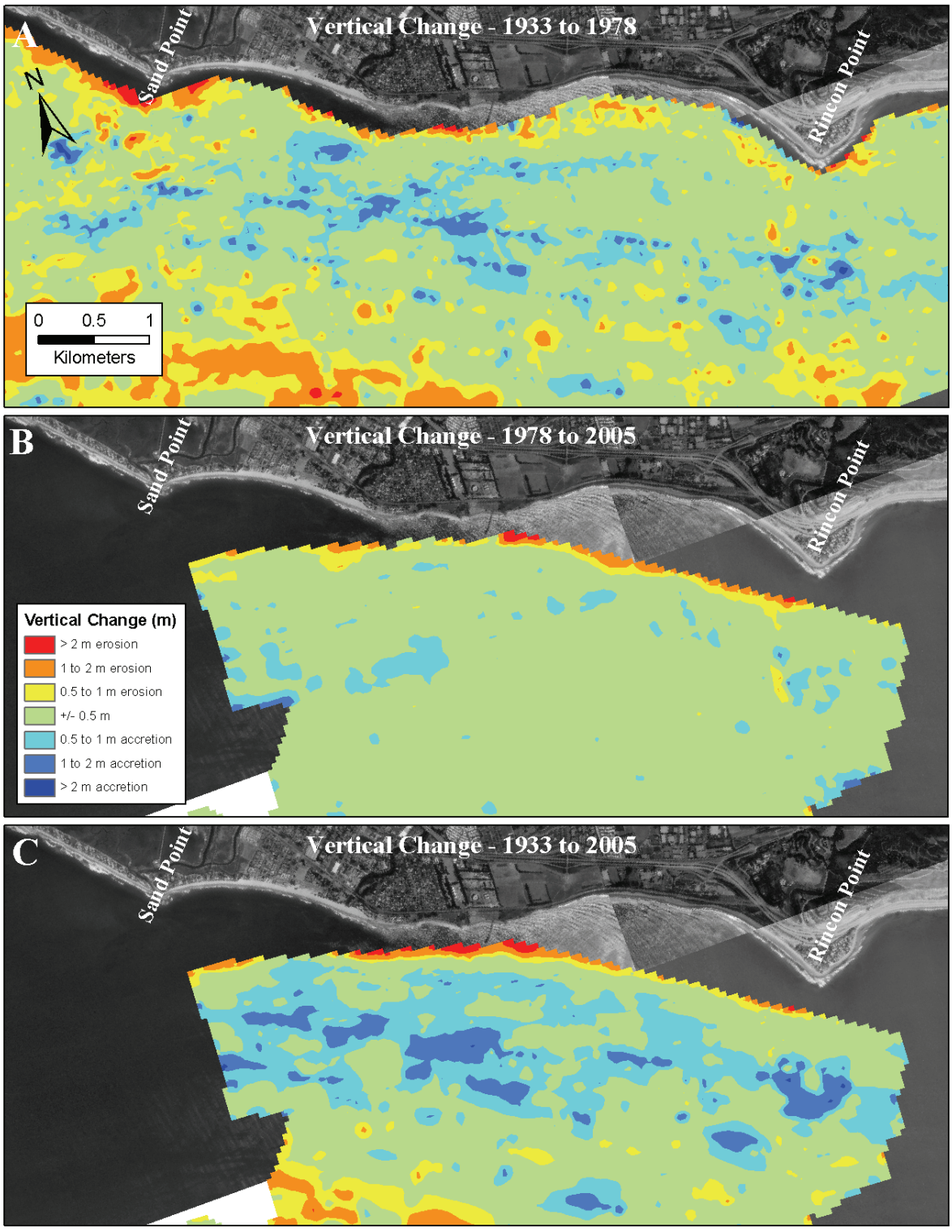

Figure 2.15. Nearshore bathymetric changes in the Carpinteria area calculated from historical NOS surveys and USGS 2005 submetrics survey gridded to 50 m cell size. A) Vertical change from 1930/33 survey to 1978. B) Vertical change from 1978 to 2005. C) Vertical change from 1930/33 to 2005.

Chapter 3- Recent Morphologic Changes

By Patrick Barnard, David Revell and Jodi Eshleman

Introduction

In October 2005, a seasonal topographic and shallow-water bathymetric surveying campaign began as part of the Carpinteria Coastal Processes Study. Lidar topographic data was also collected at this time as part of a BEACON-funded survey that covered the entire Santa Barbara littoral cell. Since then, topographic and bathymetric data have been collected bi-annually in February/March and October with All-Terrain Vehicles (ATVs) and the Coastal Profiling System (CPS), respectively (Table 3.1). Recent innovations in field techniques have made it possible to quickly collect high-quality survey data in an area where difficult conditions made surveying prohibitive in the past. This data helps to identify long-term beach and nearshore morphologic trends when compared with older survey data (see Chapter 2), seasonal patterns of sediment transport and morphologic change (this chapter), and is used to create high-resolution topographic and bathymetric grids for numerical modeling.

Methods

Lidar

Airborne light detection and ranging (Lidar) survey data were collected in partnership with BEACON, California Department of Boating and Waterways, the United States Geological Survey, the University of California Santa Cruz, and the University of Texas Bureau of Economic Geology (BEG) on October 15, 2005. The data set includes point data from a strip of Southern California coastline (including water, beach, cliffs, and top of cliffs) from Point Conception in Santa Barbara County to Point Mugu in Ventura County, which includes all beaches in the vicinity of Carpinteria. The purpose of the data was to compare with previous data sets to determine rates of shoreline change along the Santa Barbara and Ventura County coastlines. The data set was created by combining data collected using an Optech Inc. Airborne Laser Terrain Mapper (ALTM) 1225 in combination with geodetic quality Global Positioning System (GPS) airborne and ground-based receivers. The system was installed in a twin engine Partenavia P-68 Observer owned and operated by Aspen Helicopter, Inc. Elevation points were collected in the National Geodetic Survey S2003 geoid model. Heights above the GRS80 ellipsoid were converted to orthometric heights with respect to the North American Vertical Datum of 1988 (NAVD88). The horizontal datum used was the North American Datum of 1983 (NAD83, Zone 11, north) with a resolution of 1 m.

Selected portions from each Lidar data set (last return only) were used to generate a 1m x 1m digital elevation model (DEM). Data, estimated to have a horizontal accuracy of 0.01-0.03 m from ground surveys using kinematic GPS techniques, were superimposed on the Lidar DEM and examined for any mismatch between the horizontal position of the ground GPS and the corresponding feature on the Lidar DEM. Horizontal agreement between the ground kinematic GPS and the Lidar was within the resolution of the 1m x 1m DEM. Ground GPS surveys were conducted within the Lidar survey area to acquire “ground truth" information. The ground survey points are estimated to have a vertical accuracy of 0.01-0.05 m. Roads, which are open areas with an unambiguous surface, were surveyed using kinematic GPS techniques. The Lidar data set was sorted to find data points that fell within 0.5 m of a ground GPS survey point- in comparison with survey grade control points gathered at the end of Linden and Ash Avenues

coincident with the Lidar flight: the mean vertical error of 325 co-located points (within 0.5 m) is only 0.5 cm. The mean elevation difference between the Lidar and the ground GPS was used to estimate and remove an elevation bias from the Lidar. The standard deviation of these elevation differences provides estimates of the Lidar precision. The October 2005 Lidar data set was determined to have an average elevation bias of 0.045 m when compared to ground truth points. Over the calibration target area, average RMS values for the first return is 0.05 m and 0.07 m for the second return.

All-Terrain Vehicle Surveys

Four beach surveys were conducted with All-Terrain Vehicles (ATVs) using Ashtech© equipment to collect data with the Differential Global Positioning System (DGPS) (Figure 3.1). The data collected with the ATV were post-processed using data recorded at a base station, established on a USGS benchmark at the Linden Avenue Lifeguard Station, located at the eastern end of the City of Carpinteria Beach. All surveys were collected in the Universal Transverse Mercator (UTM) projection, using NAD83, Zone 11 North as the horizontal coordinate system. All elevations are relative to the North American Vertical Datum 1988 (NAVD 88), which is 2.7 cm above MLLW at the Santa Barbara Harbor Tide Station (Station # 9411340: National Oceanic and Atmospheric Association, 2007b).

Based on repeated surveys of the hardscape on Linden and Ash Avenues before and after each topographic survey, and in reference to high end control point collection in this area, the mean vertical accuracy of this system is ~ 1 cm, with the vertical uncertainty of individual points approximately +/- 3 cm. Each survey consisted of from 7,000 to 11,000 points covering the accessible portion of the beach from the Carpinteria Pier to Loon Point, with coverage often reaching below the MLLW line (Figure 3.2). This is far more efficient than traditional land surveying techniques, where only approximately one percent of the number of survey points could be gathered in the same amount of time. Grids were created with 2 m resolution using a standard inverse distance weighting method in ArcGIS to identify seasonal trends, areas of chronic erosion, shoreline position and beach volume changes. Grid differencing was conducted using the common survey areas between the two surfaces being compared. A list of the surveys to date is included in Table 3.1. The Lidar survey took place on the same day as the ATV survey on October 15, 2005. This provided an excellent test for the accuracy of each survey. A comparison of hardscape points (n=89) within 25 cm between the two surveys had a mean difference and standard deviation of 0.4 cm and 7.3 cm, respectively. The spread in the data is likely due to curbs and the Lidar bare earth filter. The entire mean survey area difference, including all beach and hardscape points, was just 0.2 cm, with a standard deviation of 8.6 cm.

Coastal Profiling System

The Coastal Profiling System (CPS), a hydrographic surveying system mounted on a Personal Watercraft, was used to collect bathymetric data for the 12 km stretch of the southwest facing Carpinteria Beach (Figure 3.3). The CPS combines the high accuracy positioning of a DGPS and the mobility of a personal watercraft to collect rapid and precise bathymetric profiles. The CPS has traditionally been used to survey cross-shore profiles perpendicular to a shoreline from approximately 15 m depth to one-meter depth (NAVD 88), depending on weather and tide conditions. The survey setup for this site consists of 36 cross-shore profiles running from ~ 1 km offshore through the surf zone and six alongshore profiles parallel to the coastline in the section just offshore of Carpinteria Beach (Figure 3.4).

The bathymetric data was collected using a third generation CPS. A more complete discussion of specifics regarding the CPS can be found in Ruggiero and others (2005) and MacMahan (2001). This bathymetric surveying technique has been shown to achieve sub-decimeter accuracy (MacMahan, 2001); however reasonable variations in water temperature can affect depth estimates by as much as two percent of the total water depth. All data are corrected to adjust the vertical coordinate for the actual speed of sound in post-processing using the average of the surface water temperature measured at the Santa Barbara National Data Buoy Center (NDBC) Buoy, Station #46053 during the survey period (National Oceanic and Atmospheric Administration, 2007a).

Ashtech© GPS equipment was used to collect bathymetric data. All survey data was collected in the UTM horizontal coordinate system, Zone 11 and referenced to NAVD 88. The CPS collected data at 5 Hz and while traveling at 3 m/s generates a depth sounding every 0.6 meters along the sea floor. All surveys were completed using Real Time Kinematic (RTK) GPS, where rovers received information by radio signal from a base station while in the field, minimizing post-processing requirements. HYPACK® (Coastal Oceanographics, Inc.) hydrographic surveying software was the platform used for navigation and data collection in the field. Ashtech© Z-Extreme receivers were used for all surveys and have manufacturer reported accuracies of approximately ±1 cm + 1ppm in the horizontal and approximately ±2 cm + 2ppm in the vertical while operating in RTK surveying mode (Magellan Navigation, Inc., 2006). These reported accuracies are, however, additionally subject to multi-path, satellite obstructions, poor satellite geometry, and atmospheric conditions. While the horizontal uncertainty of individual data points is approximately 0.05 m, the CPS operators cannot stay 'on line', in waves and currents, to this level of accuracy. Typically, mean offsets are less than 2.0 m from the preprogrammed track lines and maximum offsets along the approximately 1 km long transects are typically less than 10 m.

The control point used to set up a base station was located at the lifeguard tower in Carpinteria. When necessary, a radio repeater was set up on the rock revetment northwest of this location, or on a marine buoy at the offshore edge of the survey area to help extend radio coverage to the farthest western and eastern sections of the survey area. Due to radio range limitations, a control point in Rincon was used to set up the base station when surveying profiles one through four for surveys completed in October, 2006 and February, 2007.

Results

BEACON Profiles

BEACON profile lines BCN10 (Linden Avenue) and BN02 (Ash Avenue) (see Figure 2.2 for profile line locations) were extracted from the topographic grids to make seasonal and annual change calculations (Figure 3.5 and Table 3.2). BN02 showed greater variability but was also strongly affected by the winter beach berm activity of the February 2007 survey. This analysis shows that seasonal changes exceed the short-term annual signal, with a seasonal range of ~ +61 to -62 m^3/m of profile change at BN02, and an annual change of ~ 0 to 44 m^3/m. BCN10 showed seasonal changes that ranged from ~ +32 to -23 m^3/m and an annual change of only +9 to 13 m^3/m. The short-term annual signal is moderate beach accretion. The expected winter profile loss and summer profile gain is observed, with local vertical profile changes up to 2 m.

Beach Morphology Changes

Figures 3.6-3.8 and Table 3.3 show the seasonal and annual beach morphology changes. As with the BEACON profile lines, the seasonal variation generally exceeds the annual change. For the common survey areas, seasonal beach volume varies by +/- 60,000 m^3 (~ 23 m^3/m), with mean elevation changes that approach 0.5 m for the entire beach. The annual signal is one of accretion, with a fall and winter rate of ~ +20,000 m^3 and +38,000 m^3 (5 and 18 m^3/m), respectively. The City of Carpinteria Beach, between Ash Ave. and Linden Ave., shows more extreme seasonal variation and annual change. Seasonal changes range between +50 and -43 m^3/m, while annual accretion is between 6 (fall rate, i.e. October 2005 to October 2006) and 34 m^3/m (winter rate, i.e. March 2006 to February 2007), though the latter was heavily influenced by winter 2007 beach berm activities. Along the entire study area the largest winter erosion signal is just east (downdrift) of the revetment, near Ash Avenue.

Seasonal Beach Width and Shoreline Changes

Based on the resulting topographic grids created from the seasonal surveys from October 2005 to February 2007, the beach width changes are shown in Figure 3.9. Between October 2005 and March 2006, beach widths narrowed by an average of ~ 20 m. The highest beach width changes occurred on the City beach adjacent to the end of the structure with erosion reaching almost 40 m at the most eroded point and around 30 m immediately adjacent to the structure. The peak at transect 781 is found at the volleyball court near the east end of the City of Carpinteria state beach and the entrance to Carpinteria Creek at Transect 793; both features influence the amount of change seen at those locations. The beach width changes between March and October 2006 show that the summer beach recovery is almost a mirror image of the winter erosion. The subtle differences occur primarily in front of the revetment (transects 759-770) where the recovery in October is slightly less than the winter erosion. Seasonal changes between the October 2006 and February 2007 are disguised in part by the construction of the winter berm in front of the City of Carpinteria that was still in existence at the time of the February survey. Nevertheless, it is apparent that the location of maximum erosion occurs near the end of the revetment with maximum MSL changes reaching about 20 m of retreat.

Nearshore Bathymetry

Individual plots of profile change are included in Appendix A. The cross-shore profiles show some seasonal changes in water depths less than 5 m, but indicate very little elevation change offshore, which is a testament to survey precision as well as low sediment transport rates. Seasonal changes in shallow water show increased sediment nearshore in the spring. This is likely a result of sand moving off of the beach onto the nearshore as a result of winter storms, and moving back onshore during summer months. Alongshore lines 37-38 (Figure A9) show that seasonal changes are greatest in water depths less than 2 m (NAVD88) and almost all significant seasonal change occurs in depths less than 5 m.

There are some small offshore bars evident in profiles 7, 8 and 12 through 16 (Figures Appendix A.2-3), which are on the order of 1 m in height. The bi-annual CPS surveys did not capture any seasonal migration of these bars. Profiles 16 through 28 (Figures Appendix A.4-7) show evidence of an offshore reef in water depths between 7 and 10 meters. Many of these profiles have sections of missing data because kelp was often very thick in this region, and the echosounder cannot effectively penetrate kelp beds. Figure 3.10 shows a gridded surface of mean elevation over the survey area, which was generated by averaging individual 2-dimensional

gridded surfaces from each survey. The individual surfaces were created from profile data in Matlab© using triangle-based, weighted linear interpolation.

Discussion

Seasonal volume changes were twice as great along the City beach than the rest of the Carpinteria shoreline (e.g. max of 50 m^3/m vs. 23 m^3/m; Table 3.3). Further, volume change, profile change, shoreline change, and beach width all indicate that winter erosion for the entire Carpinteria shoreline peaks just east of the revetment near Ash Avenue, making this area the most susceptible to winter storm waves and flooding. This area is also the most developed part of the shoreline, and thus by far the most vulnerable to storm damage. This peak in erosion is likely due to the classic end around effects from the structure, which cause acceleration of longshore currents and increased sediment suspension and thus removal of sediment in front of the structure. When this transport rate drops further downdrift (i.e. in front of the State Park), the beach behaves more uniformly.

The seasonal beach width change pattern is relatively uniform across the Carpinteria coastline averaging about 20 m of retreat and recovery with intensification in changes adjacent to the revetment. This is relatively consistent with Bailard's (1982) finding of a ~21 meters (68 feet) cyclic seasonal changes between the winter/summer seasons. The beach berm that was still present during the February 2007 survey, and the relatively low energy nature of the two surveyed winters, hinder a better understanding of seasonal changes. However, the overall seasonal pattern seems to be nearly uniform retreat along the Carpinteria coastline of about 20 meters. This seasonal retreat pattern differs from the El Niño storm response rotational pattern seen in the beach widths (Figure 2.12). During an El Niño storm, the beaches erode at a far higher rate in the west and accrete in the east.

Nearshore bathymetry work shows that most cross-shore sediment transport is restricted to depths of < 5 m, owing to the relatively mild wave climate in this region, but also the relatively mild winter conditions during this study. A more substantial winter would certainly move the observed depth of closure further offshore.

Conclusions

- The Carpinteria shoreline responds in the typical seasonal pattern, with accretion in the summer and erosion in the winter of ~60,000 m^3 of sediment.
- Seasonal beach width changes show relatively uniform erosion across the Carpinteria shoreline of around 20 m during the winter surveys and a near mirror image of accretion during the summer recovery period
- The City of Carpinteria Beach is more variable than the rest of the beach, with up to 50 m^3/m of seasonal volume change, as opposed to a mean seasonal maximum change of 23 m^3/m for the rest of the study area.
- Winter erosion peaks adjacent to the east end revetment on the City of Carpinteria beach, which is reflected in the analysis of shoreline position, beach width, volume change and profile change.
- Seasonal change exceeds the observed short-term annual signal.
- Significant seasonal changes in nearshore profiles are restricted to depths < 5 m, and are reflected by patterns of accretion in spring surveys and erosion in fall surveys. The beach shows the mirror opposite pattern.

References

Bailard, J., and Jenkins, S.A., 1982. City of Carpinteria Beach Erosion and Pier Study. Final Report to the City of Carpinteria. Bailard/Jenkins Consultants. April 1982. 292 pp.

MacMahan, J., 2001. Hydrographic surveying from a personal watercraft. Journal of Surveying Engineering, v. 127, no.1, p. 12-24.

Magellan Navigation, Inc., 2006. Z-Extreme Survey System Data Sheet, http://pro.magellangps.com/en/

National Oceanic and Atmospheric Administration (NOAA), 2007a. National Data Buoy Center: Silver Spring, Maryland, http://www.ndbc.noaa.gov/

National Oceanic and Atmospheric Administration (NOAA), 2007b. Tides and Currents, Center for Operational Products and Services, Silver Spring, Maryland, http://tidesandcurrents.noaa.gov/station_info.shtml?stn=9411340%20Santa%20Barbara,%20CA

Ruggiero, P., Kaminsky, G.M., Gelfenbaum, G. and Voigt, B., 2005. Seasonal to interannual morphodynamics along a high-energy dissipative littoral cell. Journal of Coastal Research, v. 21, no. 3, p. 553-578.

Table 3.1. Topographic and nearshore bathymetric surveys and parameters for the Carpinteria Coastal Processes Study.

Lidar	# points	final grid resolution
10/15/2005	6,973,560	1 m
All Terrain Vehicles		
10/15/2005	10,073	2 m
3/25/2006	7,262	2 m
10/6/2006	11,016	2 m
2/16/2007	8,760	2 m
Coastal Profiling System		
10/15/2005	84,975	50 m
3/25/2006	266,378	50 m
10/6/2006	97,197	50 m
2/16/2007	116,184	50 m

Table 3.2. Profile changes (m^3/m) for the historical BEACON profiles.

Seasonal	**BCN10**	**BN02**
Oct05 to Mar06	-22.6	-61.9
Mar06 to Oct06	31.7	61.3
Oct06 to Feb07	-20.0	-12.9
Annual		
Oct05 to Oct06	8.7	-0.2
Mar06 to Feb07	13.3	44.4

Table 3.3. Volume changes from the ATV topographic surveys. Change data is calculated based on the common survey area between the two surveys being analyzed.

Entire Beach

Seasonal	Mean Elevation Change (m)	Surface Area (m^2)	Volume Change (m^3)	Change m^3/m
Oct05 to Mar06	-0.49	121,252	-59,413	-22
Mar06 to Oct06	0.43	141,632	60,902	23
Oct06 to Feb07	-0.21	176,496	-37,064	-11
Annual				
Oct05 to Oct06	0.12	165,663	19,880	5
Mar06 to Feb07	0.27	139,589	37,689	18

City Beach

Seasonal	Mean Elevation Change (m)	Surface Area (m^2)	Volume Change (m^3)	Change m^3/m
Oct05 to Mar06	-0.61	28,663	-17,484	-43
Mar06 to Oct06	0.66	30,856	20,365	50
Oct06 to Feb07	-0.21	30,471	-6,399	-16
Annual				
Oct05 to Oct06	0.08	28,636	2,291	6
Mar06 to Feb07	0.40	34,742	13,897	34

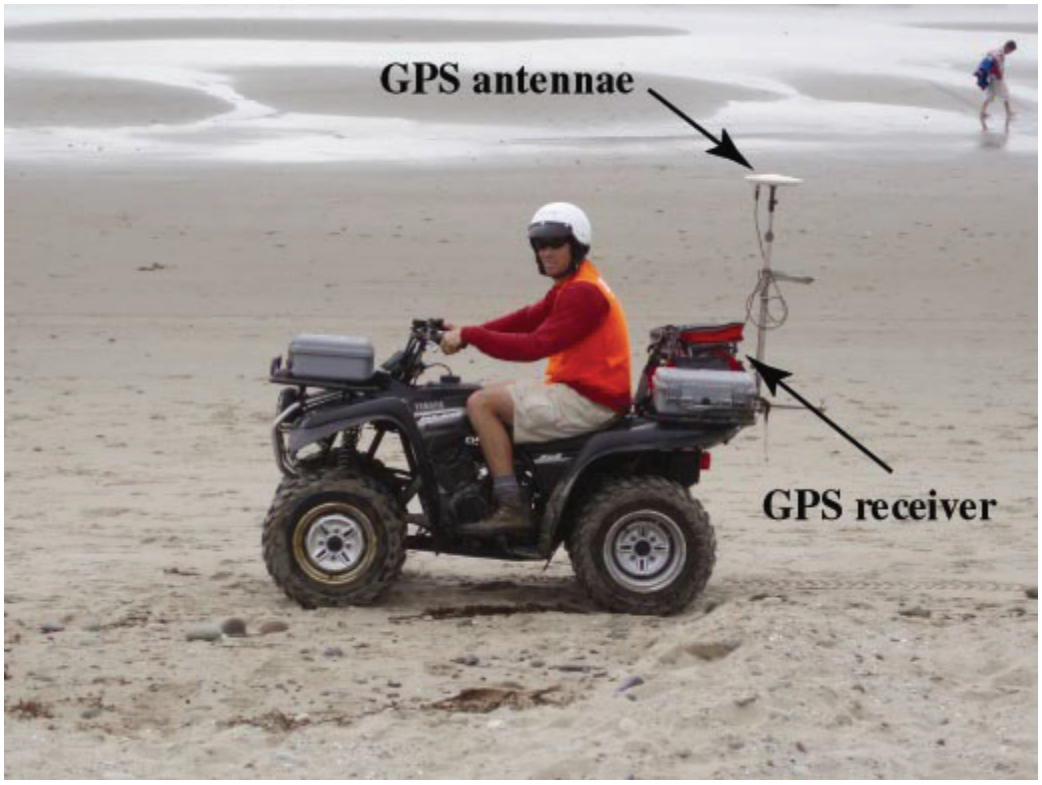

Figure 3.1. ATV set up for conducting topographic beach surveys using Differential GPS.

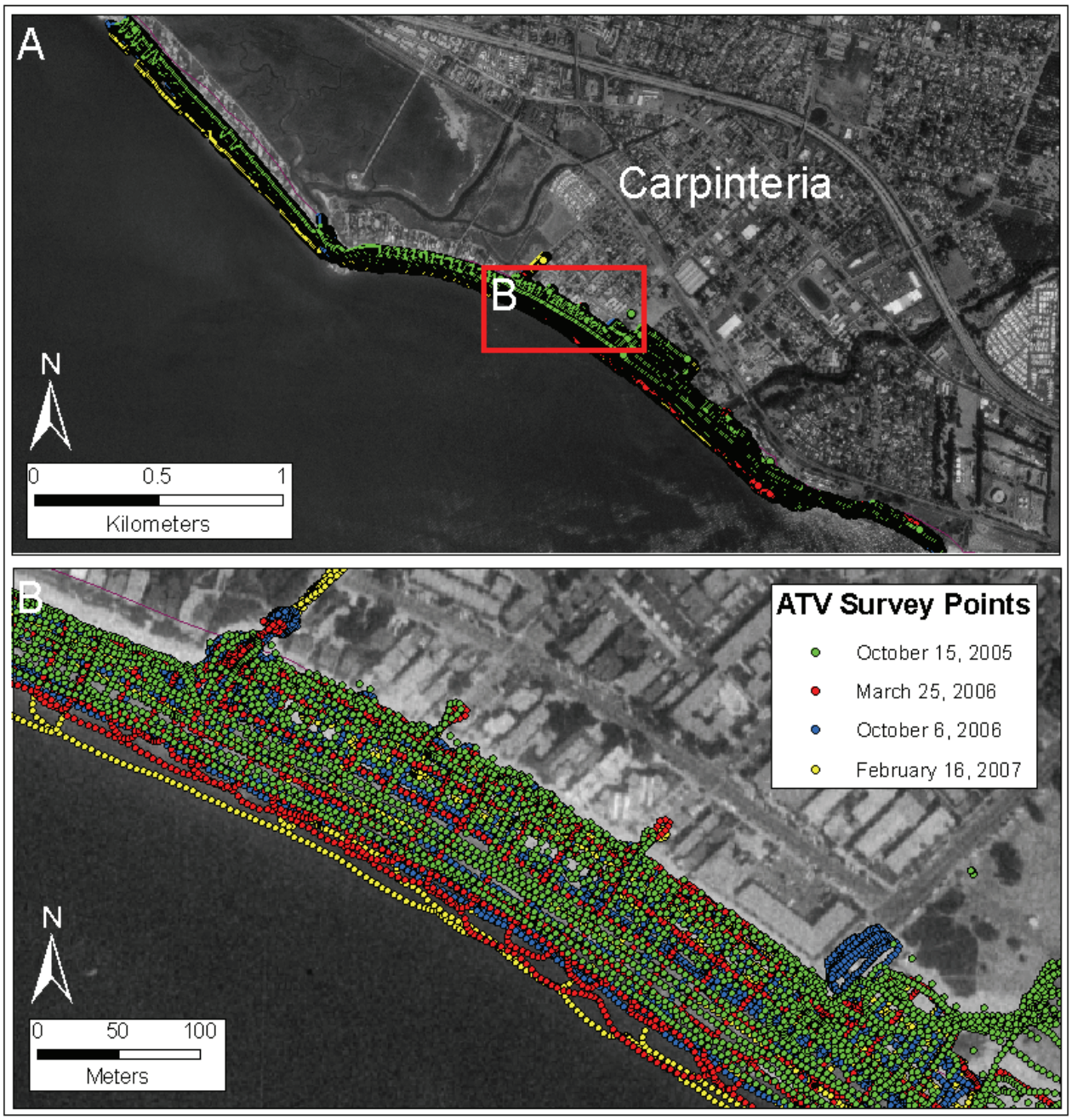

Figure 3.2. Survey points collected by ATVs at Carpinteria for A) entire survey area and B) focus study area, between Ash Avenue and Linden Avenue.

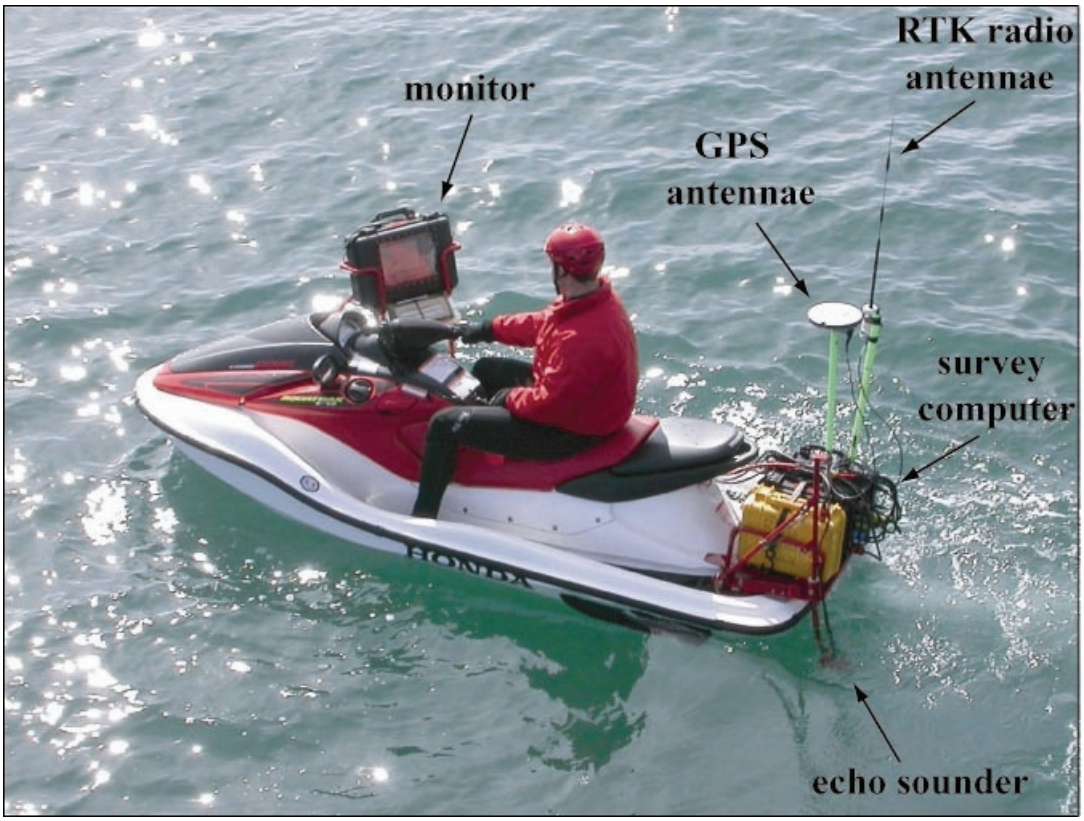

Figure 3.3 Coastal Profiling System in action.

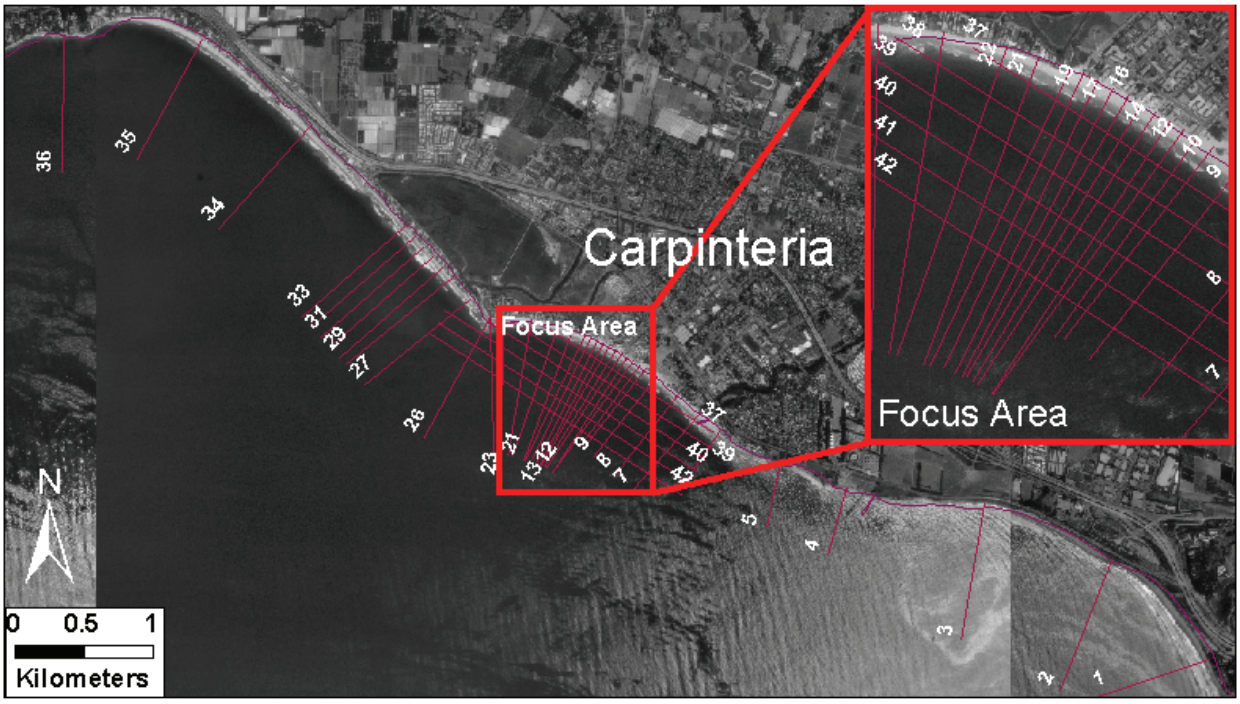

Figure 3.4. CPS profile locations. Profile data is presented in the Appendix.

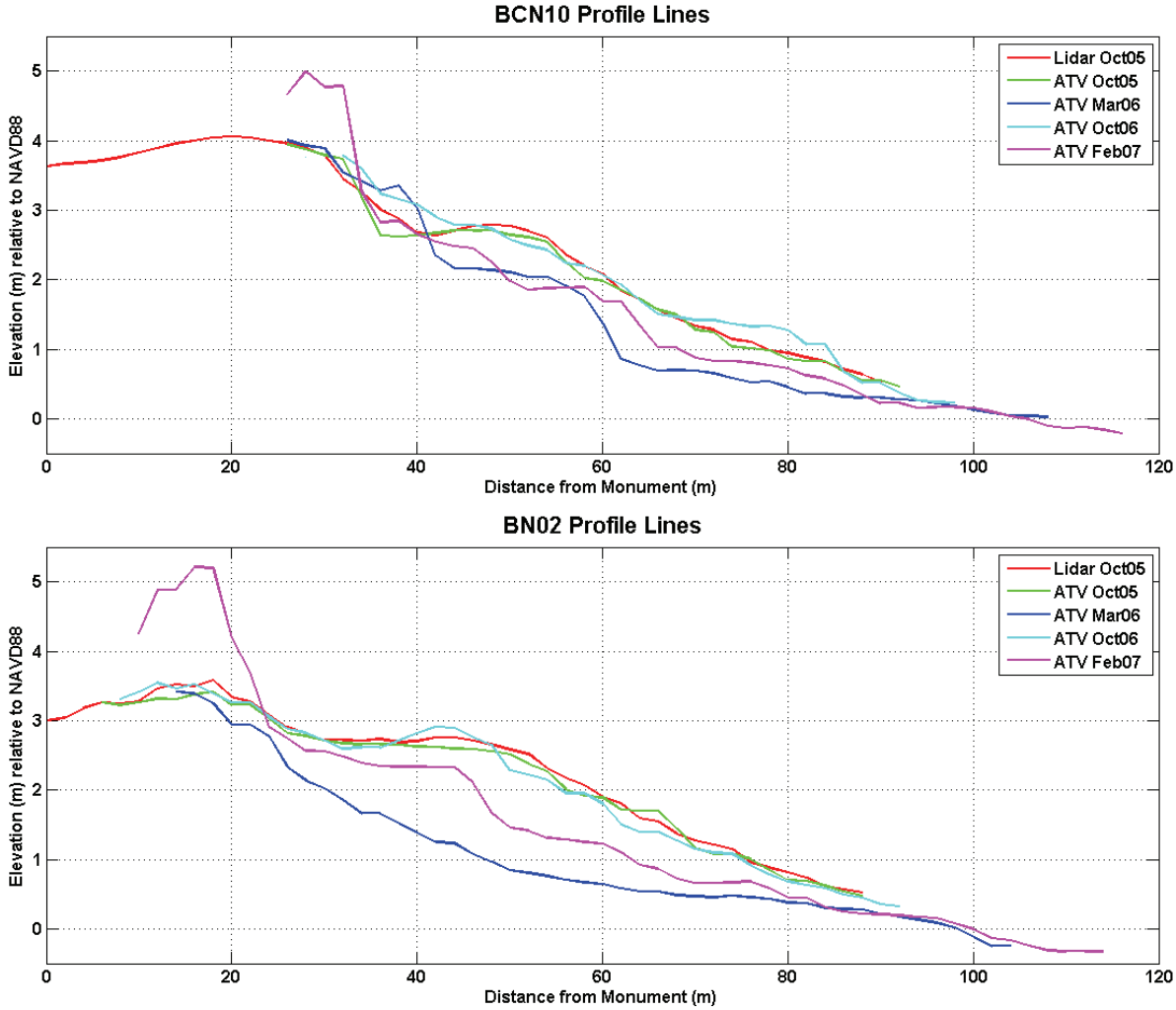

Figure 3.5. Seasonal beach profile changes for the two BEACON profiles (see Figure 2.2 for profile locations).

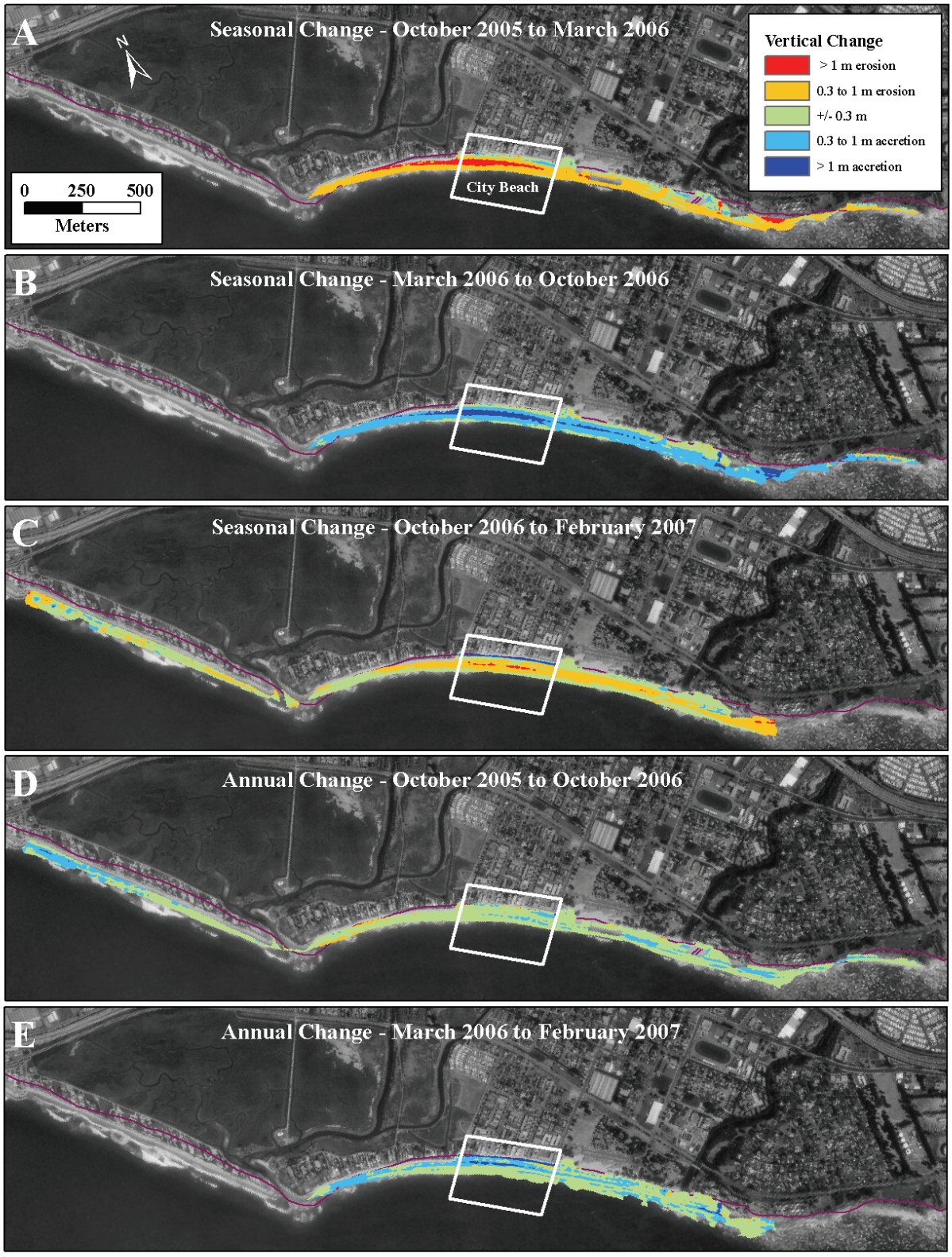

Figure 3.6. Seasonal (A-C) and annual (D-E) changes along the Carpinteria shoreline.

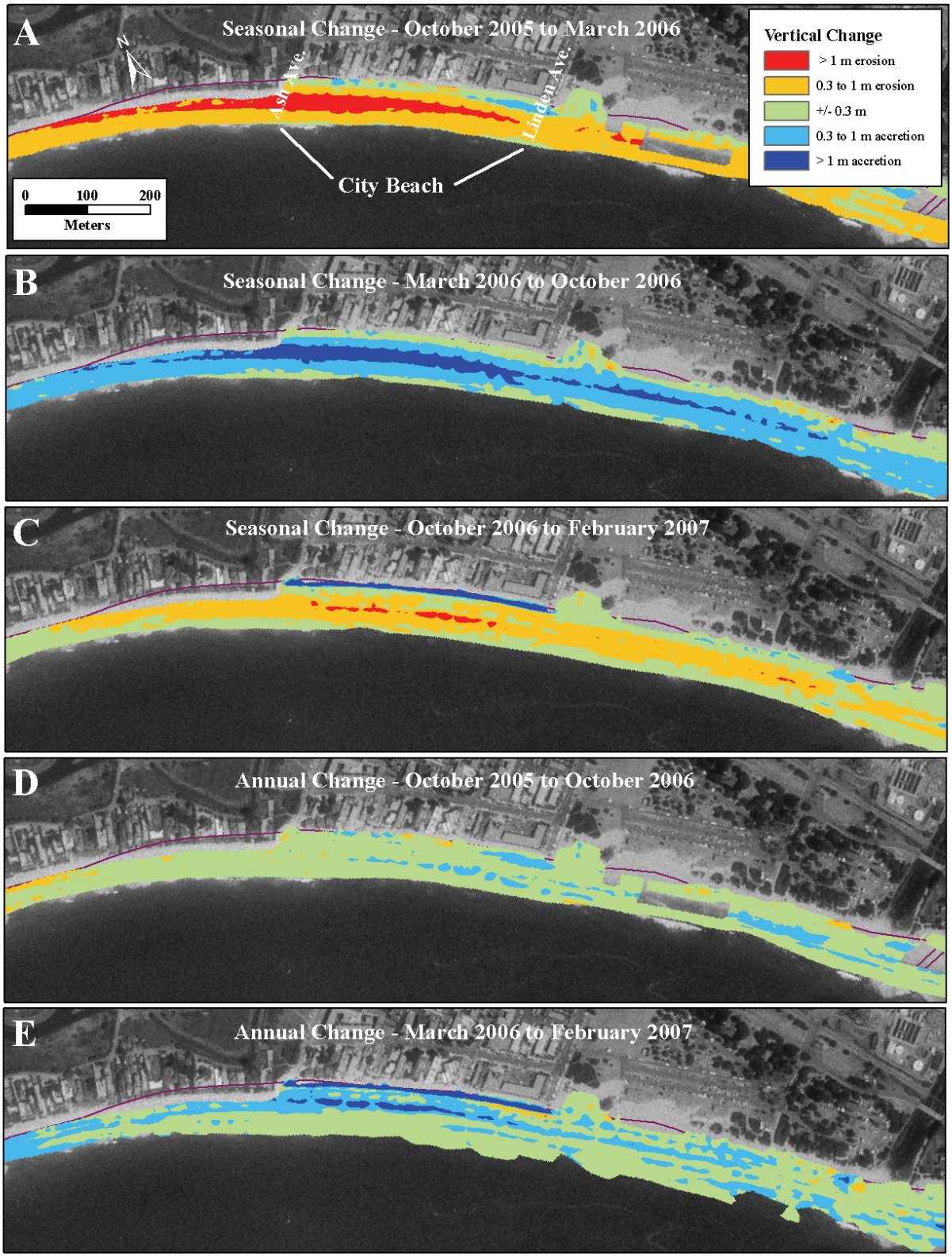

Figure 3.7. Seasonal (A-C) and annual (D-E) changes for the City of Carpinteria beach.

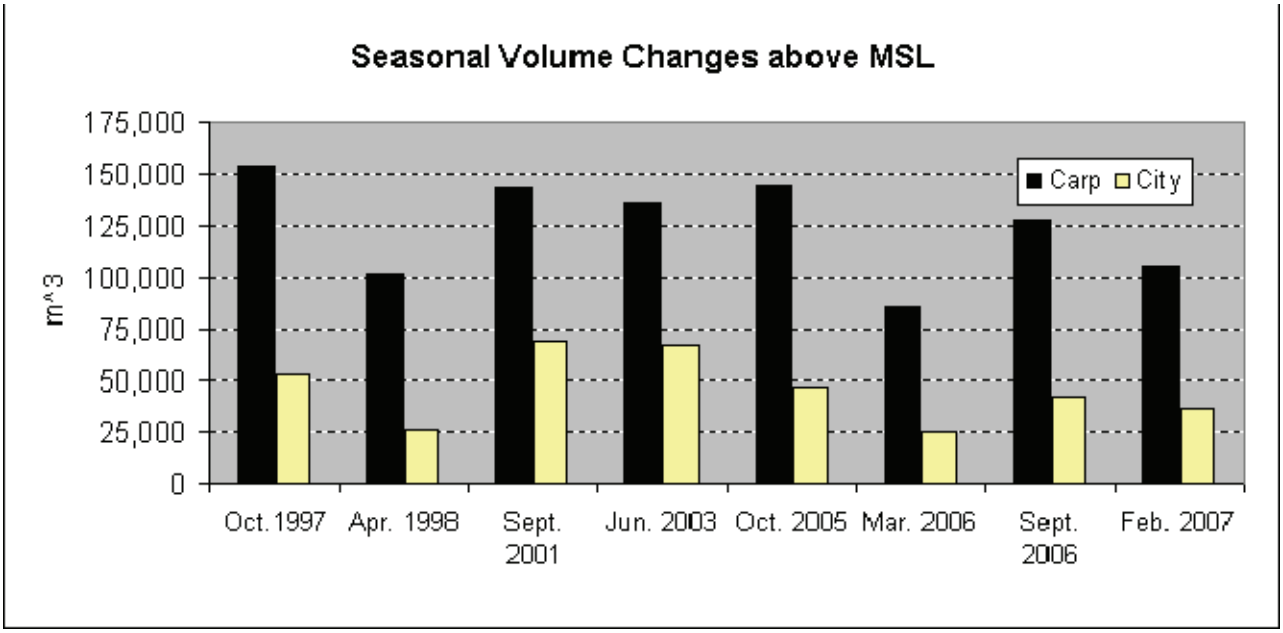

Figure 3.8. Seasonal changes in beach volume above MSL for Carpinteria and the City of Carpinteria (see volume calculation methods in Chapter 2). Note the October 2005 Lidar survey was used is in this analysis.

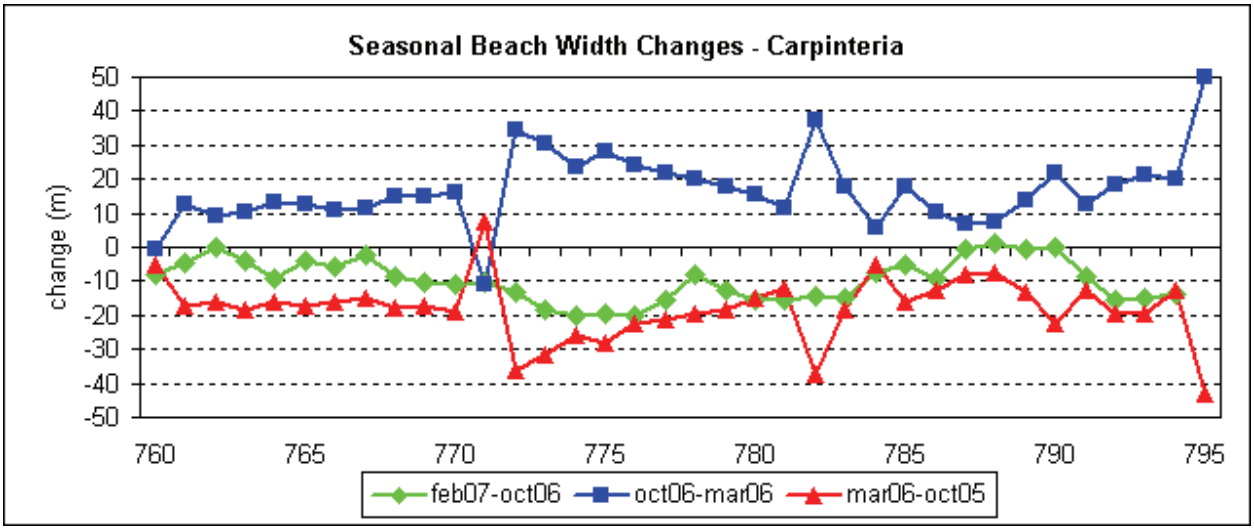

Figure 3.9. Seasonal beach width changes for the Carpinteria coastline. City Beach is located between transects 771-779. Shoreline armoring (revetment) occurs from transect 759 to 770.

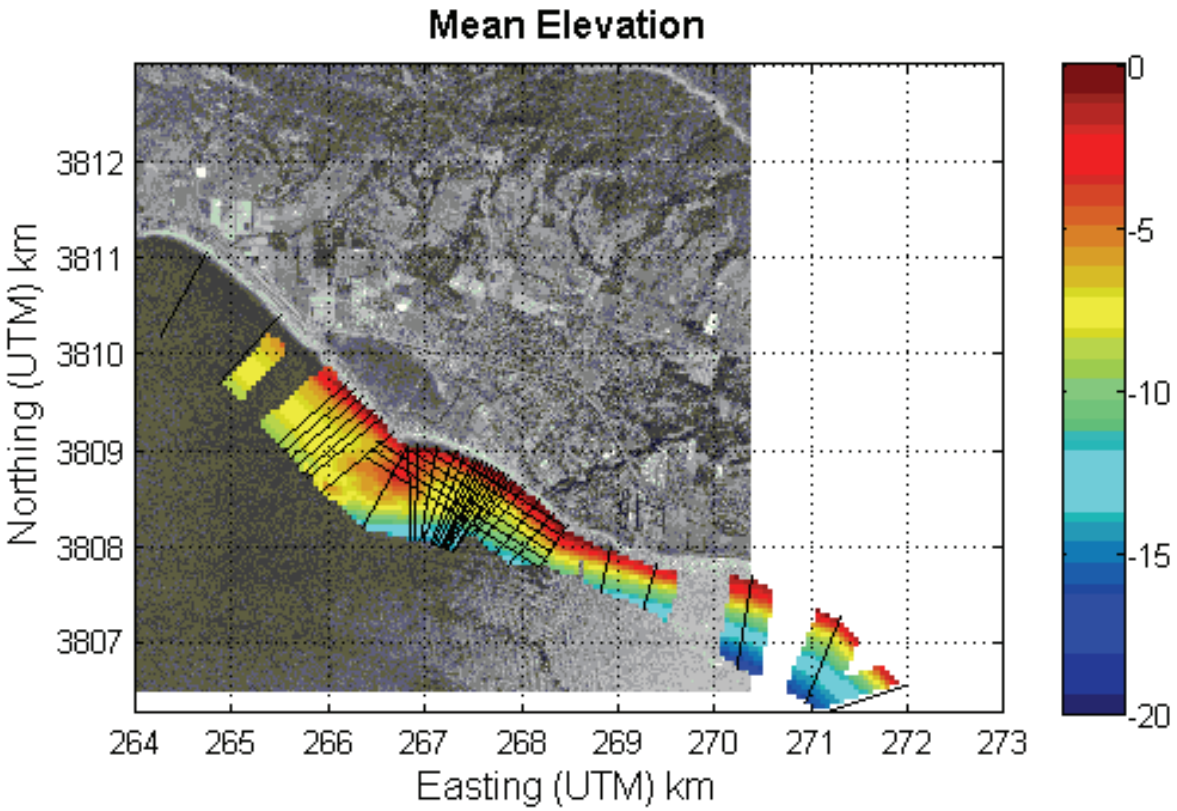

Figure 3.10. Gridded surface of mean elevation determined from four seasonal surveys with CPS profile lines shown in black.

Chapter 4- Sediment Grain-Size Analysis

By Neomi Mustain, David L. Revell and Patrick L. Barnard

Introduction

Most of the beaches of the Santa Barbara littoral cell, from Point Conception to Point Mugu, are naturally narrow (Flick, 1993; Wiegel, 1994), and the Carpinteria area is no exception. In addition, studies suggest that the beaches of this cell may also be narrowing in response to human activities (Runyan and Griggs, 2003; Willis and Griggs, 2003; Revell and Griggs, 2006). Because the beaches of California are a valuable natural resource, it is important for coastal managers to consider approaches to restore or expand existing beaches.

One possible way to restore and widen a beach is through direct beach nourishment. For a nourishment project to be successful, however, suitable sediment with a grain size equivalent to or slightly coarser than sand found naturally on the beach must be used (National Research Council, 1995; Dean, 2002; U.S. Army Corps of Engineers, 2002). In this study, the Carpinteria shoreline was examined to determine seasonal and alongshore grain size distributions and the sediment size that is stable under natural conditions. Surficial sediments throughout the nearshore inner shelf (i.e. out to 20 m water depth) were also sampled to determine if beach compatible sediment exists nearby.

Traditional methods of grain size analysis, including sieving or settling, require considerable time to process samples. As an alternative, the relatively new but well tested method of the USGS-developed digital bed sediment Eyeball camera and autocorrelation algorithms (Rubin 2004; 2006; Barnard and others, 2007; Mustain and others, 2007) were used. The speed and efficiency of both the collection process and grain size determination technique allowed for an unprecedented amount of data, over 300 sediment samples (~ 270 onshore and ~ 50 offshore), to be gathered quickly from the study area, thus allowing for a rapid assessment of the broad compatibility of nearshore inner shelf and onshore sediments in the region. This chapter describes just a portion of a much broader grain size distribution study for the entire Santa Barbara littoral cell, funded by BEACON (report release late 2008), and detailed in Mustain (2007).

Methods

Sampling Scheme

The broader field survey was designed to collect samples along a cross-shore profile from the beach face and the nearshore at 5, 10 and 20 m water depth (i.e. within the economic dredging limit), with transects spaced at least every kilometer alongshore. To compare seasonal grain size variations, winter (March 2006 and February 2007) and summer (October 2006), beach samples were also collected at a higher spatial resolution along the Carpinteria shoreline (Figure 4.1).

Eyeball Methods

Two different Eyeball camera systems were used to collect digital samples (Figure 4.2). Beach face samples were collected with the ‘Beachball’ camera, a 5-megapixel digital camera encased in a waterproof housing (Rubin, 2006; Figure 4.2, top). To sample the beach, the camera is placed flush against the sediment, which is illuminated by a ring of LED lights (Figure 4.3,

top). Camera settings such as aperture, shutter speed, zoom, focus, and pixel resolution of the image are held constant. Nearshore samples were collected with the underwater Eyeball version, the 'Flying Eyeball', which is a video camera illuminated by LED lights encased in a wrecking ball (Rubin, 2006; Figure 4.2, bottom). Live video is reviewed on deck while the instrument is repeatedly raised and lowered to the seafloor to collect digital video samples. The clearest frames of video are then captured as still images and processed for grain size (Figure 4.3, bottom). For both systems, multiple images, typically 3-5, are taken at each location and later averaged to produce a mean grain size for that station location. Images that do not pass quality control checks (e.g. overexposure, out of focus, coarse lag deposit, uneven sediment surface, air bubbles, etc.) are not included.

Images were processed by running a Matlab® script that uses a spatial autocorrelation algorithm developed by Rubin (2004). This algorithm determines the correlation (i.e. as measured by pixel intensities) between a pixel and subsequent pixels at increasing offset distances. Grain size is then interpolated by comparing the spatial autocorrelation result to a calibration matrix (Figure 4.4). The calibration matrix contains spatial autocorrelation results of calibrated sample images produced by imaging ¼ phi-interval sieved sediments collected from the study area with the same equipment and camera settings as used in the field. In addition, for Flying Eyeball samples, point-counted images were also used to produce the calibration matrix. Each calibration matrix created is valid only for sediment of similar size, shape and mineralogy as the sediment initially sieved and imaged. This technique was tested extensively by Barnard and others (2007), who showed that through a series of field tests on a range of beach types, the autocorrelation method was able to predict the mean and median grain size with a minimum of 96% accuracy.

To validate grain sizes determined from the autocorrelation method at Carpinteria, results were compared to mean grain size determined from point counting, or calculating the mean of an image by hand-measuring the size of 100 grains in the image. A high correlation (Beachball r^2=0.94 and Flying Eyeball r^2=0.93) of samples is evidence that the autocorrelation method was able to successfully determine grain size of an image accurately, with only 1% error (Figure 4.5).

However, when using the Beachball camera, a systematic bias was found: the autocorrelation method consistently slightly overestimated grain size as determined from point counting. This bias could have resulted from improper sieving techniques. For example, not enough time was allowed for all of the grains to settle into the proper sieve, or possibly small grains were caught in larger sieves, therefore misrepresenting sediment size when images for the calibration matrix were taken. To correct for this bias, a correction (i.e. solving for the equation $y = 1.157 x – 0.0151$) was applied to Beachball autocorrelation results (Figure 4.5). No correction was applied to the Flying Eyeball results, since no systematic bias resulted (i.e. because point counted images, in addition to sieved sediments, were also used to produce the calibration matrix).

The autocorrelation method is limited by pixel resolution, especially when using the Flying Eyeball: once grains become very small (e.g. $\leq$ 2-3 pixels) clusters or flocs of small grains begin to look (i.e. in terms of correlation) like larger grains. As a result, when nearshore grain size is less than 0.09 or 0.10 mm, the ability to accurately determine grain size by the autocorrelation method is diminished. Therefore, the finest grain sizes in the nearshore should only be regarded as an approximation. However, the 0.10 mm limit in the nearshore is not a significant problem for this study because the aim of offshore sampling is to determine if beach compatible material exists, and suitable sediment for Carpinteria is definitely coarser than 0.125 mm, making the Flying Eyeball results adequate and this study applicable.

Following the grain size sample processing, the seasonal distribution of all subaerial beach samples was examined. To evaluate the spatial variability of the various grain sizes on the subaerial beach, all grain size samples for each survey were gridded using an inverse distance weighting function in ESRI ArcGIS©.

Results

Beach Sampling

The mean size of the active winter/summer beach at Carpinteria is 0.28 mm. Mean grain sizes of summer beach samples were smaller than winter beach samples throughout the Carpinteria shoreline (Winter 2006 = 0.32 mm, Summer 2006 = 0.26 mm, Winter 2007 = 0.29 mm; Figure 4.6). Mean grain size fluctuated between medium and fine sand, but locally could vary by up to a factor of two between summer and winter samples (minimum = 0.18 mm, maximum = 0.5 mm). During the summer, grain size varied less alongshore than during the winter. The coarsest grain sizes found along the beach were found during winter surveys (2006 and 2007), around Transect #773. This area corresponds to the area of maximum erosion just downdrift of the rip rap revetment (e.g. see Figure 3.6a).

To analyze natural beach face variability on a small scale, 50 Beachball images were taken within a square meter at 9 different locations throughout the Santa Barbara littoral cell, including Carpinteria during February 2007. Figure 4.7 shows that there can be considerable variation (grain size can vary by a factor of 2) within a small area. The results of this analysis suggest that in future work, at least 7 to 10 images should be taken at each site to converge on the 'true' mean (Barnard and others, 2007). Despite local variations, seasonal measurements from February 2007 were compared to the analysis of 50 images within a square meter, also taken February 2007, to determine how well the beach face was represented by kilometer sampling. The three areas of intense sampling at Carpinteria were located 1 km apart and many seasonal measurements were in between. It was found that grain size did not vary significantly within a kilometer, at least not anymore than measurements within a square meter. Furthermore, seasonal summer sampling shows even less variability along the beach compared to winter sampling; thus even with local variability, kilometer alongshore sampling appears to have worked well to represent summer grain size throughout the broader study area.

The spatial distribution of sediment grain sizes shows a seasonal coarsening of sediments at the end of the winter (Figure 4.8). The sediment coarsening over the winter is not uniform along the entire study area, instead there appears to be some coarsening peaks that are co-located with the erosion hotspots seen at the end of the Sandyland Cove revetment near Ash Avenue (Figure 4.8a, c). During the summer, the sediments fine becoming relatively uniform across the study area (Figure 4.8b).

Nearshore Sampling

Figure 4.9 shows the results of the local nearshore surface sampling with the Flying Eyeball camera. From the 17 nearshore sample stations, the mean grain size exceeded 0.2 mm at only a single location, the 10 m station off Sand Point. Kelp growing on the hard bottom is visible immediately adjacent to this site (Figure 4.10). In addition it was noted in the cruise field notes that the Flying Eyeball had to be navigated through kelp to reach the seafloor at this location. As a result, the coarser deposit is likely only a thin deposit within a bedrock pocket and is therefore not considered a suitable borrow area for beach nourishment.

Discussion

Stable beach fill material, as determined by sediment grain size, is required for a successful beach nourishment project, because the grain size distribution of the fill will affect the rate that the fill is eroded from the beach, how the beach will respond to storms, and the slope of the nourished beach (U.S. Army Corps of Engineers, 2002). Stable fill material, or suitable sediment, should therefore be as coarse as, or coarser than sediment that is naturally found on the beach; finer sediment is considered unstable and is expected to be quickly winnowed out and carried offshore. The particular grain size definition of suitable sediment will vary alongshore from beach to beach, just as the native sediment composing beaches varies alongshore. As a general guideline, the Coastal Engineering Manual (CEM) suggests that if the median grain size on the native beach is 0.2 mm or coarser, then suitable sediment should have a median diameter within +/- 0.02 mm of the native sediment (U.S. Army Corps of Engineers, 2002). With a mean grain size of 0.28 mm along the Carpinteria Shoreline, and no nearshore surficial grain size > 0.2 mm, except on the reef offshore of Sand Point, the sampling in this study suggests that there are no proximal nearshore sediment sources for beach nourishment.

Sediments of previously identified borrow areas were also examined (Figure 4.11). Potential offshore deposits in the Carpinteria area were estimated to contain about 13 million m^3 of sediment in the most recent study (Noble Consultants, 1989), which reviewed, further investigated and revised all previously considered borrow areas (e.g. those of Field, 1974 and Dahlen, 1988). However, the report also indicates that most of the sediment is only marginally suitable (i.e. grain size ranging from 0.09 to 0.18 mm). Flying Eyeball surface samples agree, and in the Carpinteria area between 10 and 20 m depth, mean grain size ranged from 0.07 mm to 0.09 mm. In addition, one sample had a mean diameter of 0.24 mm, but is believed to be adjacent to exposed bedrock, thus implying thin sediment cover, and is probably not suitable for a borrow area.

The finest sand to remain on the beach (i.e. the littoral cell cut-off diameter or d_{10}) was found to be coarser than very fine-grained sand (0.125 mm). As a result, if sediments immediately offshore Carpinteria are used to nourish Carpinteria beaches, a significant portion can be expected to be easily lost back offshore. In addition, to ensure a successful project, a large overfill ratio would have to be used to compensate for nourishing with finer sediments. Furthermore, biological impacts of nourishing with fine sediment will also have to be investigated and considered. So in addition to the risks involved with nourishing with finer sediments, coastal managers will have to decide whether nourishment projects, which will have a large overfill ratio and thus large costs, are even economically justifiable.

The Eyeball cameras capture surface grain size well, as demonstrated by point counting, but the use of the cameras and the results of this study will be limited if sediments beneath the surface are not equivalent in size to those on the surface. However, grain size results determined from the Eyeball cameras in this study have been compared to grab samples and cores of other studies (Noble Consultants, 1989; Reid and others, 2006). From this analysis, results indicate that surface and subsurface sediments are comparable in the offshore. In addition, future box coring, in cooperation with the USGS, is planned for further confirmation of these results.

The seasonal coarsening in sediment grain size during the winter is consistent with other beaches in the Santa Barbara littoral cell (Mustain and others, 2007). However, the peak coarsening locations (Figures 4.8a, c) adjacent to the end of the revetment is co-located with the erosion hotspots seen in the El Niño storm event changes (Figure 2.12), and the seasonal beach width changes (Figure 3.9). This co-location of beach changes and sediment coarsening provides

evidence of accelerated longshore transport in front of the structure, with a transport reduction and subsequent deposition of the coarser material downdrift of the structure.

Conclusions

- Mean grain size for the Carpinteria shoreline averages 0.28 mm, but increases and is more variable alongshore in the winter.
- Locally, grain size can vary by a factor of two seasonally.
- Grain size peaks (coarser sediments) are co-located with the erosion hotspot immediately downdrift of the revetment at Ash Avenue.
- Together with previously collected cores, this current analysis confirms that coarser sediments suitable for beach nourishment do not exist in large quantities along the previously identified potential borrow areas offshore of Carpinteria.

References

Barnard, P.L., Rubin, D.M., Harney, J. and Mustain, N., 2007. Field test comparison of an autocorrelation technique for determining grain size using a digital beachball camera versus traditional methods. Sedimentary Geology, v. 201, no. 1-2, p. 180-195, http://dx.doi.org/10.1016/j.sedgeo.2007.05.016

Dahlen, M.Z., 1988. Seismic Stratigraphy of the Ventura Mainland Shelf, California: Late Quaternary History of Sedimentation and Tectonics. M.S. Thesis. University of Southern California, Los Angeles, CA. 147 pp.

Dean, R.G., 2002. Beach Nourishment: Theory and Practice. New Jersey: World Scientific.

Field, M.E., 1974. Preliminary "Quick Look" Report on Offshore Sand Resources of Southern California: Unpublished Report for Department of the Army, Coastal Engineering Research Center. Fort Belvoir, VA. 42 pp.

Flick, R.E., 1993. The myth and reality of Southern California Beaches. Shore & Beach, v. 61, no. 3, p. 3-13.

Mustain, Neomi, 2007. Grain size distribution of beach and nearshore sediments of the Santa Barbara Littoral Cell: Implications for Beach Nourishment. MS Thesis in Earth Sciences, University of California, Santa Cruz, 107 pp.

Mustain, N., Griggs, G. and Barnard, P.L., 2007. A rapid compatibility analysis of potential offshore sand sources for beaches of the Santa Barbara littoral cell. In: Kraus, N.C., Rosati, J.D. (eds.), Coastal Sediments '07, Proceedings of the 6th International Symposium on Coastal Engineering and Science of Coastal Sediment Processes, American Society of Civil Engineers, New Orleans, LA, Volume 3, p. 2501-2514

National Research Council, 1995. Beach Nourishment and Protection. National Academy Press, Washington, D.C., 334 pp.

Noble Consultants, 1989. Coastal Sand Management Plan Santa Barbara / Ventura County Coastline. Prepared for BEACON, Beach Erosion Authority for Control Operations and Nourishment, Santa Barbara, CA.

Reid, J.A., Reid, J.M., Jenkins, C.J., Zimmermann, M., Williams, S.J., and Field, M.E., 2006. usSEABED: Pacific Coast (California, Oregon, Washington) Offshore Surficial-sediment Data Release: U.S. Geological Survey Data Series 182. http://pubs.usgs.gov/ds/2006/182/.

Revell, D. L. and Griggs, G. B., 2006. Beach width and climate oscillations along Isla Vista, Santa Barbara, California. Shore & Beach, v. 74, no. 3, p. 8-16.
Rubin, D.M., 2004. A Simple Autocorrelation Algorithm for Determining Grain Size from Digital Images of Sediment. Journal of Sedimentary Research, V. 74, No. 1, p. 160-165.
Rubin, D.M., Chezar, H., Harney, J.N., Topping, D.J., Melis, T.S. and Sherwood, C.R., 2006. Underwater Microscope for Measuring Spatial and Temporal Changes in Bed-sediment Grain Size. U.S. Geological Survey. Open-file report 2006-1360, 15 pp.
Runyan, K.B. and Griggs, G.B., 2003. The effects of armoring seacliffs on the natural sand supply to the beaches of California. Journal of Coastal Research, v. 19, no. 2, p. 336-347.
U.S. Army Corps of Engineers, 2002. Chapter 4: Beach Fill Design. In: Coastal Engineering Manual-Part V. Vicksburg, Mississippi, 113 pp.
Wiegel, R.L., 1994. Ocean beach nourishment on the USA Pacific Coast. Shore & Beach, v. 62, no. 1, p. 11-36.
Willis, C.W. and Griggs, G.B., 2003. Reductions in fluvial sediment discharge by coastal dams in California and implications for beach sustainability. Journal of Geology, v. 111, no. 2, p. 167-182.

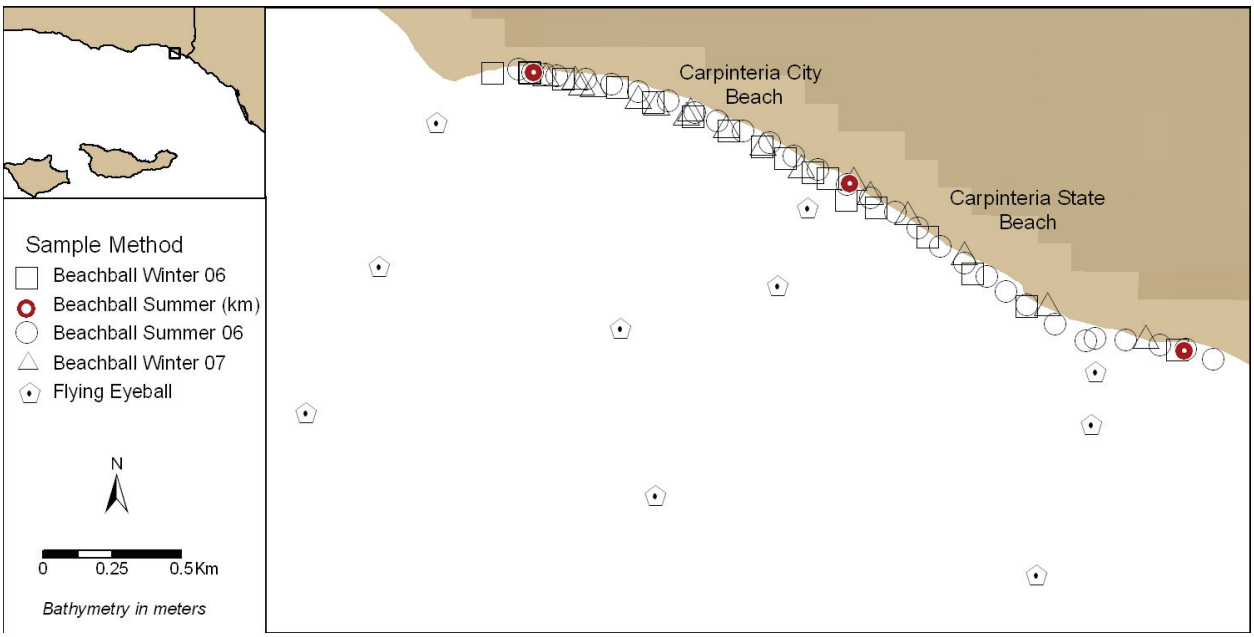

Figure 4.1. Locations of summer nearshore samples, summer kilometer spaced samples, and seasonal beach face samples collected at Carpinteria.

Figure 4.2. Top: Beachball camera: digital camera encased in waterproof housing. Bottom: Flying Eyeball: video camera encased in wrecking ball.

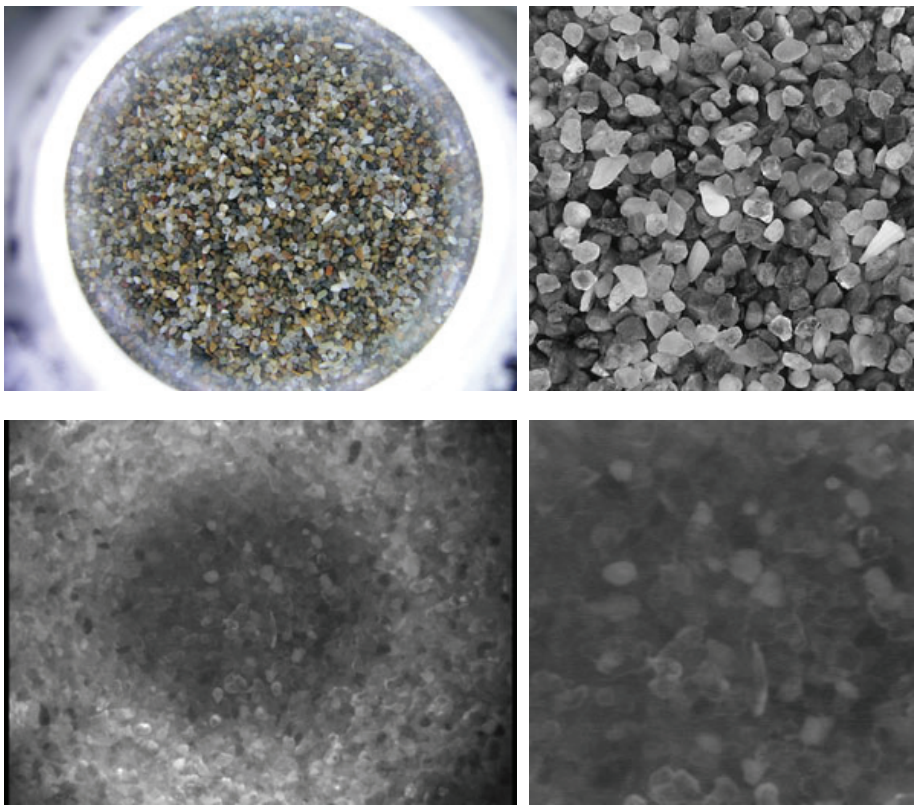

Figure 4.3. Top: Beachball image and processed image in grayscale, cropped from center (images have been rescaled). Bottom: Flying Eyeball image and processed image cropped from center (images have been rescaled).

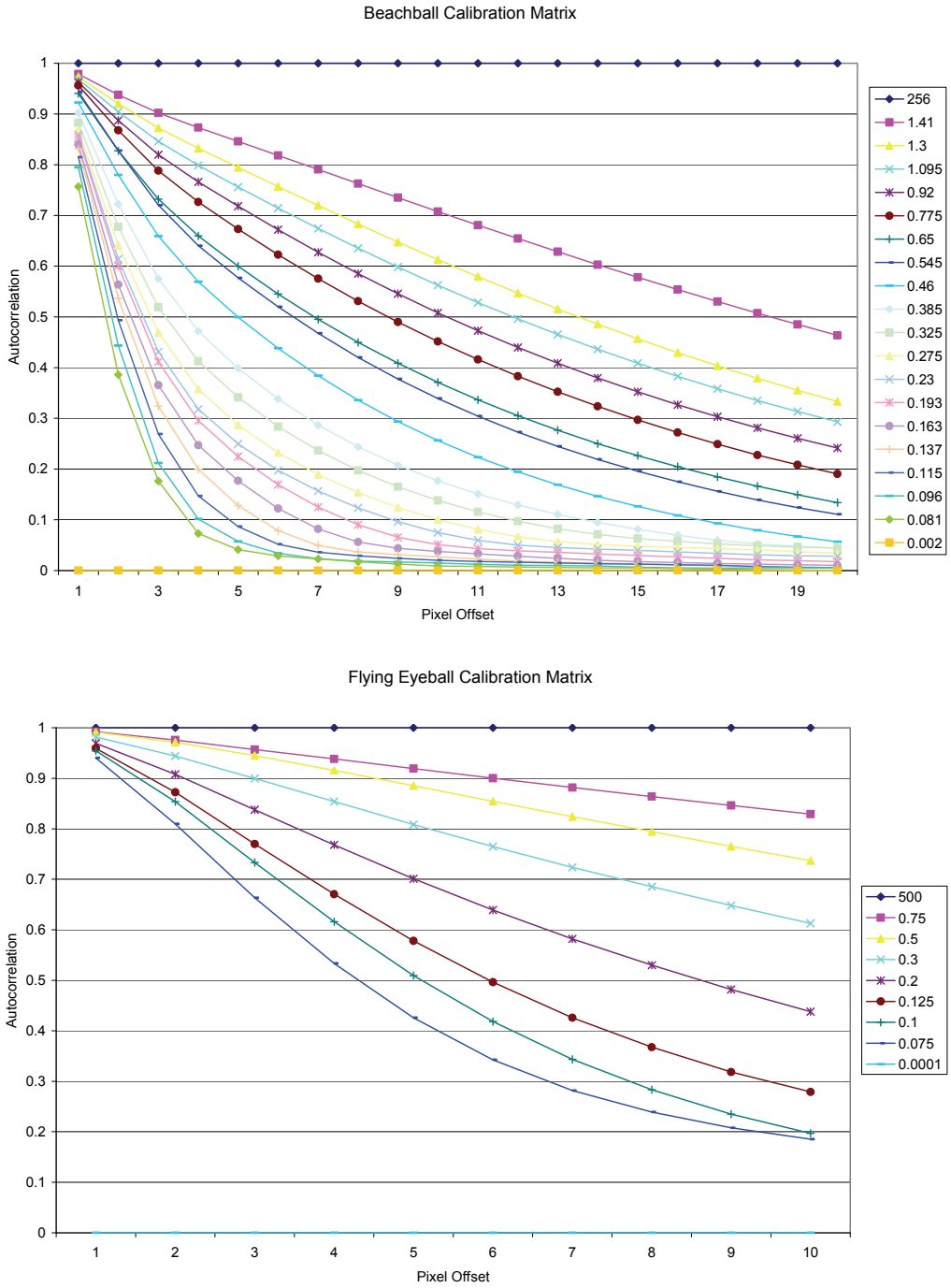

Figure 4.4. Beachball (top) and Flying Eyeball (bottom) calibration matrices, used to interpolate grain size in mm.

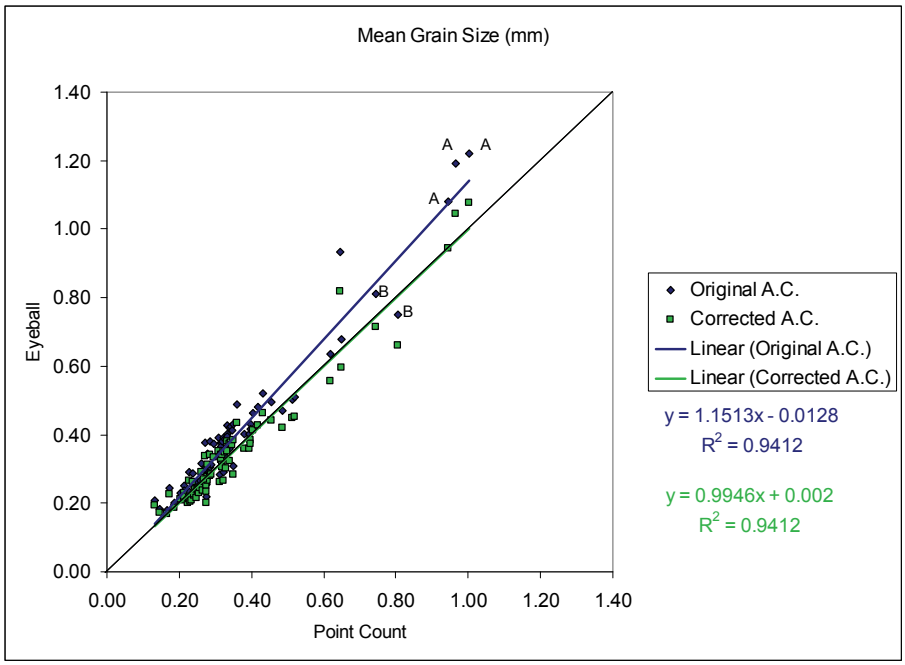

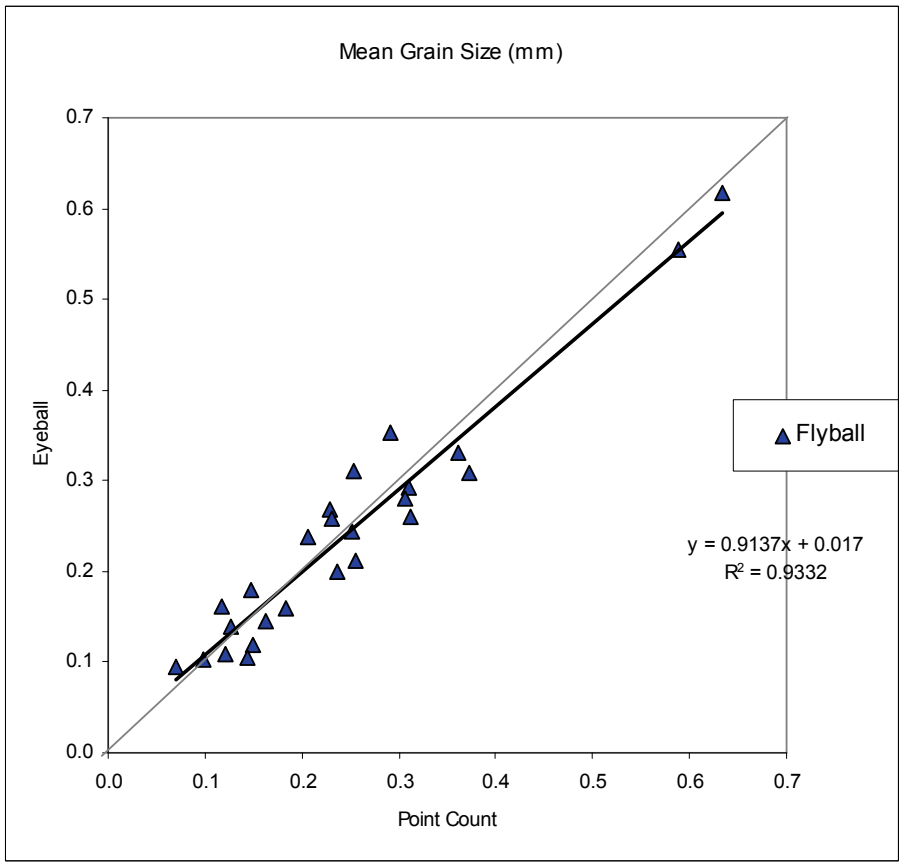

Figure 4.5. Top: Point counted Beachball grain size result vs. autocorrelation result: original and corrected (for systematic sieving bias). Bottom: Flying Eyeball point counted result vs. autocorrelation result.

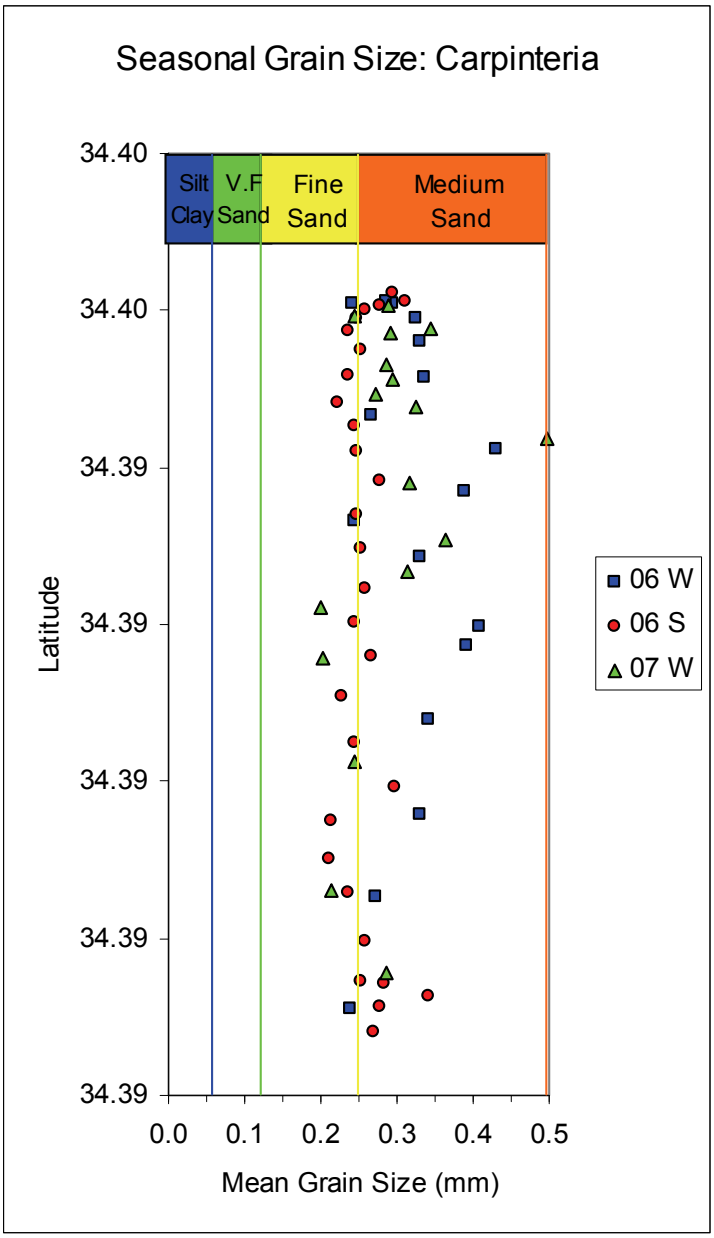

Figure 4.6. Seasonal mean grain size changes along the Carpinteria shoreline.

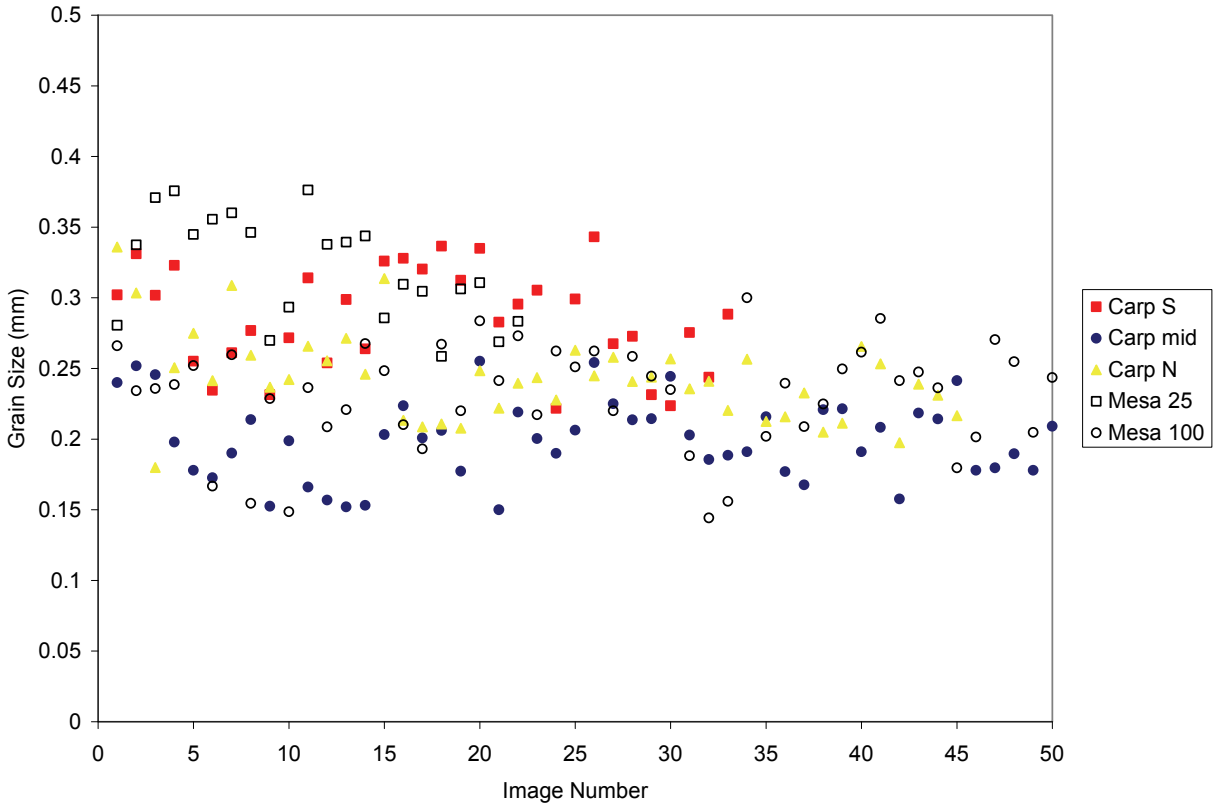

Figure 4.7. Mean grain size of ~50 Beachball beach face images takes in a square meter in February 2007.

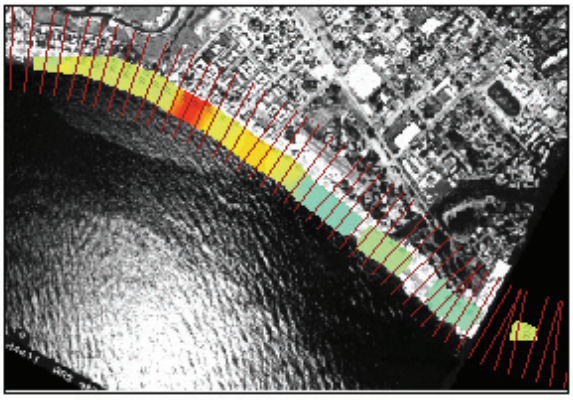

Winter 2006

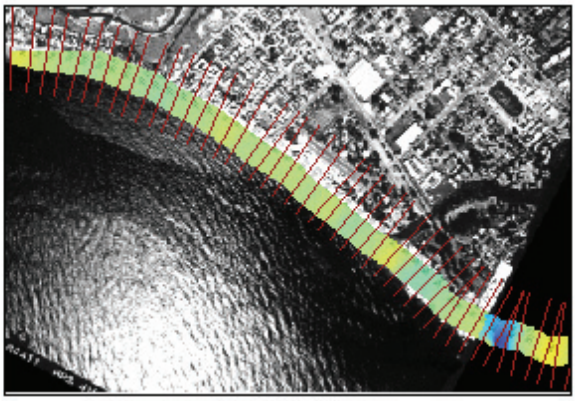

Summer 2006

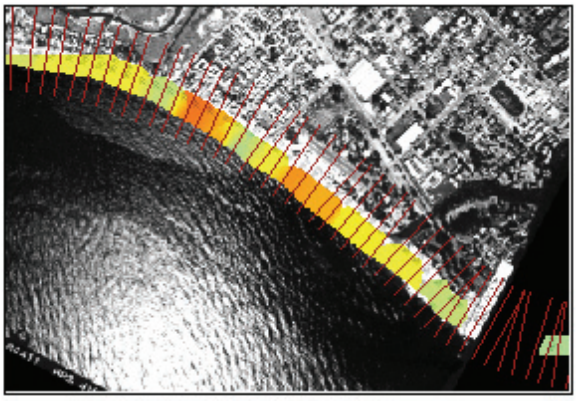

Winter 2007

Figure 4.8. Gridded sediment grain size samples. The hotter colors represent coarser grain materials while the cooler colors represent finer grained material. A) Winter 2006, B) Summer 2006, and C) Winter 2007. Note the coarsening of grain sizes at the end of the revetment near the Ash Avenue erosion hotspot.

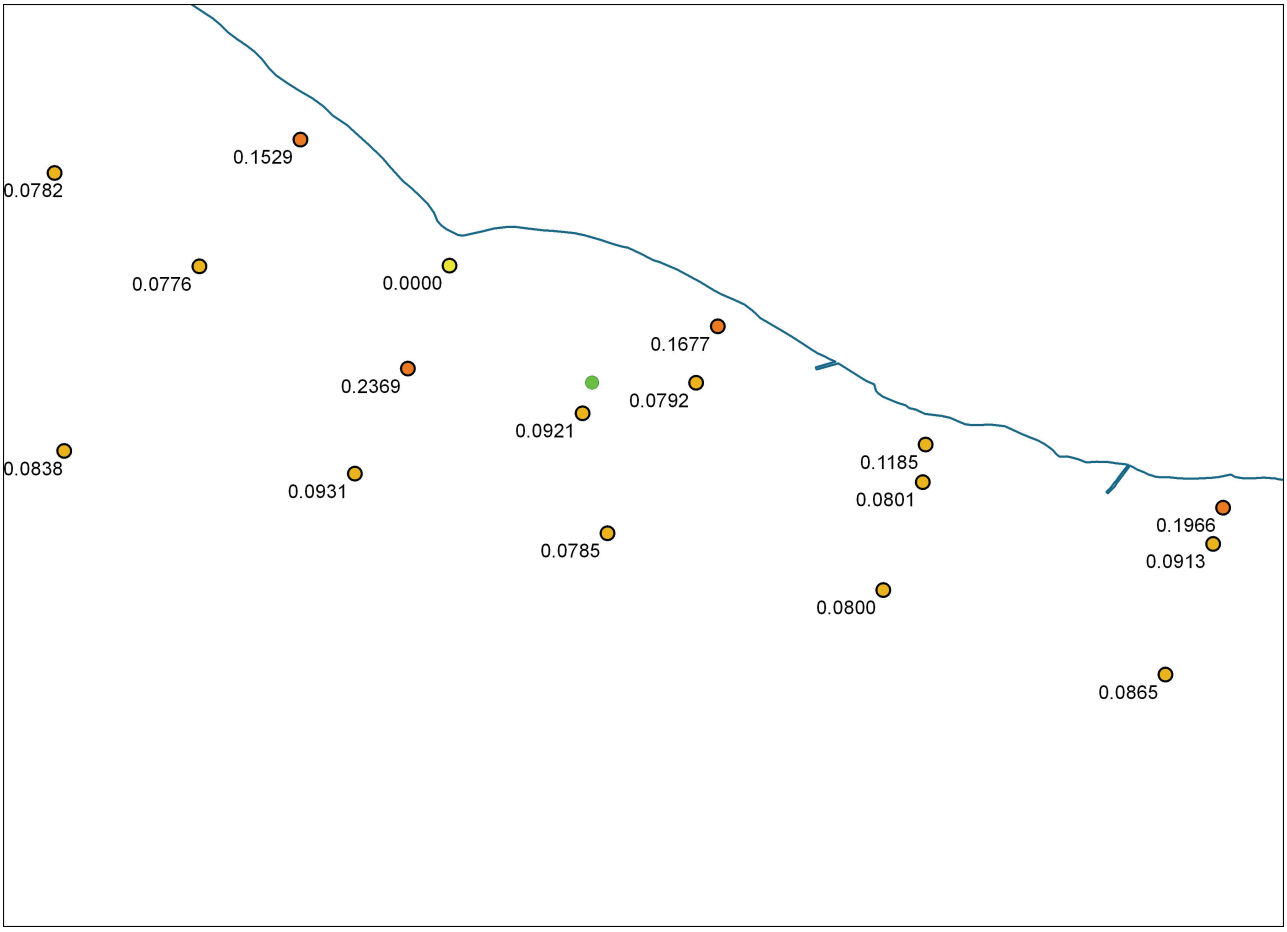

Figure 4.9. Map of surficial median grain size measurements in millimeters from the Flying Eyeball study completed in summer 2006 (green dot shows AWAC deployment location in winter 2006-see Chapter 6).

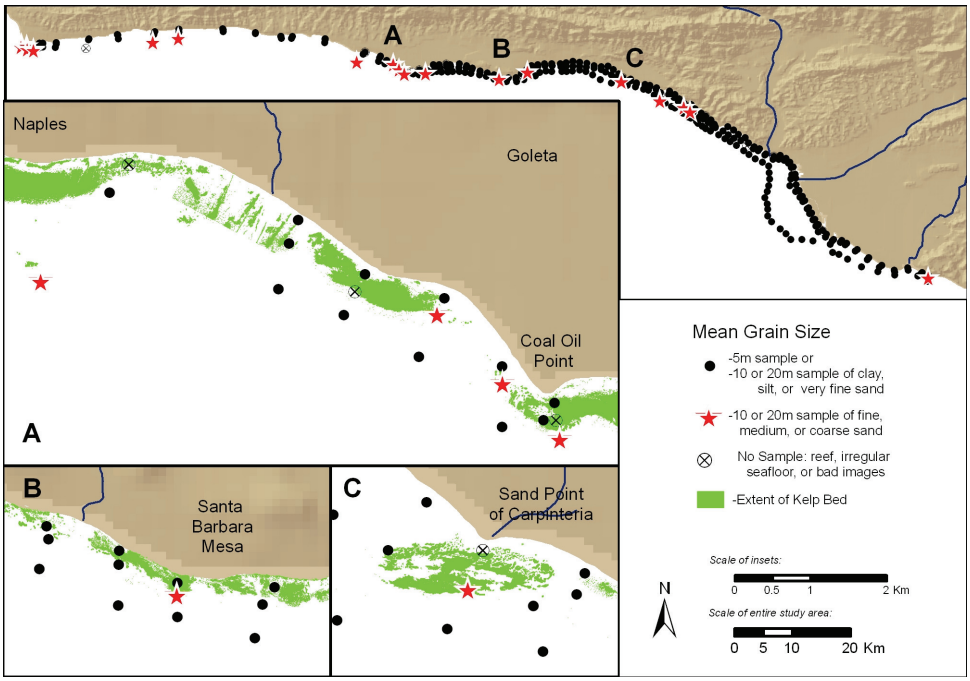

Figure 4.10. Prominent kelp beds in the Santa Barbara littoral cell . Data from this study, usSEABED (Reid and others, 2006) and BEACON (Noble Consultants, 1989).

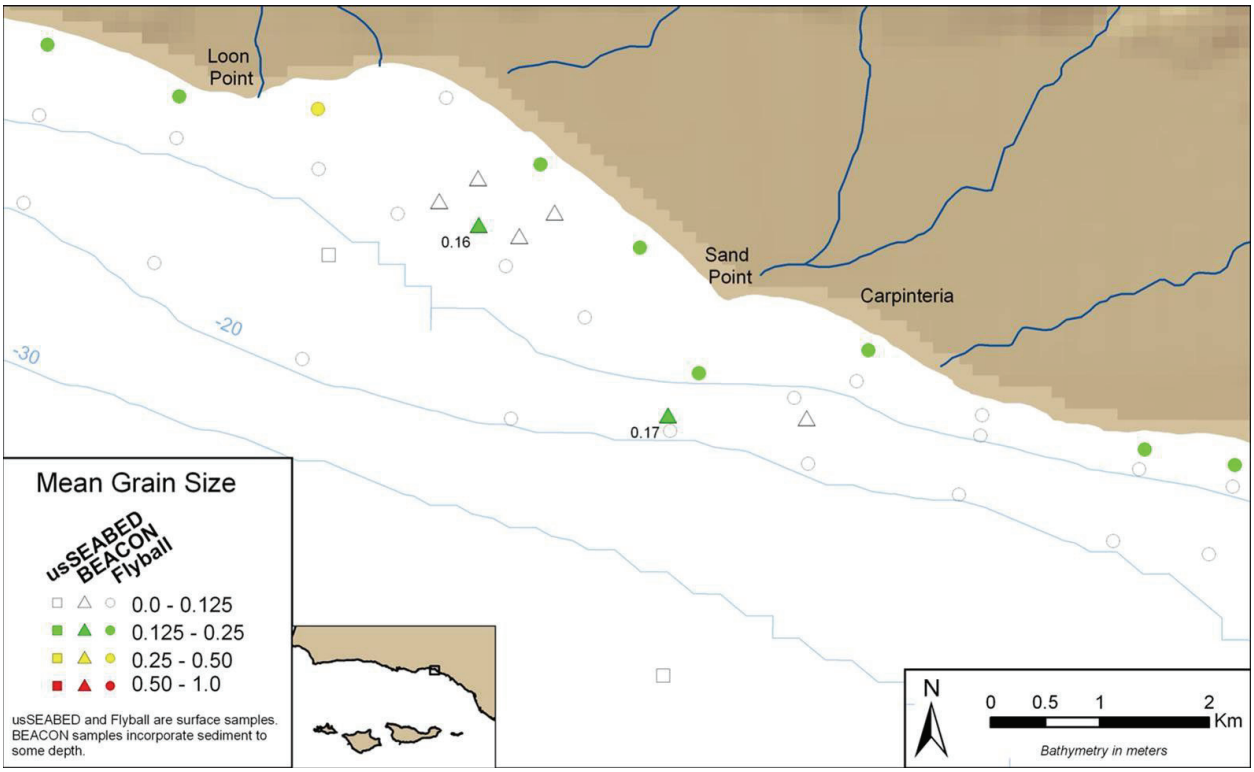

Figure 4.11. Samples offshore Carpinteria. Data from this study, usSEABED (Reid and others, 2006) and BEACON (Noble Consultants, 1989).

Chapter 5- High Resolution Nearshore Mapping and Habitat Classification

By Patrick Barnard

Introduction

This chapter is taken, in large part from the USGS report, "Seafloor Mapping and Benthic Habitat GIS for Southern California, Volume III" (Cochrane and others, 2007). Therefore, this chapter is meant to be only a brief summary of the more extensive report that can be found at: http://pubs.usgs.gov/of/2007/1271/.

From August 8-27, 2005, more than 75 km of the continental shelf (Fig. 5.1) in water depths of 20-70 m southeast of Santa Barbara, were surveyed during the USGS cruise S-1-05-SC (http://walrus.wr.usgs.gov/infobank/s/s105sc/html/s-1-05-sc.meta.html), including offshore of Carpinteria, between Rincon Pt. and Sand Pt. The region between Sand Point and Loon Point was surveyed in 2006, but that data will not be processed and released until 2008. Both Interferometric sonar and 14 hours of both vertical and oblique georeferenced submarine digital video were collected to (1) obtain geophysical data (bathymetry and acoustic reflectance), (2) examine and record geologic characteristics of the sea floor, and (3) construct maps of seafloor geomorphology and habitat distribution. Substrate distribution was predicted using a modified version of Cochrane and Lafferty (2002) video-supervised statistical classification of sonar data that includes derivatives of bathymetry data. Specific details of the methods can be found in the metadata of the bathymetry data file at http://pubs.usgs.gov/of/2007/1271/. In the context of this report, this survey serves to provide updated bathymetry for the nearshore area offshore of Carpinteria, information on substrate type and sediment transport potential, and analysis of long-term nearshore change when compared with historical National Ocean Service (NOS) surveys (see Chapter 2).

Methods

Interferometric sonar data were collected using a 468 kHz SEA Swathplus Interferometric sonar. Interferometric sonar imaging provides high-resolution images of the sea floor by recording the intensity of sound reflected off the sea floor (acoustic backscatter). Seafloor depth data were estimated from the phase difference between seafloor reflections received by spaced receivers. The sonar was mounted on a pole manufactured expressly for use on the *R/V Shearwater*.

Video observations of the seafloor were logged real-time in the field by a team of geologists and biologists who examined areas of transition between contrasting substrate types, resolved and characterized unique seafloor features, and linked the geology and biology of benthic environments. Common substrates observed include a mixture of mud and sand. Common subtidal biota observed include benthic and demersal fish and sessile invertebrates such as gorgonians, sea pens, echinoderms, anemones, sponges, and urchins.

Bathymetric and acoustic backscatter data were compiled with geologic and biologic video observations in an ESRI Geographic Information Systems database (ArcGIS) and used to construct maps of geologic substrate and habitat distribution per Greene and others (1999). These map products enable scientists, parks, and resource managers to better understand benthic habitat characteristics. This information is increasingly important in making decisions about the management of critical environments and resources, the design and utility of marine protected areas, and policies on tourism and development.

For more detailed information about the Methods for the data collection presented in this chapter go to http://pubs.usgs.gov/of/2007/1271/.

Results and Discussion

Bathymetry

Figure 5.2 shows the nearshore bathymetry derived from the Interferometric sonar data. In general, nearshore, there is a gently sloping bottom, except for the steeply sloping, prominent extension of Rincon Point at depth (see also Figure 5.1). This data will be used as a boundary condition for future modeling efforts in 2008 along with the survey data from Sand Point west to Loon point, to be released in 2008. See Figure 2.14 for historical changes in nearshore bathymetry.

Habitat Classification

The 77 sq. km study area is located entirely on the continental shelf (Figure 5.3). Within this area 95% of the seafloor is composed of flat and soft mud or sand. 1.19% of the area is hard bottom (Figure 5.4); the remainder is a mix of low relief hard bottom and sand or coarser sediment bottom. The sand content increases in the nearshore waters and video observations suggest mud is lacking in waters less than 20 m deep. The hard seafloor is divided into two main rocky regions. One area of rocks is located at the crest of an east-west trending bathymetric ridge in the western and central part of the study area above the 50 m contour and north of the oil platforms. There are 0.373 sq. km of exposed bedrock along the ridge of Tertiary age. The only other significant rocky area is a 0.392 sq. km area in the east, above the 30 m contour line, and directly offshore of Rincon Point. Video over the area shows boulders and larger rocks that are likely a submerged extension of the large delta visible at Rincon Point. Locally, onshore outcrops exist of sedimentary rocks of Miocene and Pliocene age.

Sand ripples were observed in the nearshore region between Carpinteria and Rincon Point (Figure 5.5). As depth increases offshore there is an increase in the number of burrowing and bioturbation that decreases the continuity of the bedforms (Figures 5.6-5.8). The bedforms suggest stronger bottom currents, and based on the video the nearshore rippled zone was separated from the more bioturbated zone by dividing polygons using the 20 m depth contour. Video data were collected in the innershelf, north-east section of the study area to determine at what depth the transition from soft, muddy, bioturbated sediment to sand ripples occurs. Figure 5.5 shows the location of the three lines as well as the points where sand ripples were observed. In the figure, sand ripple observations appear bright blue over the yellow observation point markers. Video observations of these lines confirmed that at 20 m there is degradation of ripples by bioturbation. Figure 5.6 shows a bioturbated view at the deepest point on camera line 15. Figure 5.7 shows an image in the zone of transition between bioturbated and sand ripples in the center on camera line 15. Figure 5.8 shows the shallowest point on camera line 15 where the seafloor is predominately sand ripples.

Conclusions

- Sand dominates the substrate in water depths < 20 m, where clearly visible wave-induced ripples are present

- The only prominent hard bottom area mapped in the nearshore is the extension of Rincon Point., which is dominated by boulders and large rocks. Additional information on the reef complex off of Sand Point will be available in 2008.

References

Cochrane, G.R., Golden, N.E., Dartnell, P., Schroeder, D.M., and Finlayson, D.P., 2007. Seafloor Mapping and Benthic Habitat GIS for Southern California, Volume III. U.S. Geological Survey Open-File Report 2007-1271. Available online at http://pubs.usgs.gov/of/2007/1271/

Cochrane, G.R. and Lafferty, K.D., 2002. Use of acoustic classification of sidescan sonar data for mapping benthic habitat in the Northern Channel Islands, California. Continental Shelf Research, v. 22, p. 683-690.

Greene, G.H., Yoklavich, M.M, Starr, R.M., O'Connell, V.M., Wakefield, W.W., Sullivan, D.E., McRea, J.E. and Cailliet, G.M., 1999. A classification scheme for deep seafloor habitats. Oceanologica Acta, v. 22, p. 663-678.

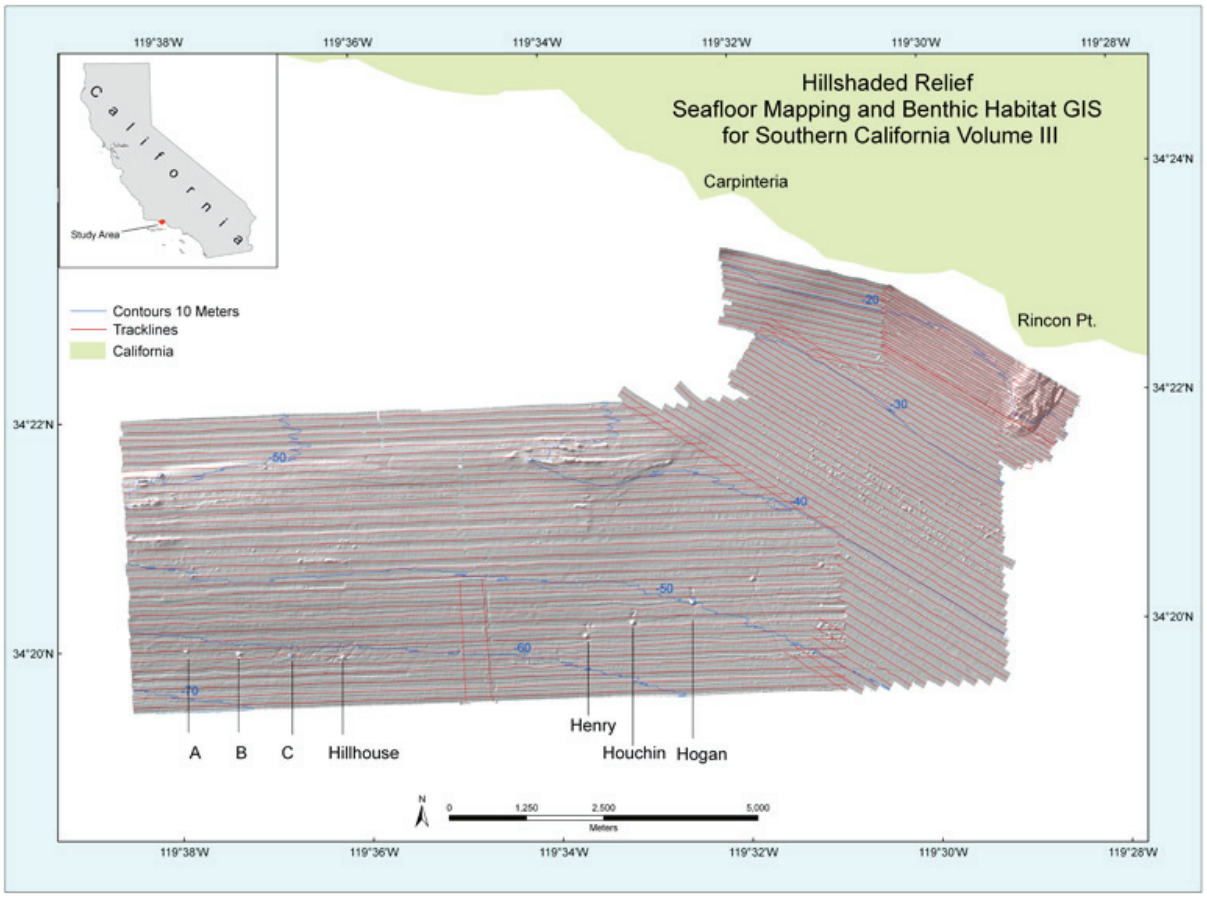

Figure 5.1. Coverage area for the 2005 offshore bathymetric survey.

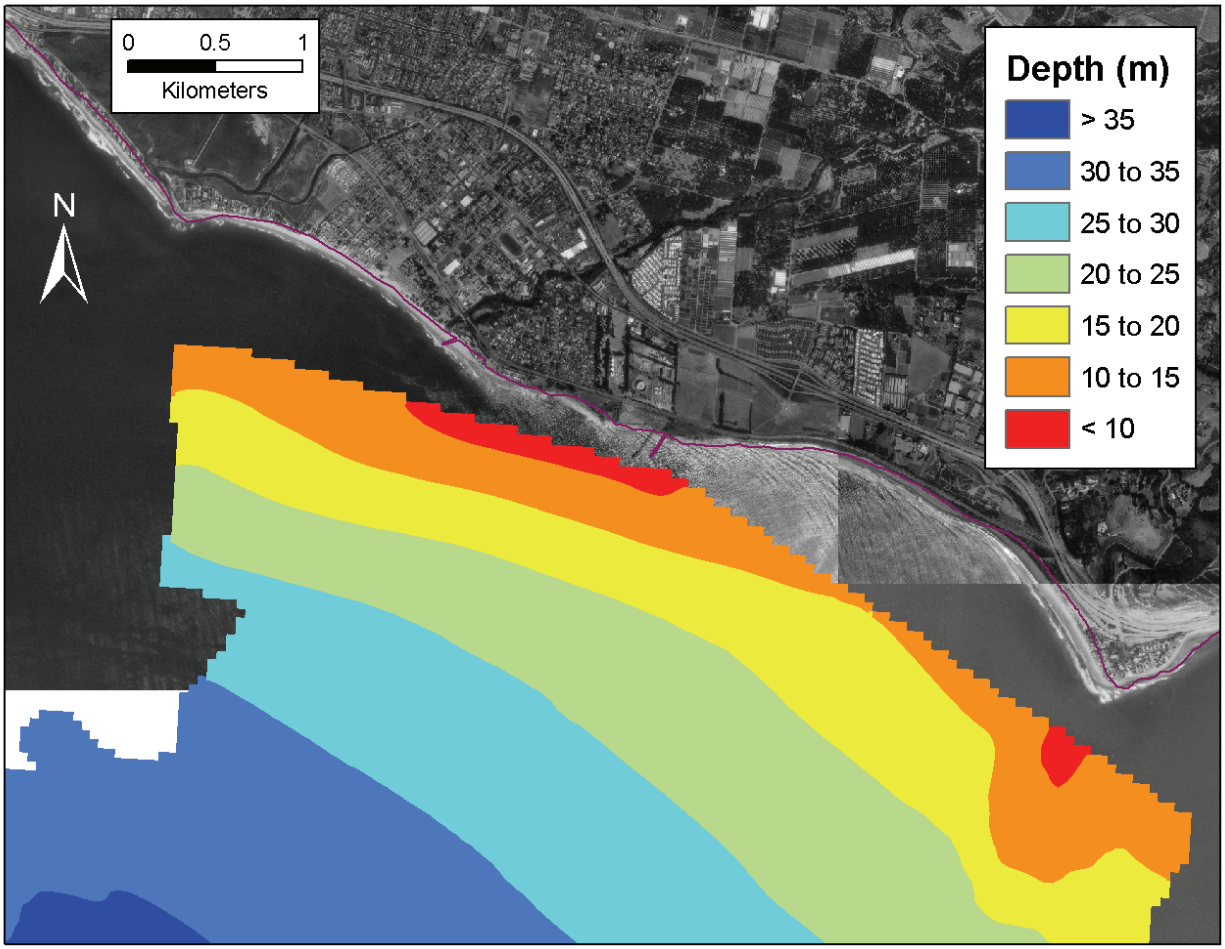

Figure 5.2. Bathymetry from the 2005 USGS offshore bathymetric survey.

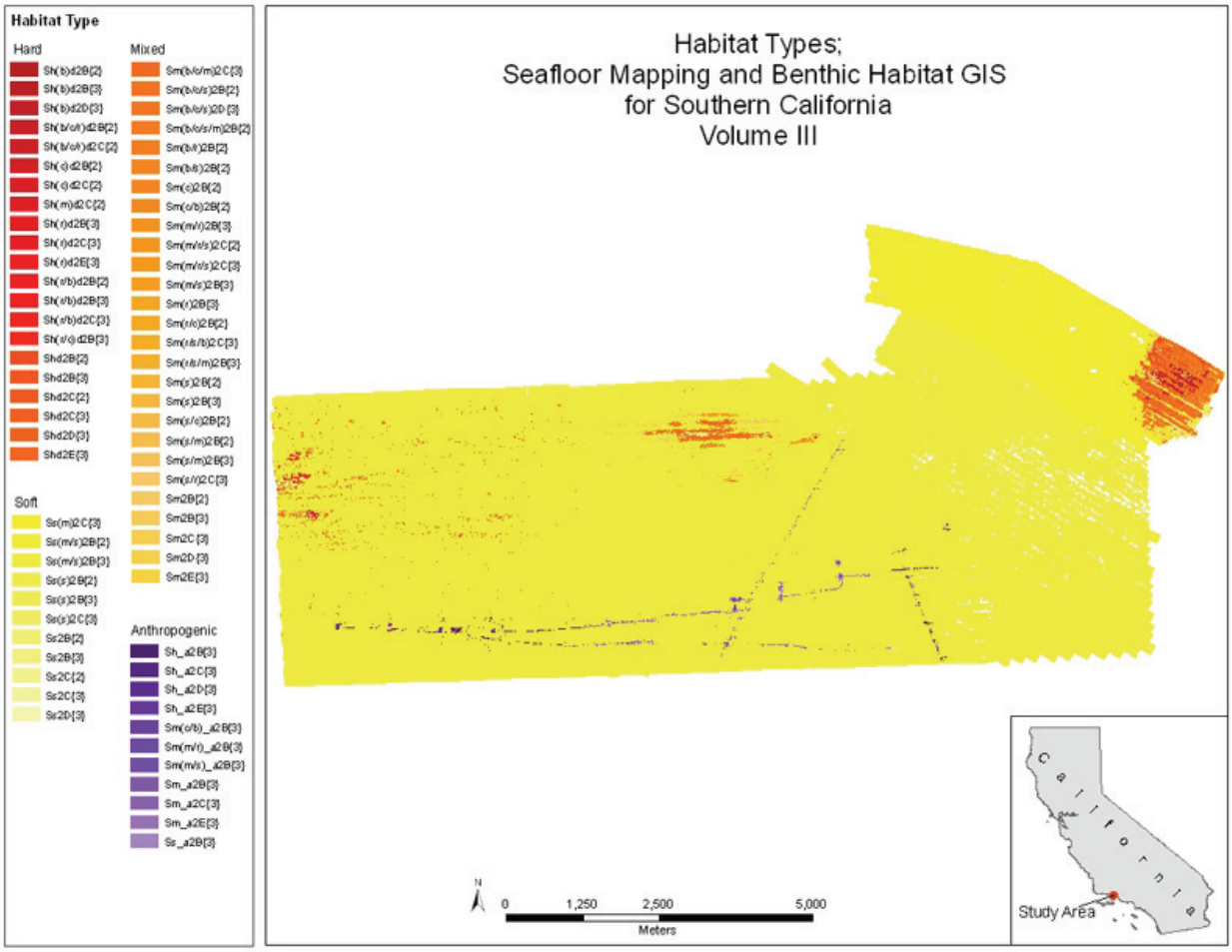

Figure 5.3. Habitat map as determined from the backscatter data and ground truthing in the Carpinteria study area. See http://pubs.usgs.gov/of/2007/1271/ for more details.

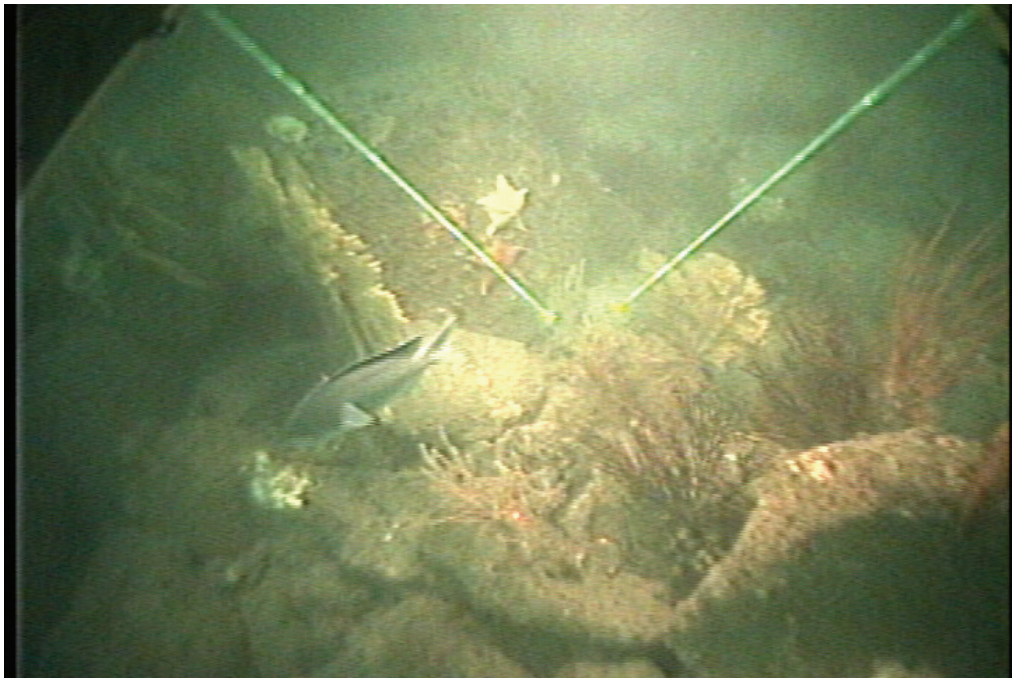

Figure 5.4. Offshore bedrock reef habitat off of Loon Point near Carpinteria (U.S. Geological Survey, 2006).

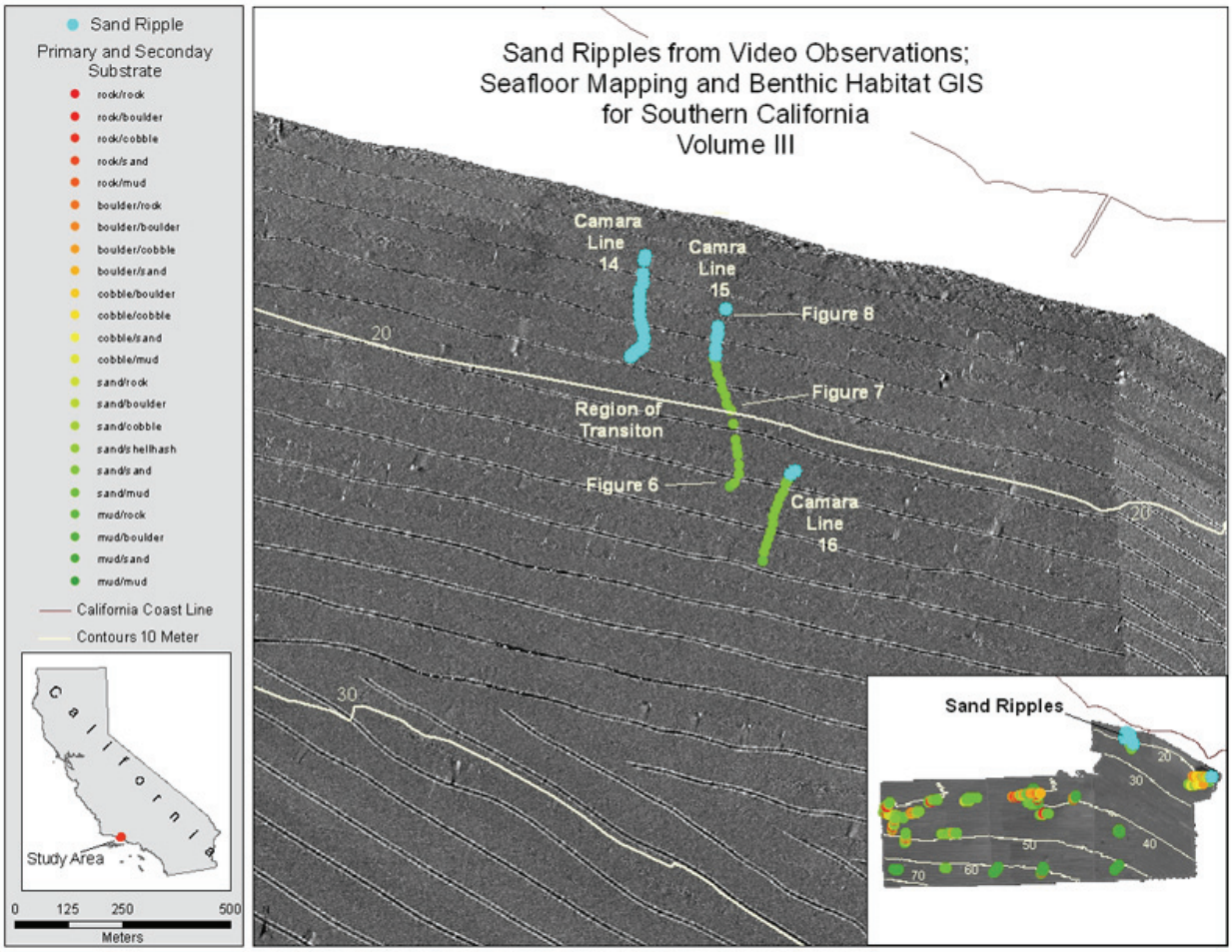

Figure 5.5. Location map of sand ripple features in the nearshore region between Carpinteria and Rincon Point. Blue dots represent locations where ripples were observed and yellow dots represent locations where ripples were not observed.

Figure 5.6. Image of the deepest point of camera line 15 at a depth of 19.7 m, showing ripples degraded by bioturbation.

Figure 5.7. Image showing the zone of transition between bioturbated sand ripples in the center of camera line 15 at a depth of 18.4 m.

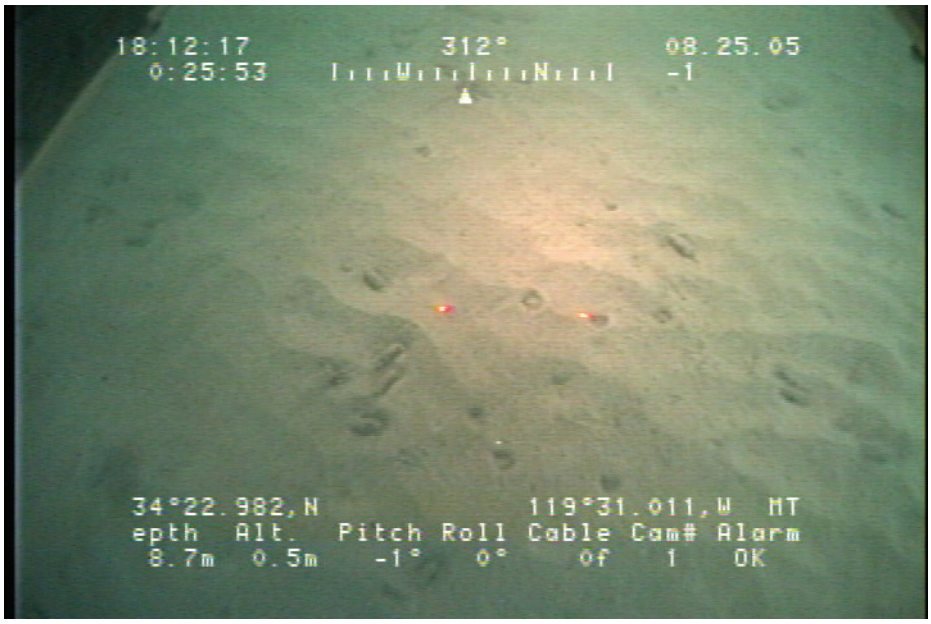

Figure 5.8. Image along the shallowest point on camera line 15 at a depth of 16.9 m, where the seafloor is predominately sand ripples.

Chapter 6- Wave and Current Analysis

By Jodi Eshleman

Introduction

A Nortek Acoustic Wave and Current Meter (AWAC) was deployed off of Carpinteria Beach in 10 m of water during the winter of 2006 to help characterize nearshore wave and current conditions (Figure 6.1). This nearshore current profiler provides detailed current measurements throughout the water column. The deployment was part of a larger regional campaign, with other instruments placed in similar water depths in Goleta and Ventura. In addition, there are buoys from the Coastal Data Information Program (CDIP) and the National Data Buoy Center (NDBC) located in these regions that collect wave data in water depths ranging from to 20 m to 400 m (Figure 6.2).

Methods

The Nortek AWAC collected current profile data every 30 minutes from February through March of 2007. The deployment was designed for a two month duration; therefore sampling intervals were chosen to maximize battery life. Detailed information pertaining to sampling design and deployment location is included in Table 6.1. The AWAC is designed to measure velocity profiles, surface track and pressure with separate sampling regimes for the wave and current measurements. However, a malfunction in the Nortek AWAC AST software set the surface track and pressure data time series to zero throughout the entire deployment. As a result, the velocity measurements that were saved for wave array processing were in the very bottom bins just above the instrument head, and at this water depth, the signal was too weak to recover any wave data.

Current data was saved internally in the AWAC and extracted to individual text files using the Nortek proprietary AWAC AST software. These text files were read into Matlab©. In order to eliminate 'bad' velocity data, several steps were undertaken as part of data post-processing:

1) Time-series records recorded when the instrument was out of the water were removed based on deployment dates and pitch and roll readings.
2) Current data was corrected for magnetic declination at the site using a value of 13º19'E, determined from the NOAA Geophysical Data Center (NGDC; NOAA 2007c).
3) Constructed water level time series was used to remove the signal above the water surface.
4) Data with amplitude readings less than 30 counts were removed since this is the threshold for noise (Nortek, 2004).

For Step 3 above, water level data recorded at the National Oceanic and Atmospheric Administration (NOAA) Santa Barbara station # 9411340 was used to generate a water level time series at the instrument site (NOAA, 2007b). This station is located approximately 14 km from the site, so time differences in tidal elevation would be on the order of minutes and are neglected in this analysis. The measured tide level was subtracted from the water depth reading recorded by the boat's echo sounder at the time of the instrument deployment to determine the

mean water depth at the instrument site. Then, the tide level time series was interpolated to the same time spacing as the current measurements and added to the mean water depth to generate a water level time series at the instrument site. Data recorded in bins above mean sea level plus one standard deviation of the water level time series were removed. Finally, the upper 10% of the water column near the surface was removed to eliminate effects from side-lobe interference (Nortek, 2004).

To help characterize wave conditions in the vicinity of Carpinteria, wave measurements from local CDIP and NDBC buoys were compiled for comparison (Figure 6.2; SCRIPPS, 2007; NOAA, 2007a). CDIP station # 131 was located approximately 7 km southeast of the instrument site in the nearshore region at Rincon in 22 m of water, so this provides the closest wave measurements to the study area. The outer buoys show the sheltering effects of the Channel Islands for varied wave directions. Detailed processing information describing how wave bulk parameters and spectral data are calculated is available on the websites where data is accessed (SCRIPPS, 2007; NOAA, 2007a).

Results

Currents

Weekly plots of current profiles of speed and direction, depth-averaged current vectors, and water surface elevation are included in the appendix for the duration of the winter 2006 deployment (Figures A.11-A.19). Overall, currents were mild and magnitudes rarely exceeded 20 cm/s, with depth-averaged values often less than 5 cm/s. There was some stratification throughout the water column, with strong surface currents decaying with depth. These stratified flows often occur on the ebbing tide of the spring tidal cycle, when current magnitudes are stronger and can reach 15-20 cm/s. Changes in tidal elevations during the neap cycle are much less defined than during the spring cycle, appearing more like a diurnal cycle than semi-diurnal. Some individual profiles of current speed and direction are included in Figure 6.3, which highlight strong current events and general direction characteristics of ebbing, flooding, and slack tides. These show examples of strong currents throughout the water column on an ebbing and flooding tide (February 15, 27); currents measured just after slack tide (February 18, March 28); and highly stratified currents at the surface (February 17) and throughout the entire top half of the water column (March 3).

Current directions are generally northeast (ebbing tide) to southwest (flooding tide), along a principal axis that is 20 to 40 degrees south of the onshore direction at the instrument site, depending on water depth (Figure 6.4). The principal axis moves more onshore with depth, with surface currents (10 m above bottom) angled further south than bottom currents (2 m above bottom). However, the shoreline is curved in this section of coast so the onshore direction would vary significantly with location.

Waves

Bulk wave statistics from local buoys measured during the summer/fall of 2006 are shown in Figure 6.5. Waves never exceeded 2 m at the inshore buoy during the summer, and rarely exceeded 2 m offshore. Wave directions were generally onshore, and refracted slightly southward as they reached the nearshore buoy in 22 m of water at Rincon. Peak period estimates show most energy in the range of 5 to 10 seconds, although there was some south swell in the 15-20 second range. This is further reflected in plots of energy spectra at each buoy (Figure 6.6). In September and October there was more energy in the 10 to 20 second range coming from all

directions. Many times the south swell that was captured at the CDIP buoy at Anacapa Passage (#111), doesn't make it past the Channel Islands and, therefore, doesn't show up in measurements at Goleta Point (#107). Most times this energy did exist at Rincon (#131), although not necessarily as the dominant peak. Mean values of wave statistics from the Rincon buoy for the summer/fall time period are H_s=0.70 m, T_p=9.2 sec, and D_p=241º.

Figure 6.7 shows bulk wave statistics from local buoys measured during the winter of 2006/2007. There were several events where waves were greater than 2 m at Rincon. There was a marked increase in the peak period from early December through late February from the 5-15 sec range to the 10 to 20 second range (Figure 6.7, 6.8). Mean values of waves statistics from the Rincon buoy for the winter time period are Hs=0.84 m, Tp=11.5 sec, and Dp=242º. Peak wave directions measured at the outer buoys are almost always onshore, with very little evidence of dominant energy coming from the south, even in the Anacapa Passage (#111) record. This onshore directed energy refracts and comes inshore at a smaller angle at Rincon then it did in the summer/fall. Angle histograms of wave data by month in Figure 6.9 show an increase in the energy coming from the 210º- 240º bin from October through February, where the 240º-270º bin dominates in summer months. There is evidence of south swell in the increased amount of observations in the 180º-210º bin from May through September.

Discussion

There are distinct seasonal differences in bulk wave parameters measured at local wave buoys. Measurements of peak periods show sharp changes from summer to fall in early September and fall to winter in early December. Wave directions in the winter are oriented further south than in the summer/fall. This is likely due to their longer wave period, causing them to refract more before reaching the Rincon location. Although the Channel Islands do appear to shelter southern waves from the Goleta buoy location, most of this energy still reaches the Rincon site, evident in frequency spectral plots.

The threshold current velocity for sediment movement was estimated using the method outlined by Soulsby (1997). The grain size used for this analysis was 0.09 mm, which was the closest surficial median grain size measurement to the instrument site from the flying eyeball study in the summer of 2006 (see Figure 4.8). This grain size is classified as fine sand and the corresponding threshold current velocity is 41 cm/s. Figure 6.10 shows the velocity magnitude measured in the bottom bin throughout the instrument deployment. Measured velocities were always less than 20 cm/s; suggesting that the currents were not strong enough to put sediments into suspension.

Conclusions

- Tidal current magnitudes were mild and rarely exceeded 20 cm/s.
- Measured currents were not strong enough to suspend sediment based on the threshold current velocity and closest measured sediment grain size.
- Current profiles show stratification throughout the water column with strong surface currents decaying with depth, especially on the ebbing tide of the spring tidal cycle.
- Current directions are oriented northeast to southwest, with a principal axis that is skewed slightly south of onshore.
- Wave heights never exceed 2 m in the summer and rarely do in the winter at inshore locations. Average values are less than one meter.

- Wave directions are generally slightly south of onshore at Rincon, with waves refracting more in the winter as a result of lower frequency energy.

References

National Oceanic and Atmospheric Administration (NOAA), 2007a. National Data Buoy Center: Silver Spring, Maryland, http://www.ndbc.noaa.gov/

National Oceanic and Atmospheric Administration (NOAA), 2007b. Tides & Currents, Center of Operational Products and Services, http://tidesandcurrents.noaa.gov/

NOAA Satellite and Information Service, 2007c. National Geophysical Data Center, http://www.ngdc.noaa.gov/seg/geomag/jsp/Declination.jsp

Nortek AS, 2004. AWAC Acoustic Wave and Current Meter User Guide.

SCRIPPS Institution of Oceanography, 2007. The Coastal Data Information Program. San Diego, Integrative Oceanography Division, Scripps Institution of Oceanography, http://cdip.ucsd.edu

Soulsby, R, and Whitehouse, R, 1997. Threshold of sediment motion in coastal environment. Proceedings of the Pacific Coasts and Ports'97 Conference, University of Canterbury, Christchurch, New Zealand, p. 149-154.

Table 6.1. Winter 2006 AWAC Sampling Design.

Setup Parameters	Value
Deployment Date	2/2/2007
Recovery Date	4/4/2007
Deployed Latitude	119.3141 W
Deployed Longitude	34.3894 N
Instrument Serial Number	WAV 5179
Frequency (kHz)	1000
Coordinate System	ENU
Blanking distance (m)	0.52
Current Sampling:	
Cell size (m)	0.5
Profile Interval (sec)	1800
Average Interval (sec)	90
Sampling Rate (Hz)	6[1]

[1] Internal sampling rate is 6 Hz but the quickest the instrument can write out data is 1 Hz (Nortek, 2004).

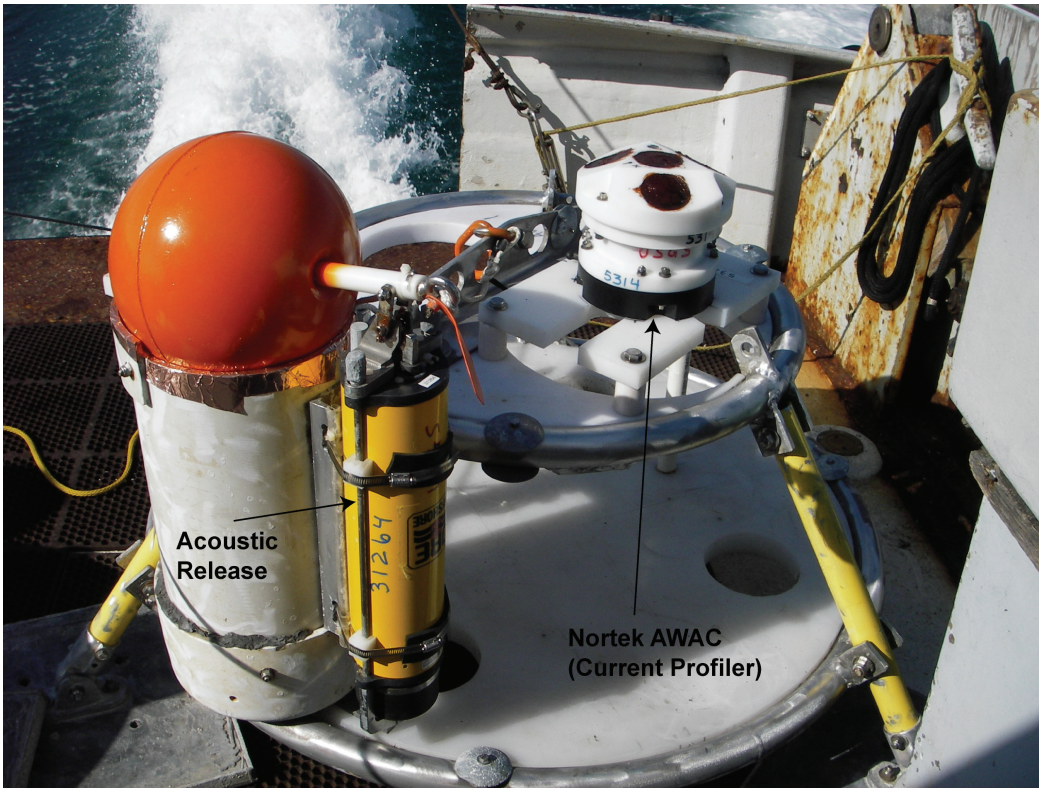

Figure 6.1. Photograph of instrumented tripod deployed in Carpinteria in the winter of 2006.

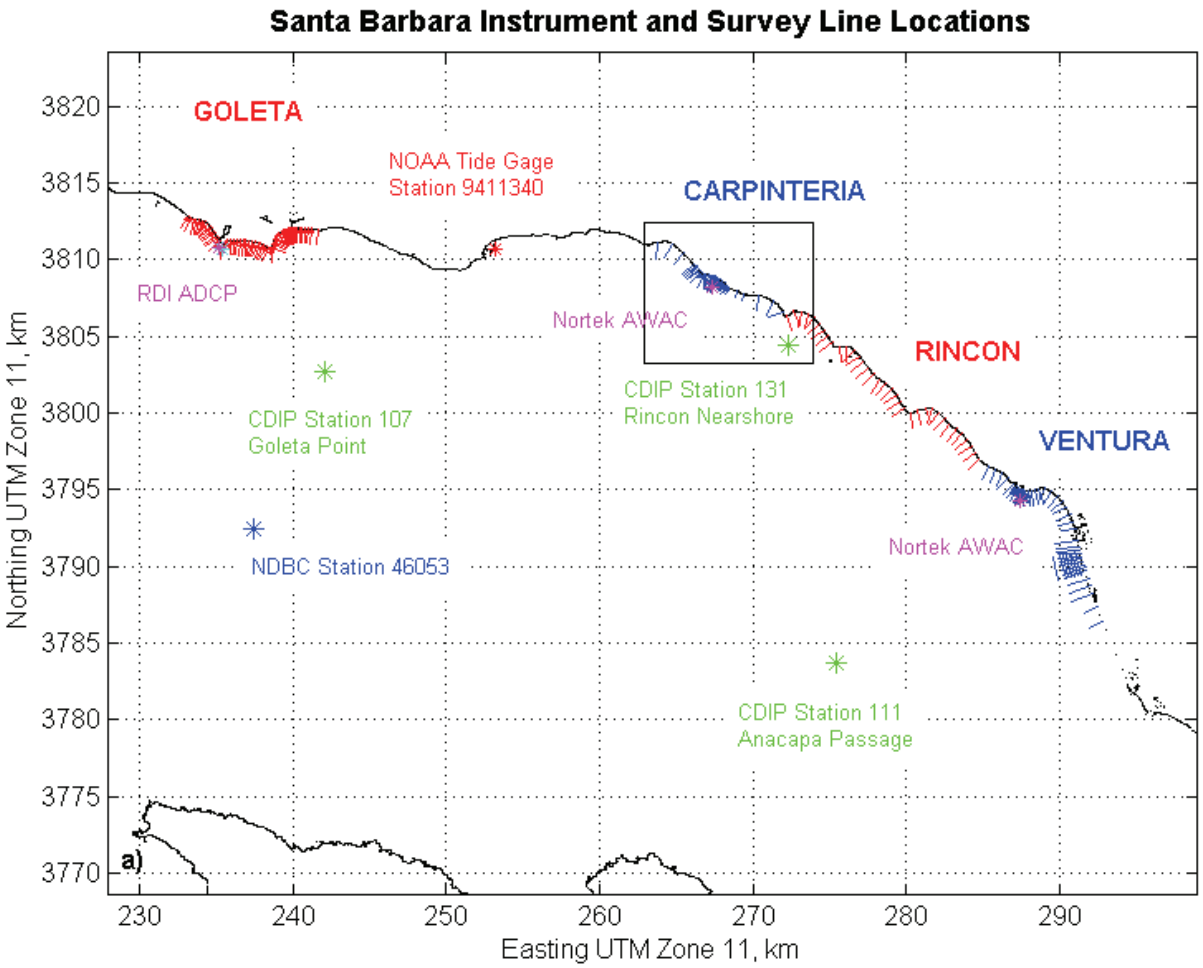
Santa Barbara Instrument and Survey Line Locations
GOLETA
NOAA Tide Gage
Station 9411340
CARPINTERIA
RDI ADCP
Nortek AWAC
RINCON
CDIP Station 131
Rincon Nearshore
CDIP Station 107
Goleta Point
VENTURA
NDBC Station 46053
Nortek AWAC
CDIP Station 111
Anacapa Passage
a)
Northing UTM Zone 11, km
Easting UTM Zone 11, km
3820
3815
3810
3805
3800
3795
3790
3785
3780
3775
3770
230
240
250
260
270
280
290

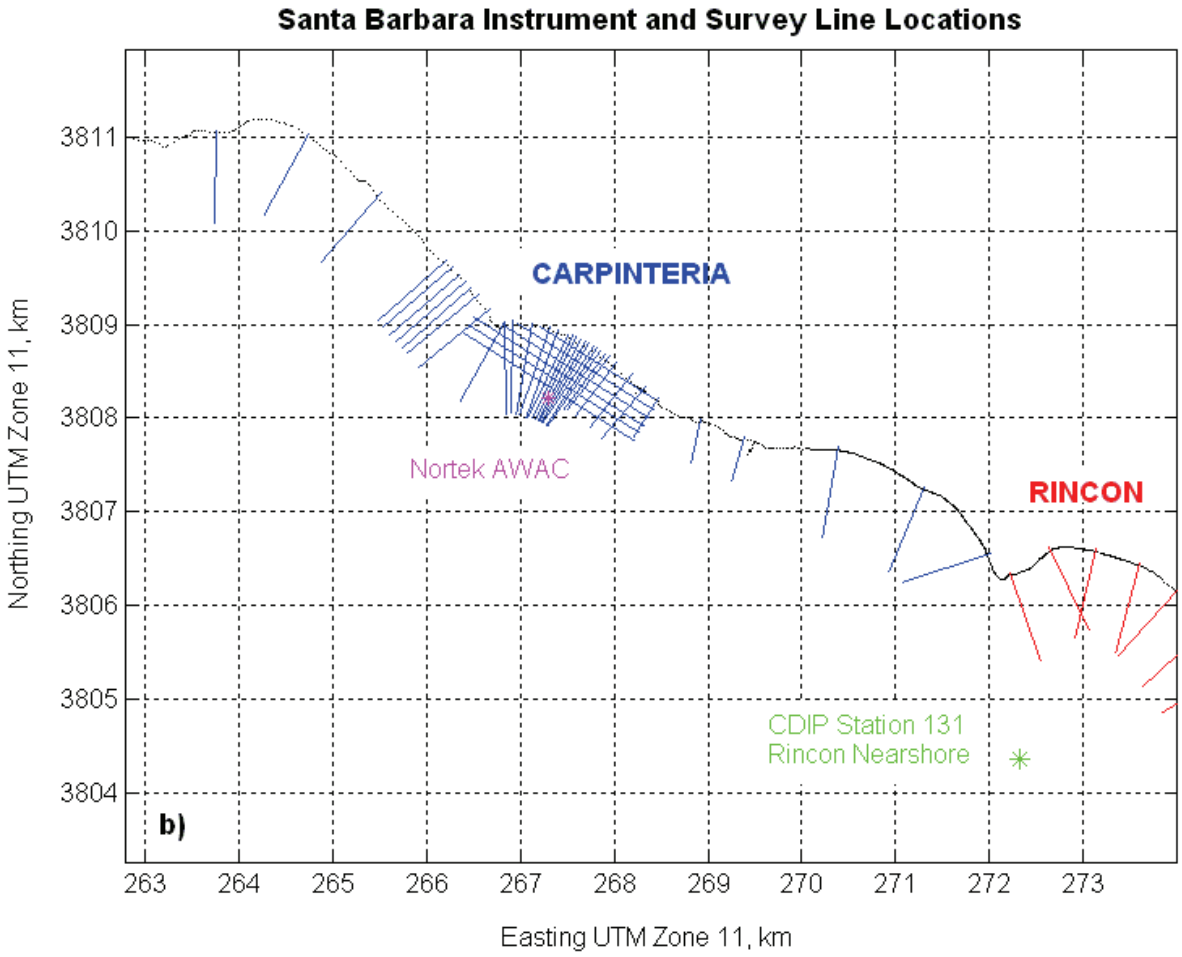

Figure 6.2. Locations of CPS profiles, wave buoys, deployed instruments and tide gages in the **A)** region of the Santa Barbara Coastal Erosion Study and **B)** of the focus area at Carpinteria.

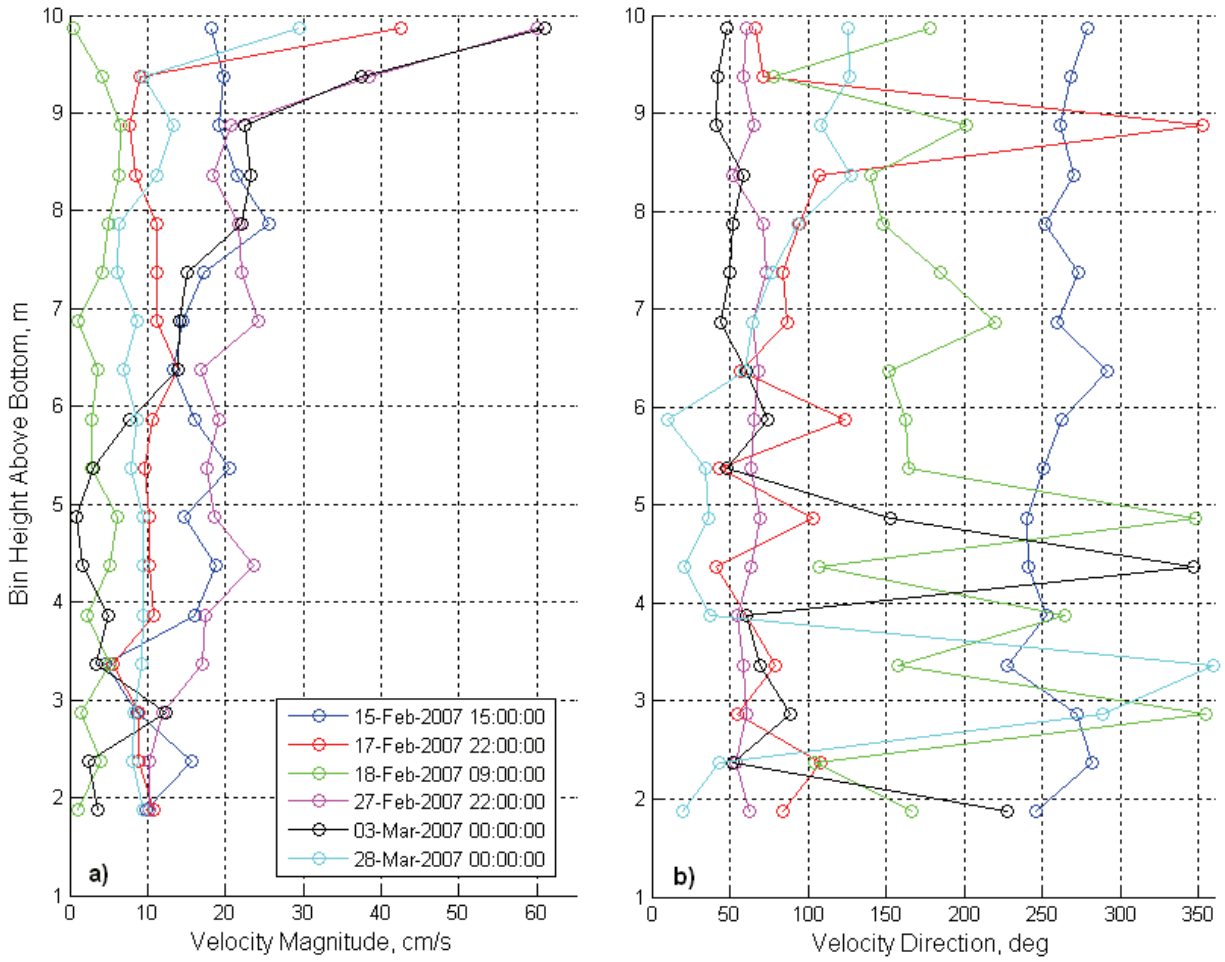

Figure 6.3. Individual current profile A) speed and B) direction measured by the AWAC for select events that occurred during the winter 2006 deployment period.

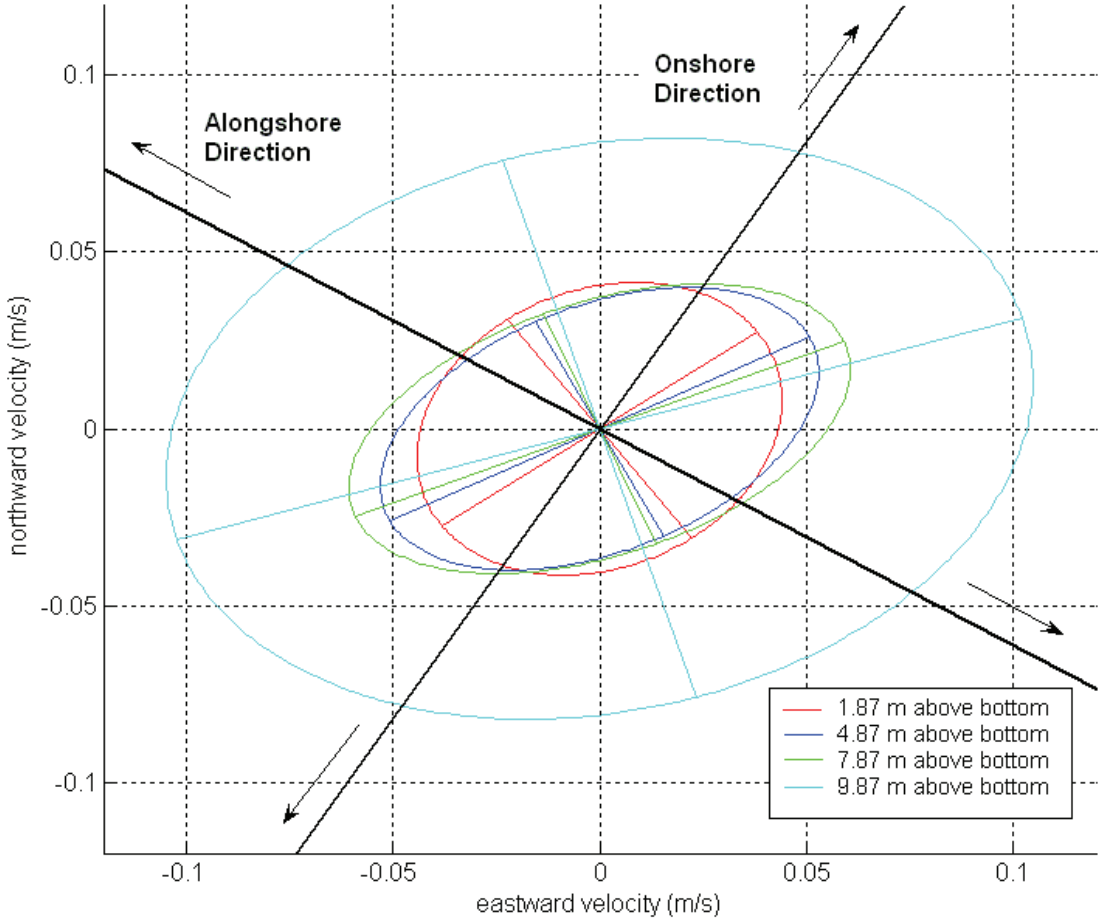

Figure 6.4. Principal axis plots of currents measured with the AWAC at different depths within the water column (solid black line shows onshore and alongshore directions).

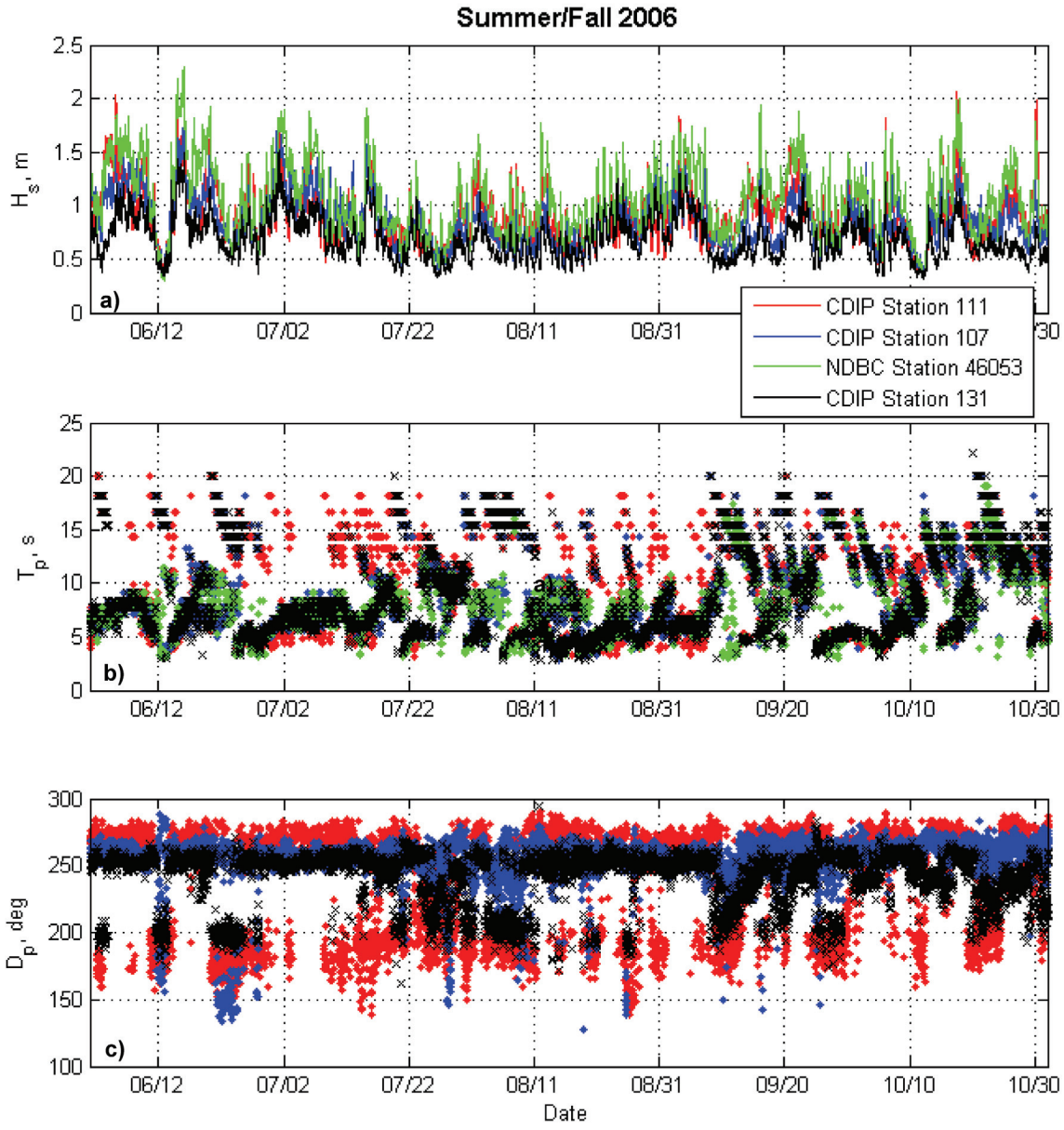

Figure 6.5. Measurements of A) significant wave height B) peak wave period and C) peak wave direction from local wave buoys during the summer/fall of 2006 (NOAA, 2007a; SCRIPPS, 2007).

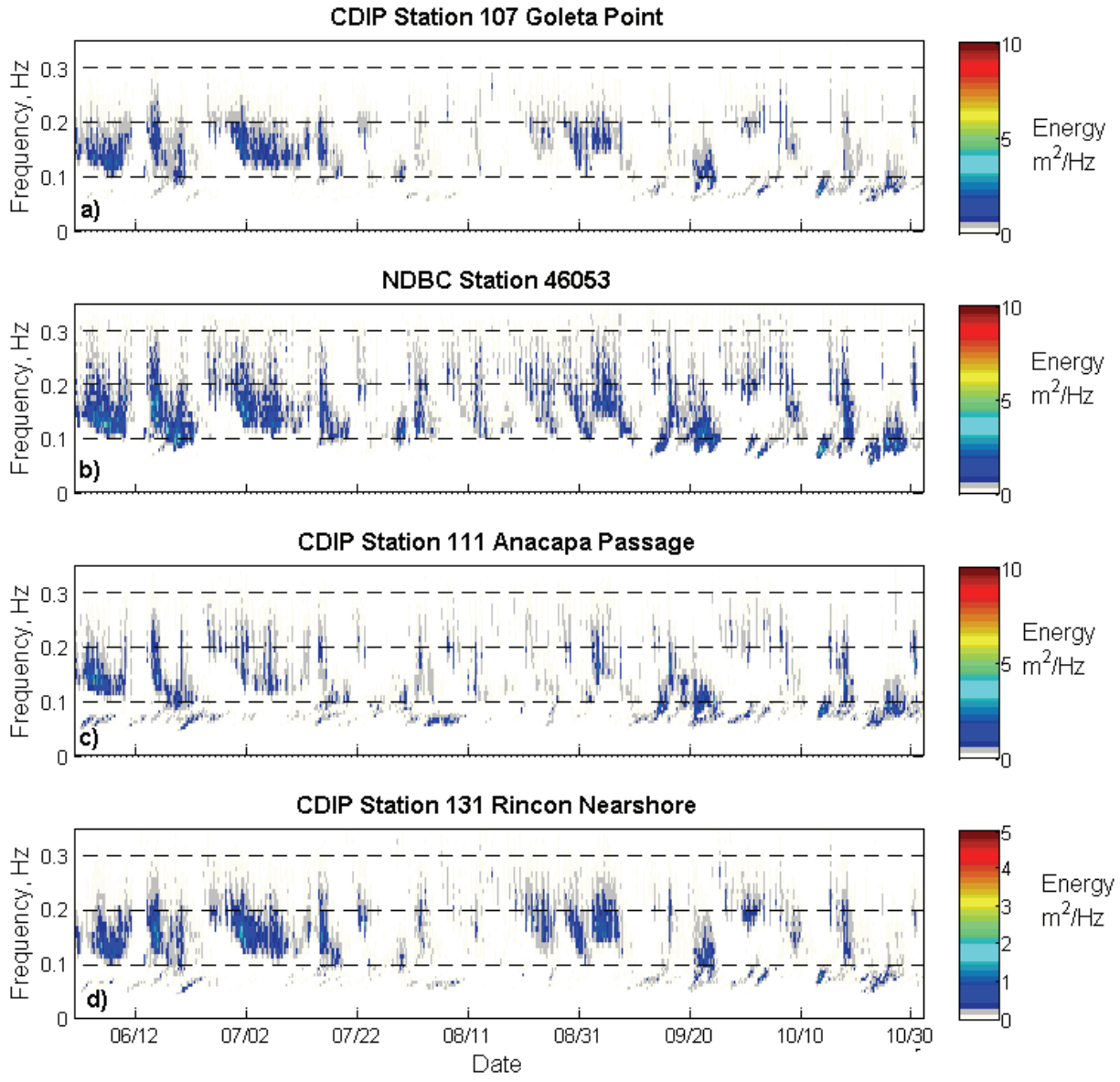

Figure 6.6. Energy spectra measured at A) CDIP Goleta Point Station 107 (183 m water depth) B) NDBC Station 46053 (417 m water depth) C) CDIP Anacapa Passage Station 111 (105 m water depth) and D) CDIP Rincon Nearshore Station 131 (22 m water depth) during the summer/fall of 2006 (NOAA, 2007a; SCRIPPS, 2007).

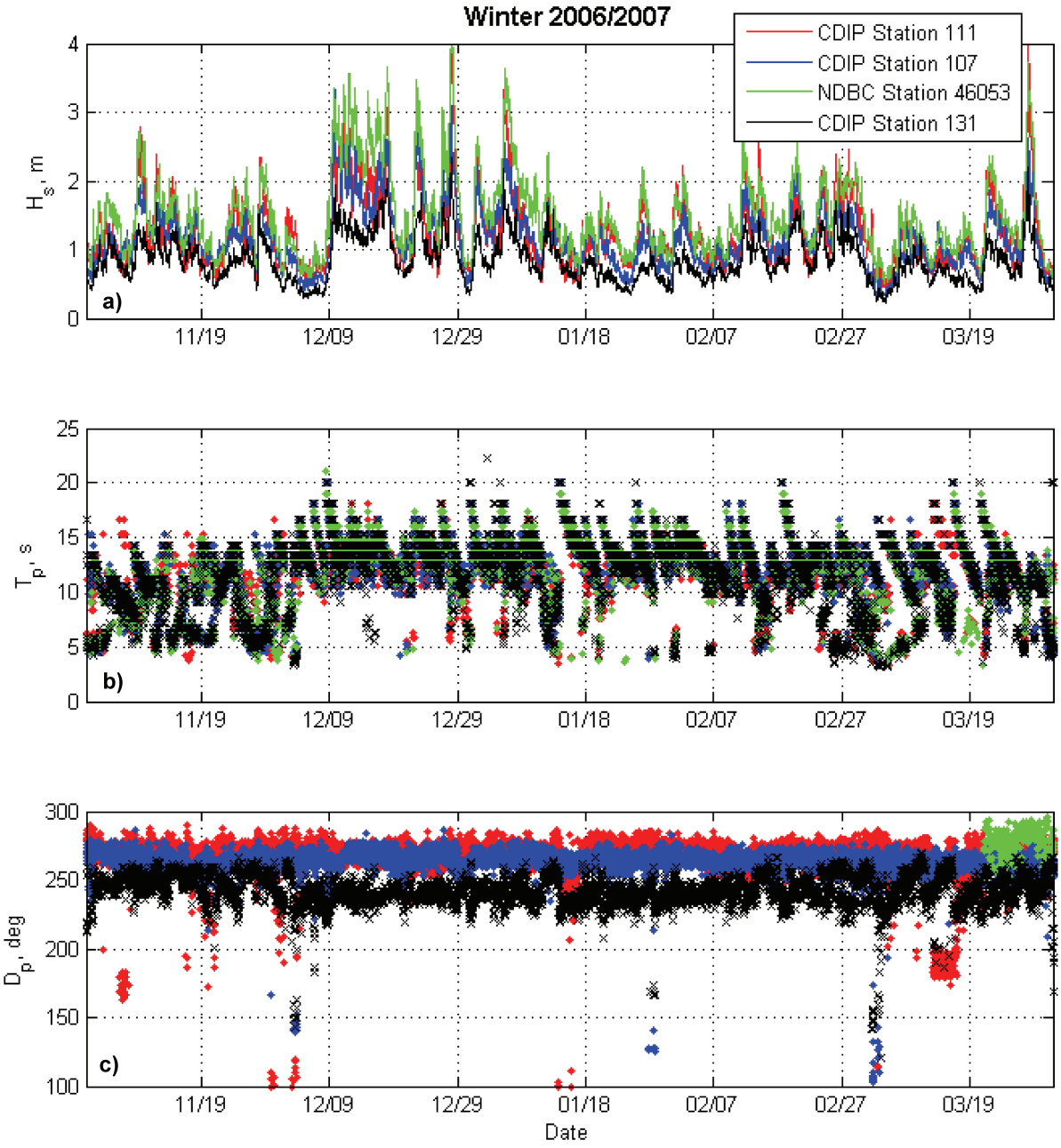

Figure 6.7. Measurements of a) significant wave height b) peak wave period and c) peak wave direction from local wave buoys during the winter/spring of 2006/2007 (NOAA, 2007a; SCRIPPS, 2007).

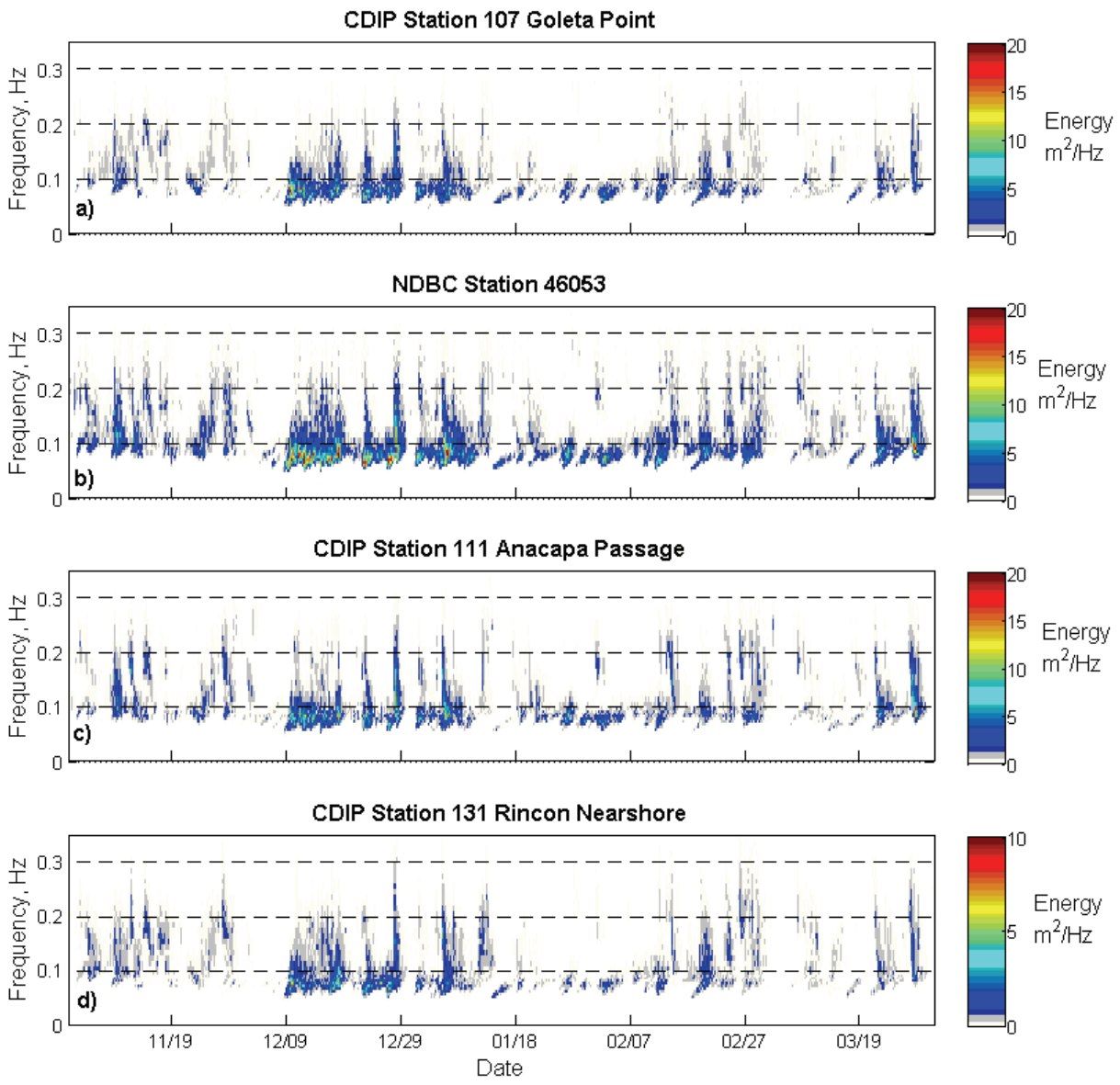

Figure 6.8. Energy spectra measured at a) CDIP Goleta Point Station 107 (183 m water depth) b) NDBC Station 46053 (417 m water depth) c) CDIP Anacapa Passage Station 111 (105 m water depth) and d) CDIP Rincon Nearshore Station 131 (22 m water depth) during the winter/spring of 2006/2007 (NOAA, 2007a; SCRIPPS, 2007).

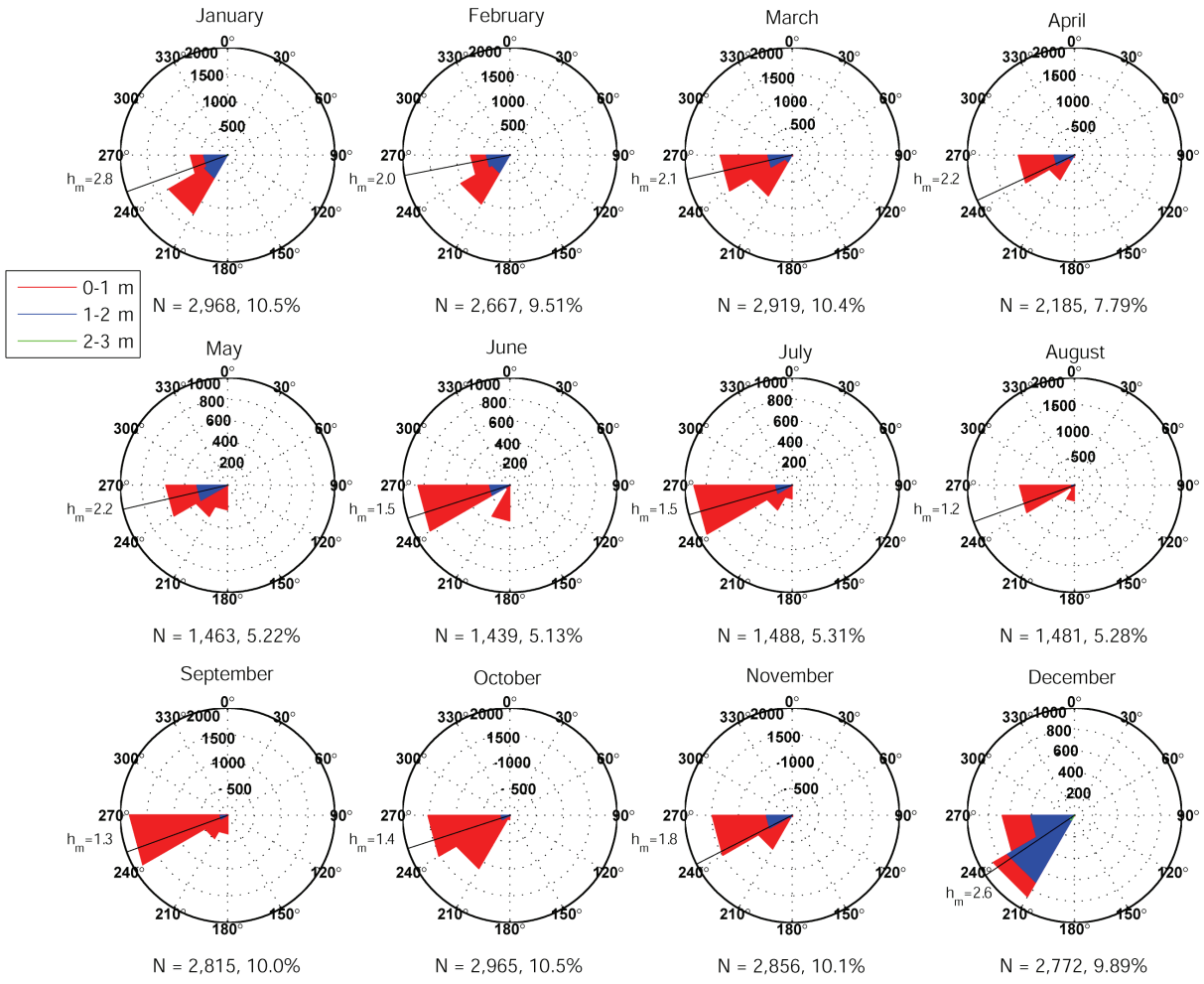

Figure 6.9. Direction histograms for Rincon Nearshore CDIP buoy #131 by month for all available wave data measured from May 2006 through April 2007 (N is number of observations out of a total 28,018, the percentage is for the total data that occurred in that month, and h_m is the maximum wave height for the month which came from a direction marked by the solid black line) (SCRIPPS, 2007).

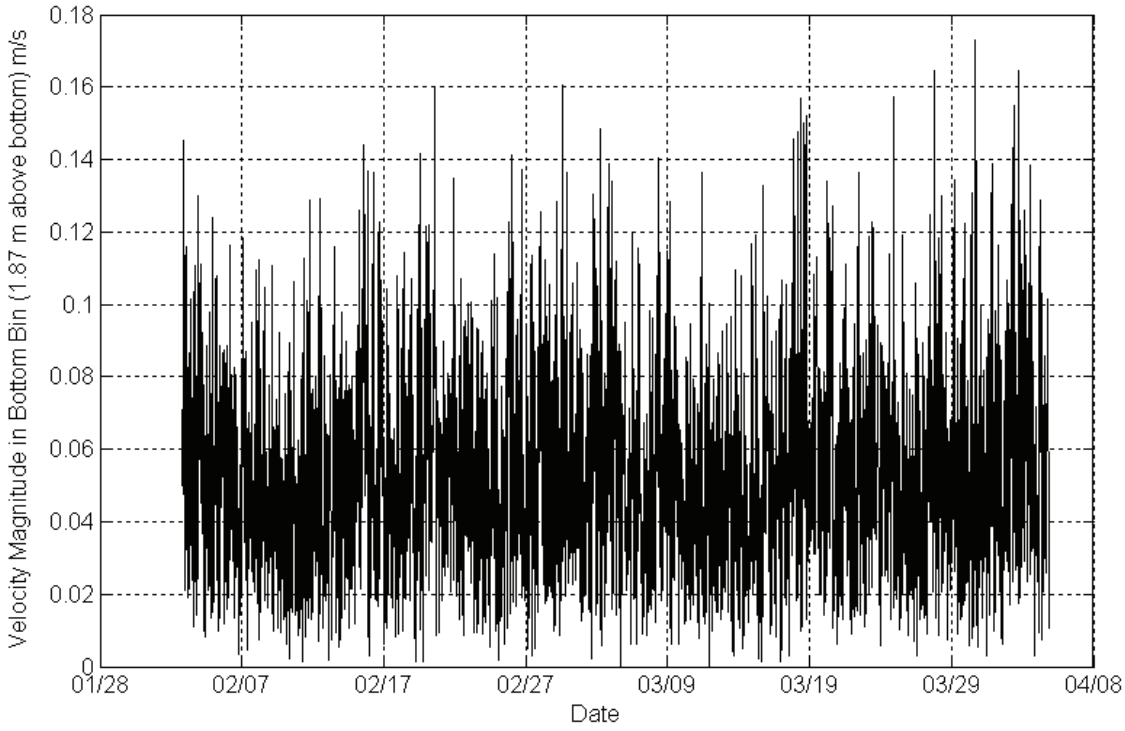

Figure 6.10. Time series of velocity magnitude measured in the bottom bin for the instrument site.

Chapter 7- Project Synthesis

Summary

Sand impoundment caused by the construction of the Santa Barbara Harbor in the late 1920s created an erosion wave that impacted downcoast (southeast) beaches. Downdrift beaches at Sandyland and Carpinteria were especially hard hit. At Carpinteria Beach, California, a recurring erosion hotspot requires regular beach maintenance and periodically threatens oceanfront property during large storm events. Using a combination of historic air photos, Lidar, and physical measurements, historic shoreline and beach width changes were analyzed spanning the last 138 years. The initial erosion wave dramatically reduced beach widths by about 50 m. The long-term beach width and shoreline change analyses show preferential erosion (-0.35 m/yr) at the west end of Carpinteria and accretion in the east (0.3 m/yr). The net result of this has been a clockwise beach rotation with the updrift west end narrowing ~50 m while the downdrift eastern end of the beach has widened about 40 m over the same time period.

El Niño storm impacts measured before and after the 1982-83 and 1997-98 El Niño seasons are shown to have a similar west end erosion and east end accretion pattern that match the 138-year long-term shoreline change rates providing evidence that strong El Niños may be driving the long term coastal evolution. Between 1983 and 1985, following the 1982-83 El Niño, construction of a revetment at the western end of the beach was completed. Analyses following the 1997-98 El Niño show that the erosion hotspot present following both events had shifted downdrift onto the City of Carpinteria beach.

Seasonal beach width change analyses show that the seasonal cyclical pattern is a systematic retreat of the shoreline and narrowing of the beach width by about 20 m. The seasonal analyses do show an erosion hotspot at the end of the revetment that is evidenced by increased narrowing of the beach width and loss of sand volumes. During the seasonal surveys, relatively low wave conditions dominated with changes to the nearshore and beach occurring above 5 m water depth. Tidal currents offshore are relatively low (<20 cm/sec) and not of sufficient velocity to move sand-sized sediment.

Sediment sampling shows that there is a seasonal coarsening of sediments in the winter and a fining in the summer. There is alongshore variability in the winter coarsening pattern with the coarsest materials co-located with the erosion hotspot seen in the El Niño storm impacts and the seasonal beach width changes.

Offshore sediment samples show that most of the offshore sand is finer than that found on the beaches indicating that there is not a significant source of suitable nourishment material in the project study area. Any nourishment project would have to acquire sand from outside the study area, or commit to a large overfill nourishment. Given the low energy wave conditions, depth of closure (< 5 m), and low tidal currents a successful nourishment project would most likely have to be done directly on the beach.

Finally, a significant lag correlation analyses with a peak lag of 4 years indicates that most of the sand volumes dredged from Santa Barbara harbor arrive on the beaches of Carpinteria after 4 years and may continue to supply the beaches for up to 10 years.

Acknowledgements

This study was funded by the City of Carpinteria, through a grant from the California State Department of Boating and Waterways. Thanks to Thomas Reiss, Gerry Hatcher, Jeffrey Hansen, and Brian Spear for their field support. Curt Storlazzi assisted with the lag correlation analysis. Amy Draut and Li Erikson provided excellent internal reviews.

Appendix

USGS Field Activity IDs and Web Links

Survey	Field Activity ID	Survey Date	URL For Field Activity ID
High Res Bathymetry	*S-1-05-SC*	8/8/05 – 8/27/05	http://walrus.wr.usgs.gov/infobank/s/s105sc/html/s-1-05-sc.meta.html
Lidar, ATV, PWC	*C-N2-05-CA*	10/15/05	http://walrus.wr.usgs.gov/infobank/c/cn205ca/html/c-n2-05-ca.meta.html
ATV, PWC, Eyeball	*I-V1-O6-CA*	3/25/06	http://walrus.wr.usgs.gov/infobank/i/iv106ca/html/i-v1-06-ca.meta.html
ATV, PWC, Eyeball	*S-V2-06-CA*	10/6/06	http://walrus.wr.usgs.gov/infobank/s/sv206ca/html/s-v2-06-ca.meta.html
ATV, PWC, Eyeball	*S-V1-07-CA*	2/18/07	http://walrus.wr.usgs.gov/infobank/s/sv107ca/html/s-v1-07-ca.meta.html
GPS Control Survey	*C-N1-05-CA*	9/12/2005-9/14/2005	http://walrus.wr.usgs.gov/infobank/c/cn105ca/html/c-n1-05-ca.meta.html
ATV, GPS survey	*C-N2-05-CA*	10/15/2005-10/20/2005	http://walrus.wr.usgs.gov/infobank/c/cn205ca/html/c-n2-05-ca.meta.html
GPS Control Survey	*I-V1-05-CA*	9/12/2005-9/14/2005	http://walrus.wr.usgs.gov/infobank/i/iv105ca/html/i-v1-05-ca.meta.html
ATV, PWC	*I-V2-05-CA*	10/15/2005-10/20/2005	http://walrus.wr.usgs.gov/infobank/i/iv205ca/html/i-v2-05-ca.meta.html
GPS Control Survey	*V-N1-05-CA*	9/12/2005-9/14/2005	http://walrus.wr.usgs.gov/infobank/v/vn105ca/html/v-n1-05-ca.meta.html
ATV, PWC	*V-N2-05-CA*	10/15/2005-10/20/2005	http://walrus.wr.usgs.gov/infobank/v/vn205ca/html/v-n2-05-ca.meta.html
ATV, PWC, Eyeball	*V-N1-06-CA*	3/25/2006-3/30/2006	http://walrus.wr.usgs.gov/infobank/v/vn106ca/html/v-n1-06-ca.meta.html

Coastal Profiling System Profiles

This section includes plots of bathymetric profile evolution for each of the 42 profiles included in the Carpinteria planned line file. Profiles 35 and 36 are not included since radio coverage was intermittent and surveyors were not able to collect RTK DGPS data at those locations.

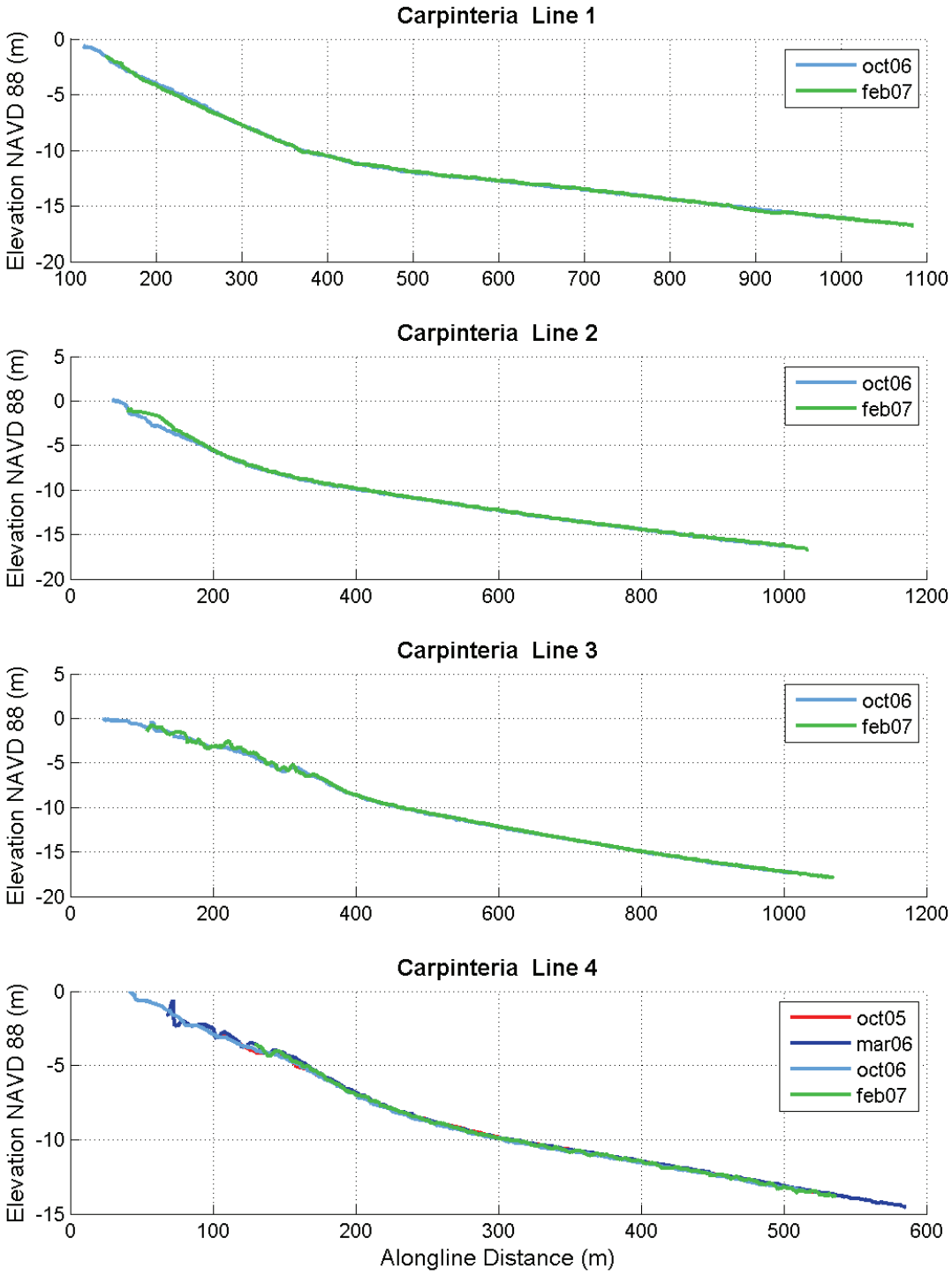

Figure A.1 Carpinteria cross-shore profiles 1-4.

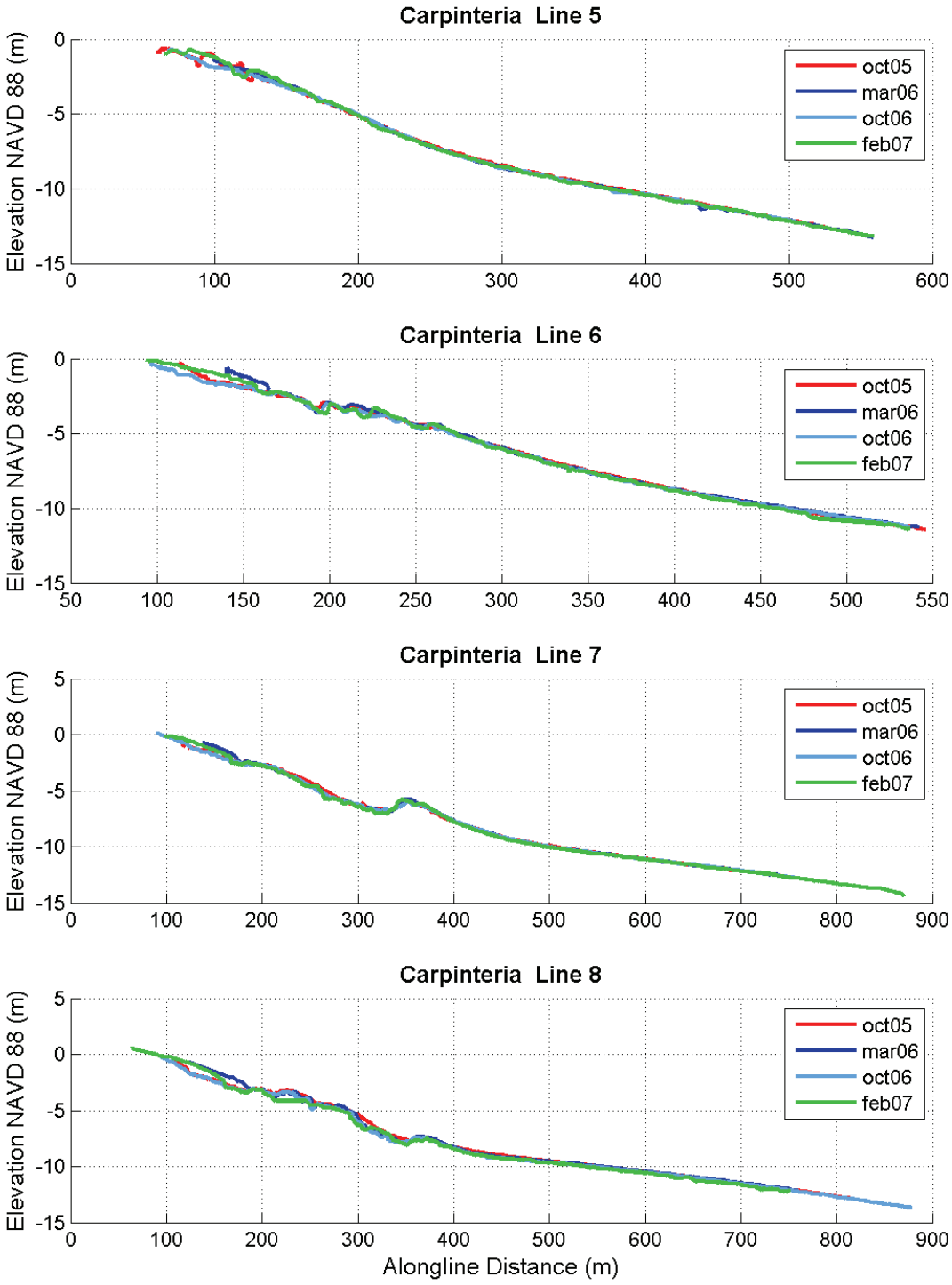

Figure A.2 Carpinteria cross-shore profiles 5-8.

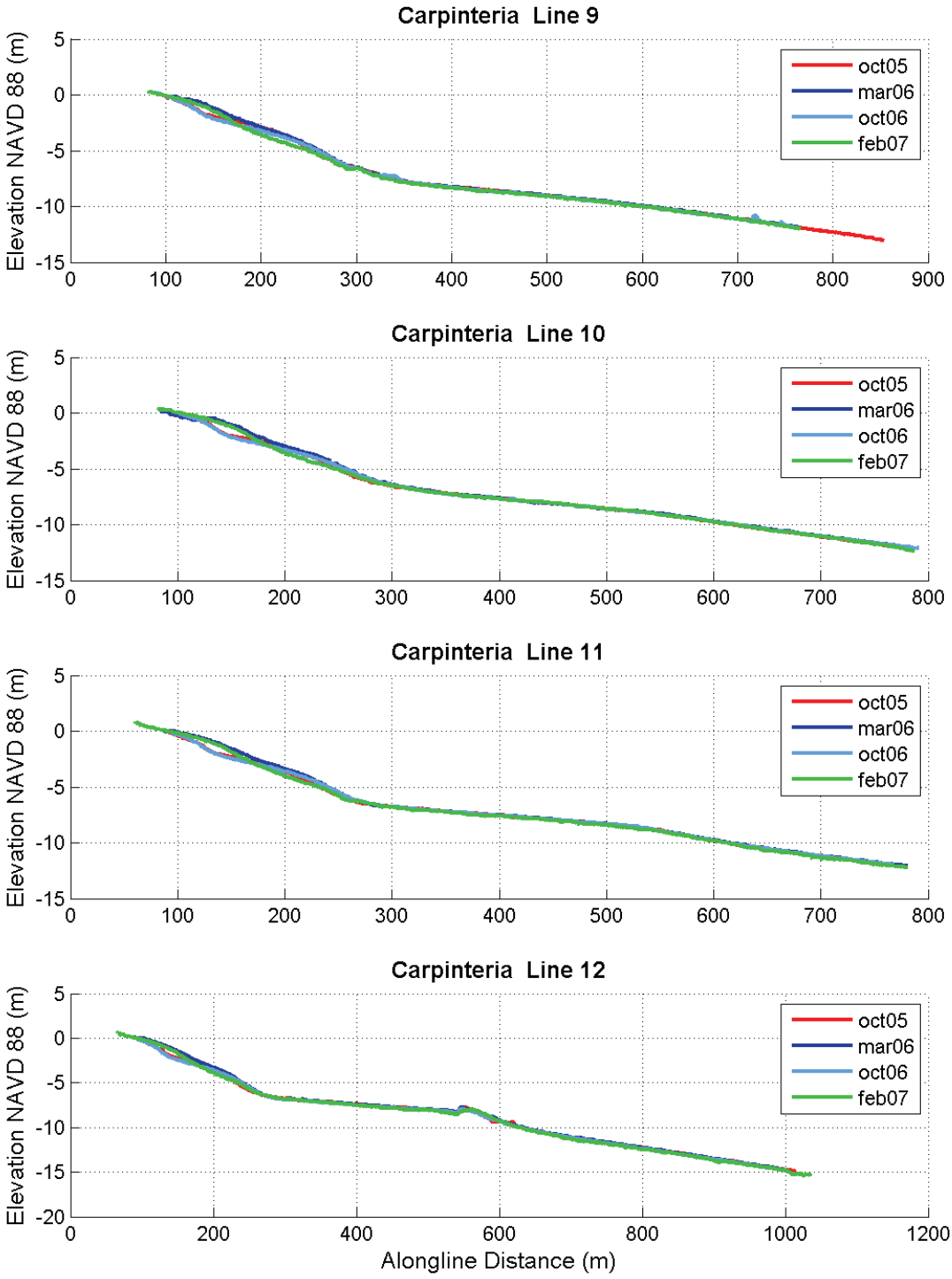

Figure A.3 Carpinteria cross-shore profiles 9-12.

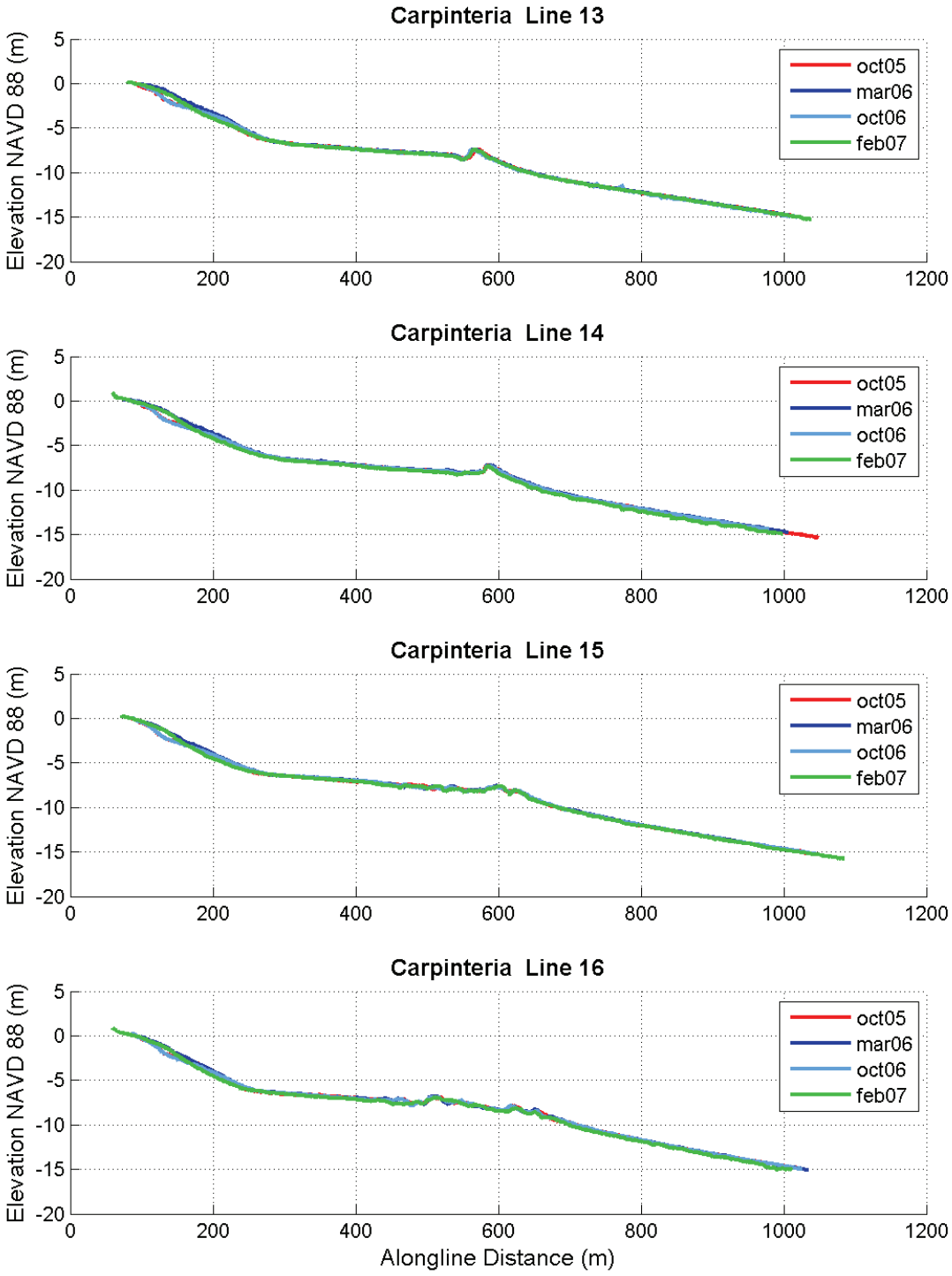

Figure A.4 Carpinteria cross-shore profiles 13-16.

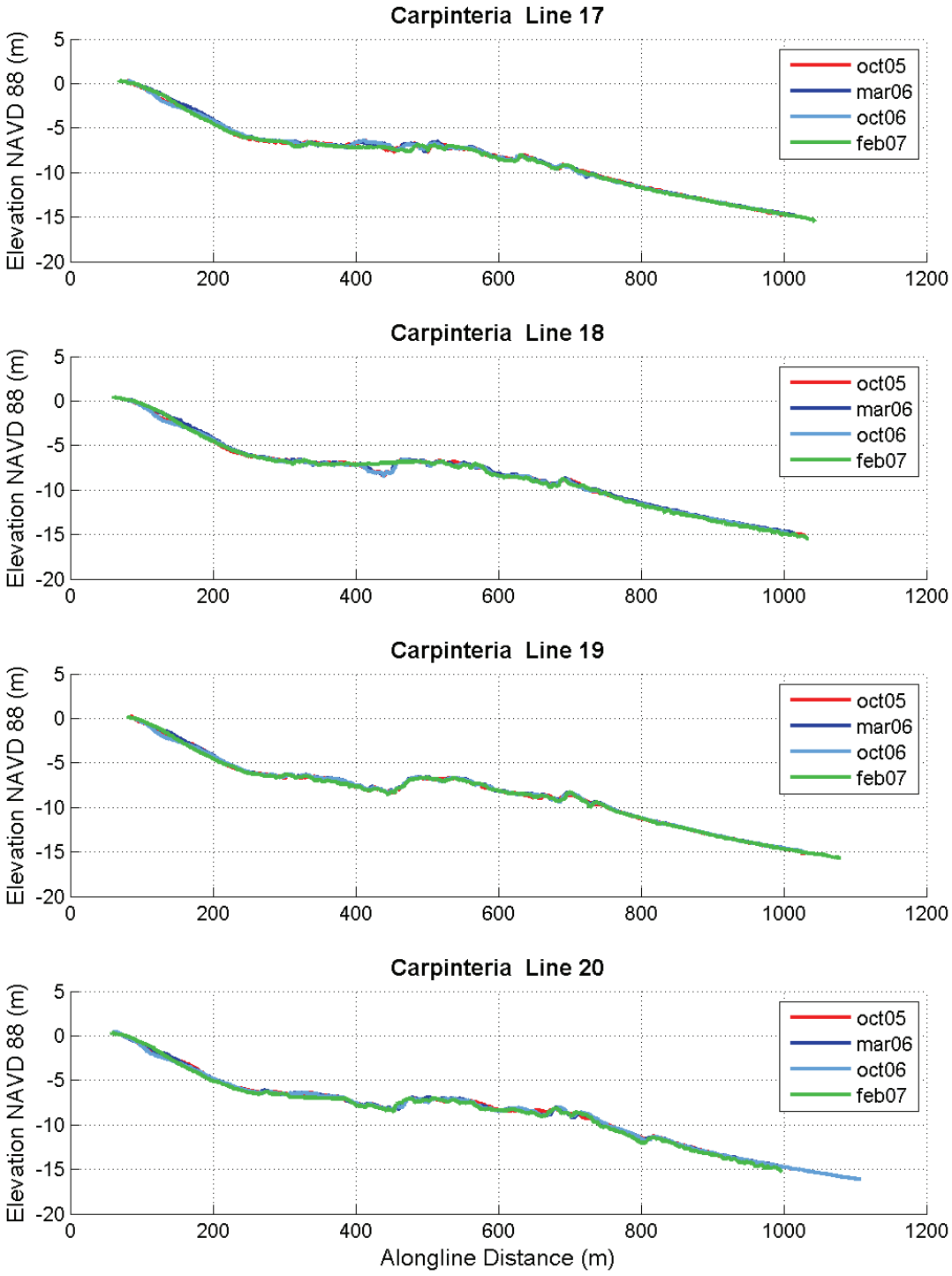

Figure A.5 Carpinteria cross-shore profiles 17-20.

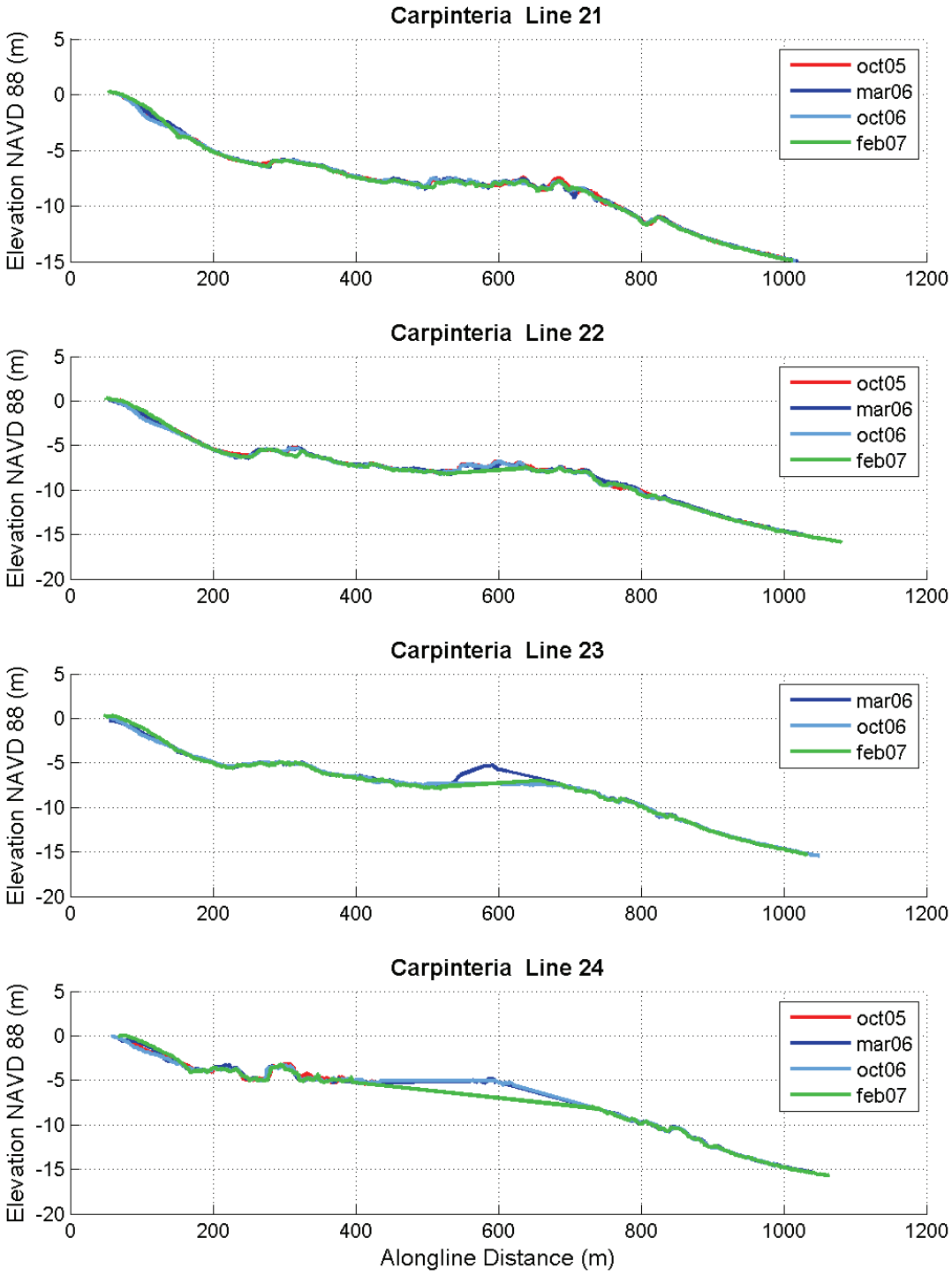

Figure A.6 Carpinteria cross-shore profiles 21-24.

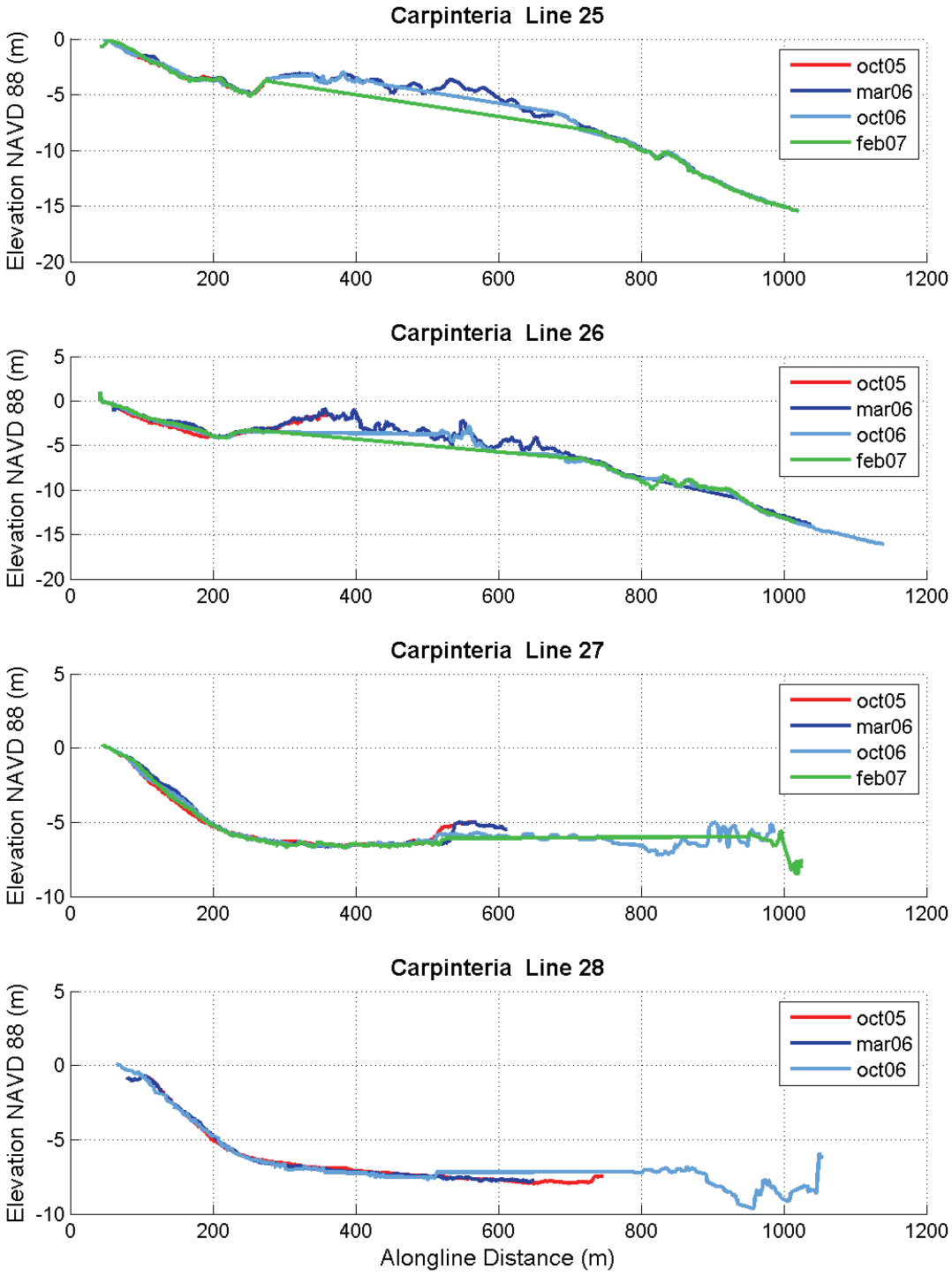

Figure A.7 Carpinteria cross-shore profiles 25-28.

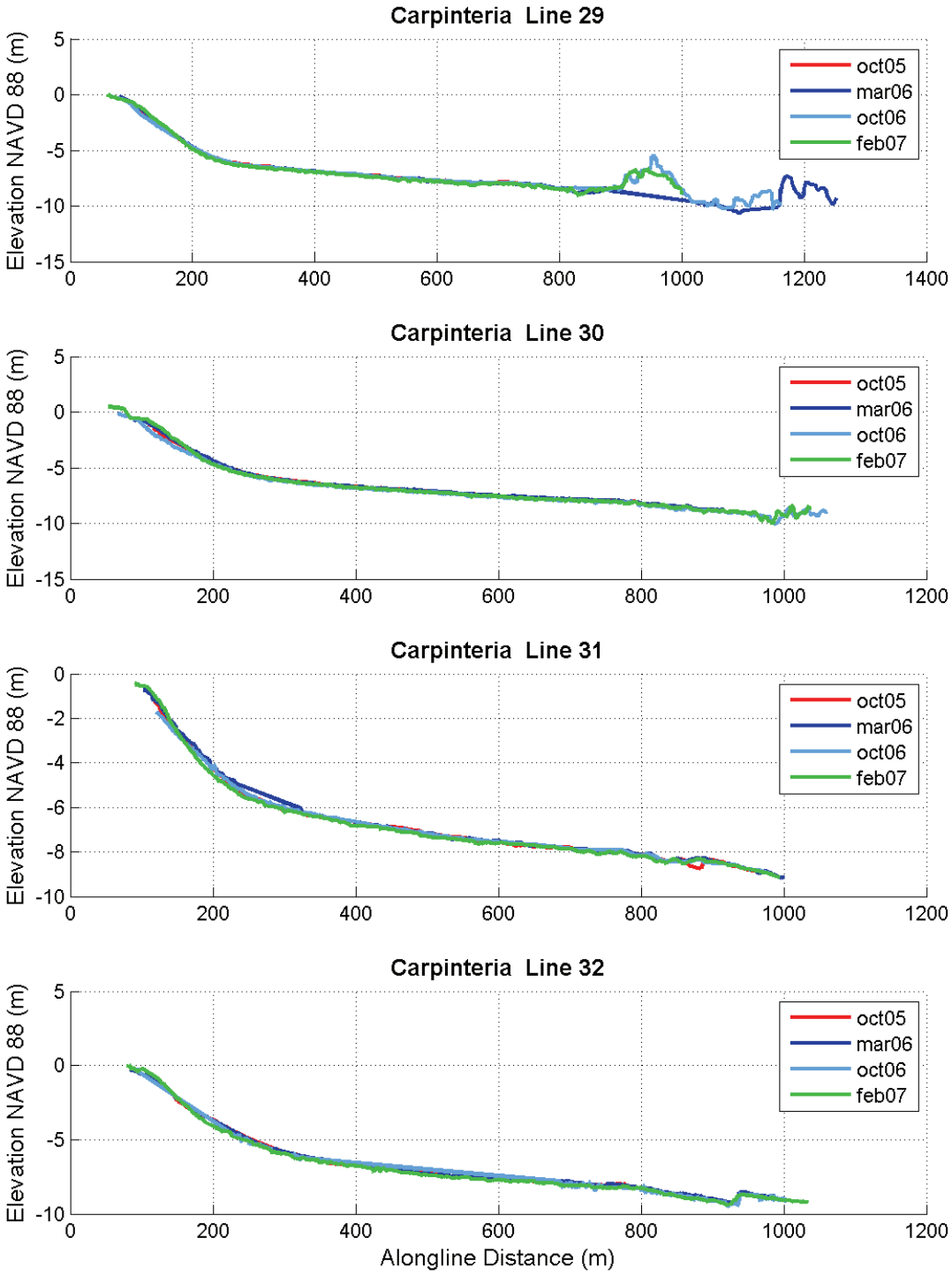

Figure A.8 Carpinteria cross-shore profiles 29-32.

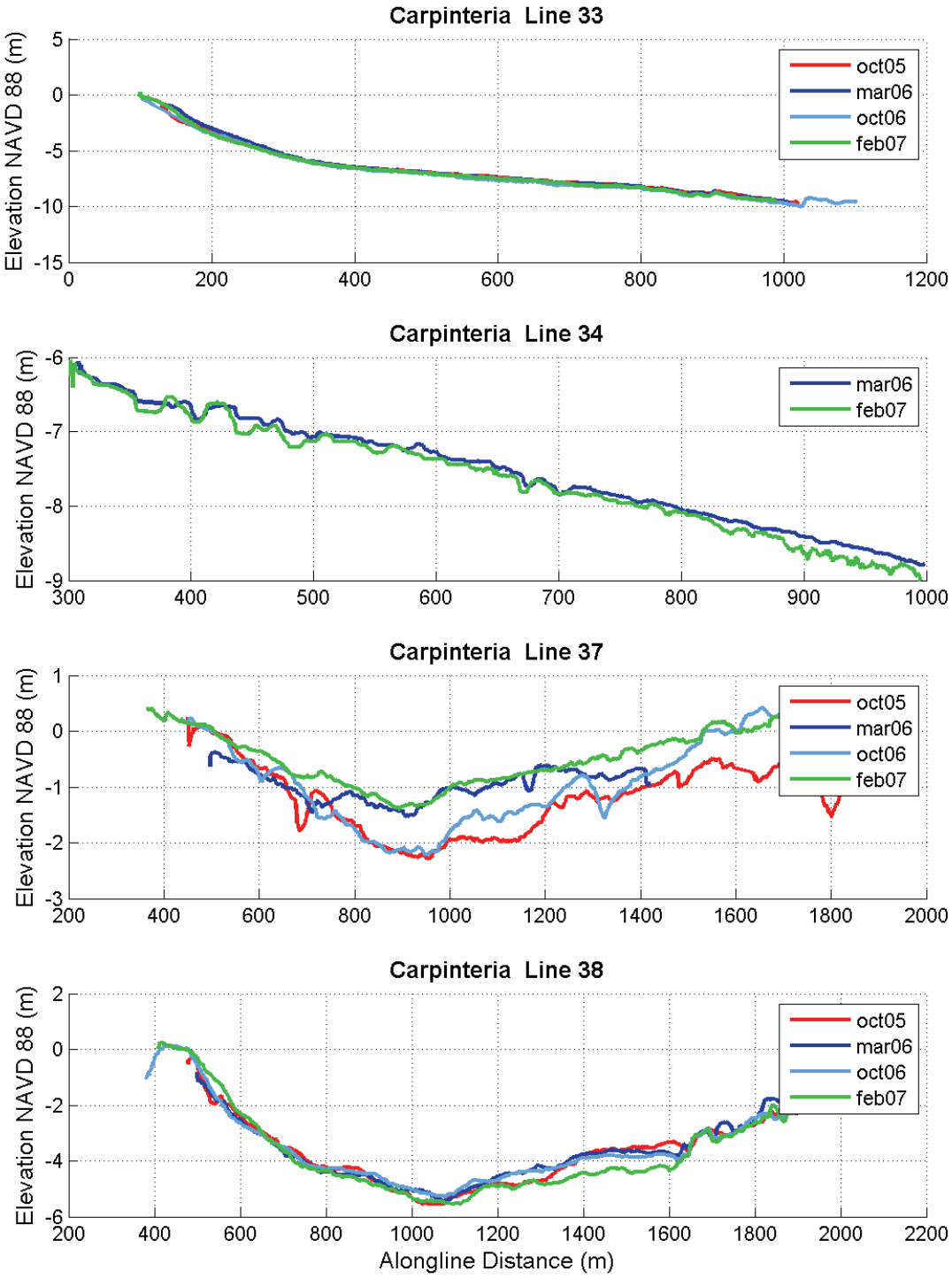

Figure A.9 Carpinteria cross-shore profiles 33-34 and alongshore profiles 37-38.

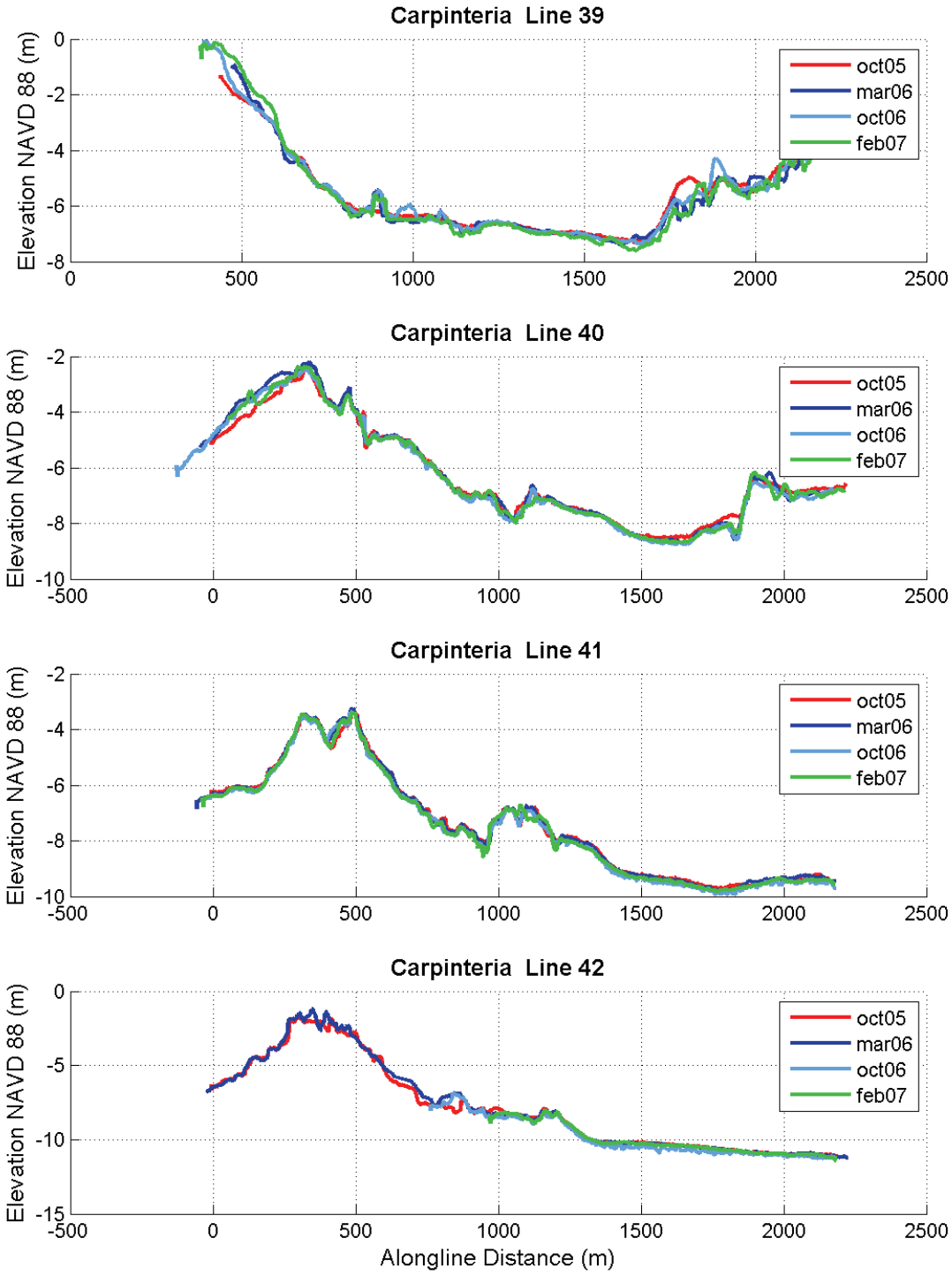

Figure A.10 Carpinteria alongshore profiles 39-42.

Nortek AWAC Measurements

This section includes weekly plots of current speed and direction for the entire water column measured by the Nortek AWAC during the winter 2006 instrument deployment. The current direction is the direction that the current is going to. The top panel shows the section of the tidal cycle that is included in the lower panels. The water depth included in the top panel was constructed from water level measurements recorded at the NOAA Santa Barbara Tide Gage Station # 9411340 (NOAA, 2007b).

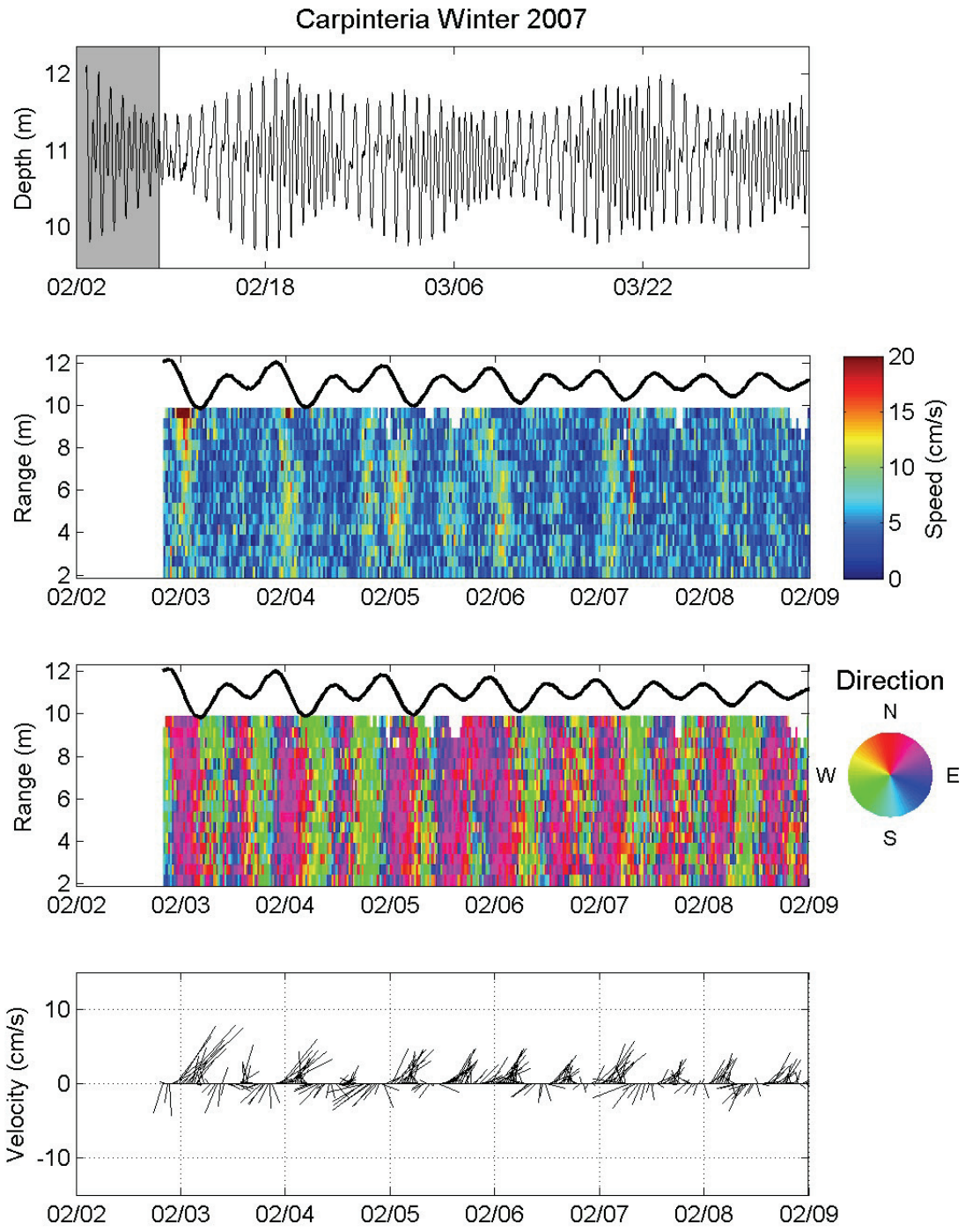

Figure A.11 Measured current data from Nortek AWAC for the week of February 2-9, 2007.

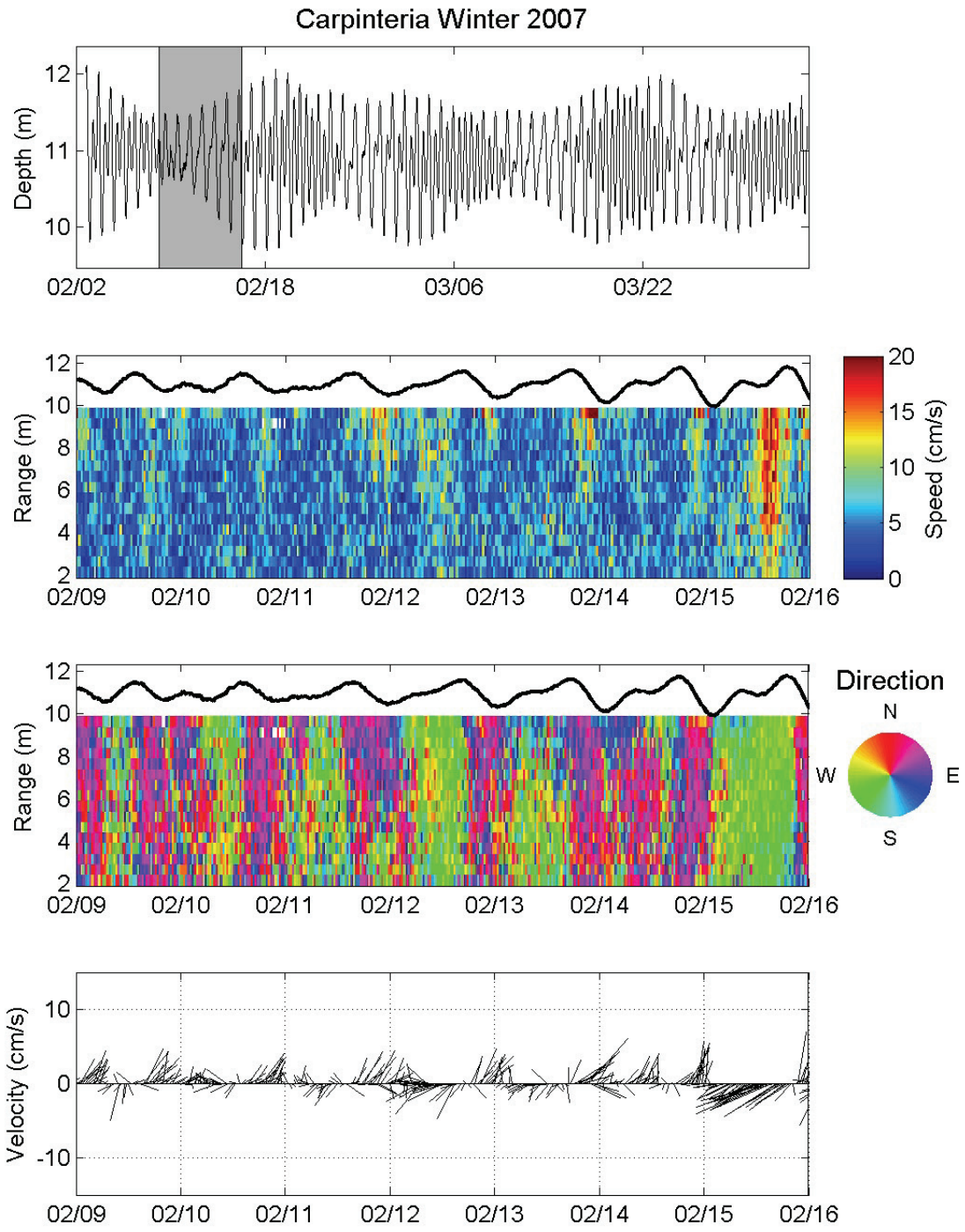

Figure A.12 Measured current data from Nortek AWAC for the week of February 9-16, 2007.

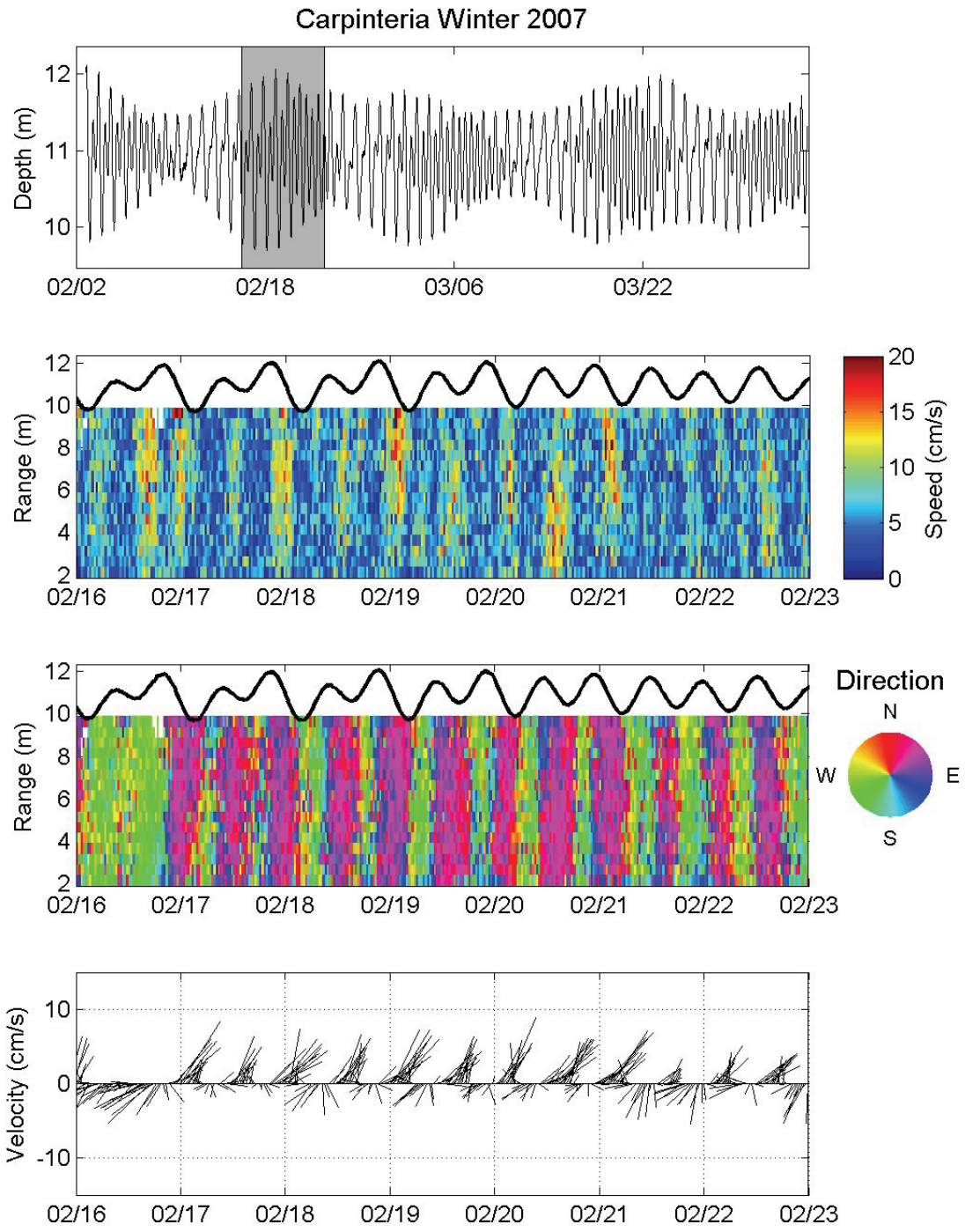

Figure A.13 Measured current data from Nortek AWAC for the week of February 16-23, 2007.

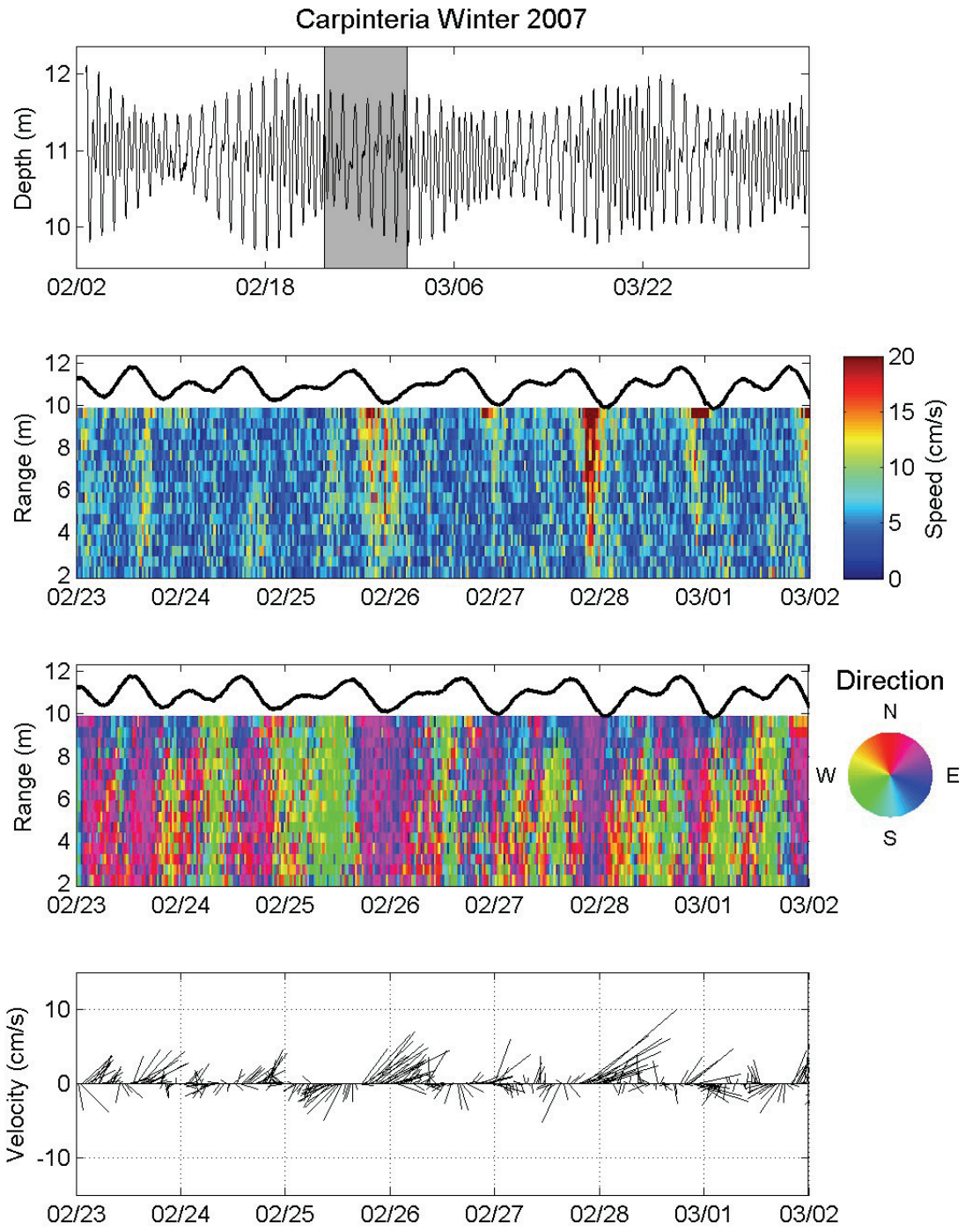

Figure A.14 Measured current data from Nortek AWAC for the week of February 23- March 2, 2007.

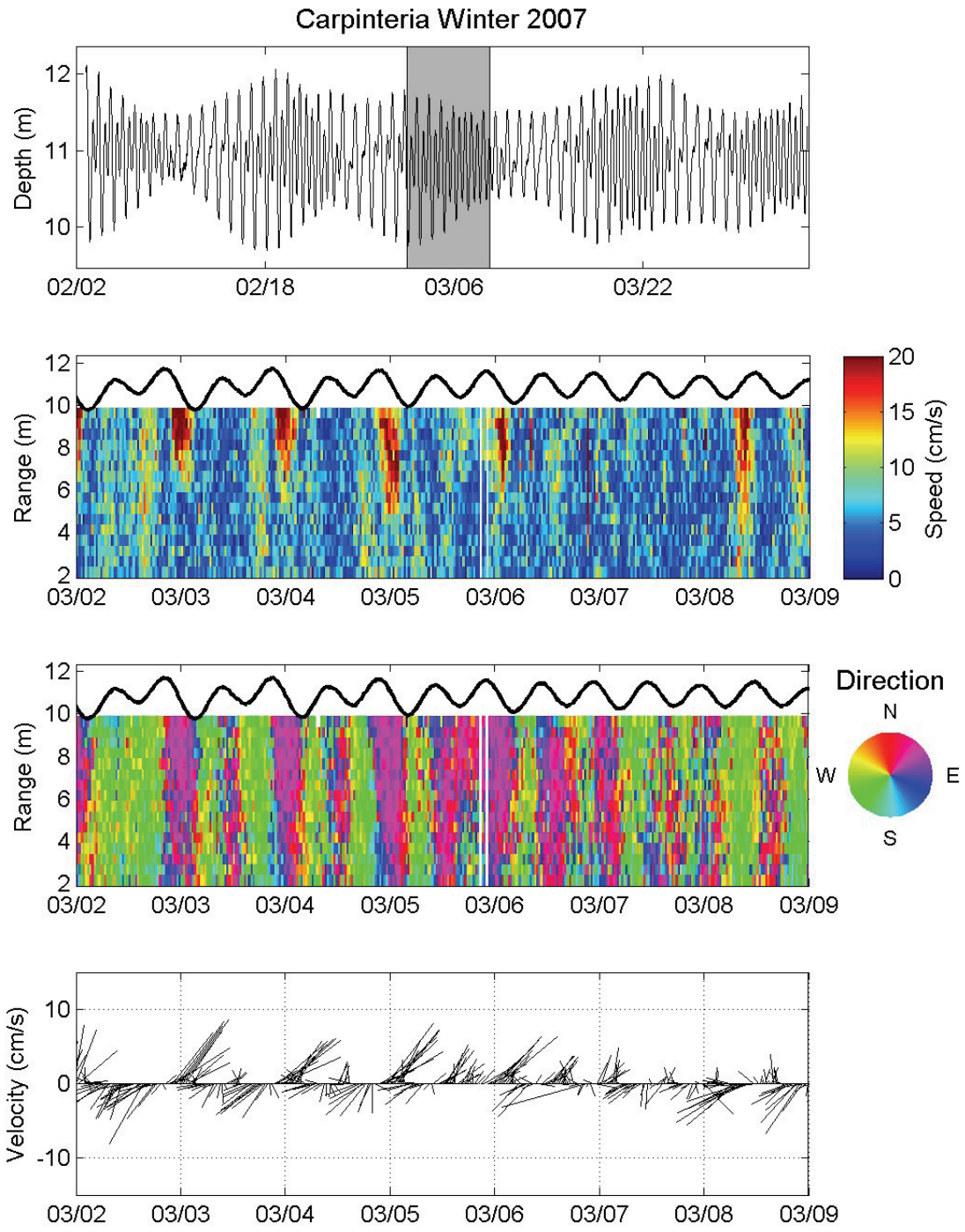

Figure A.15 Measured current data from Nortek AWAC for the week of March 2-9, 2007.

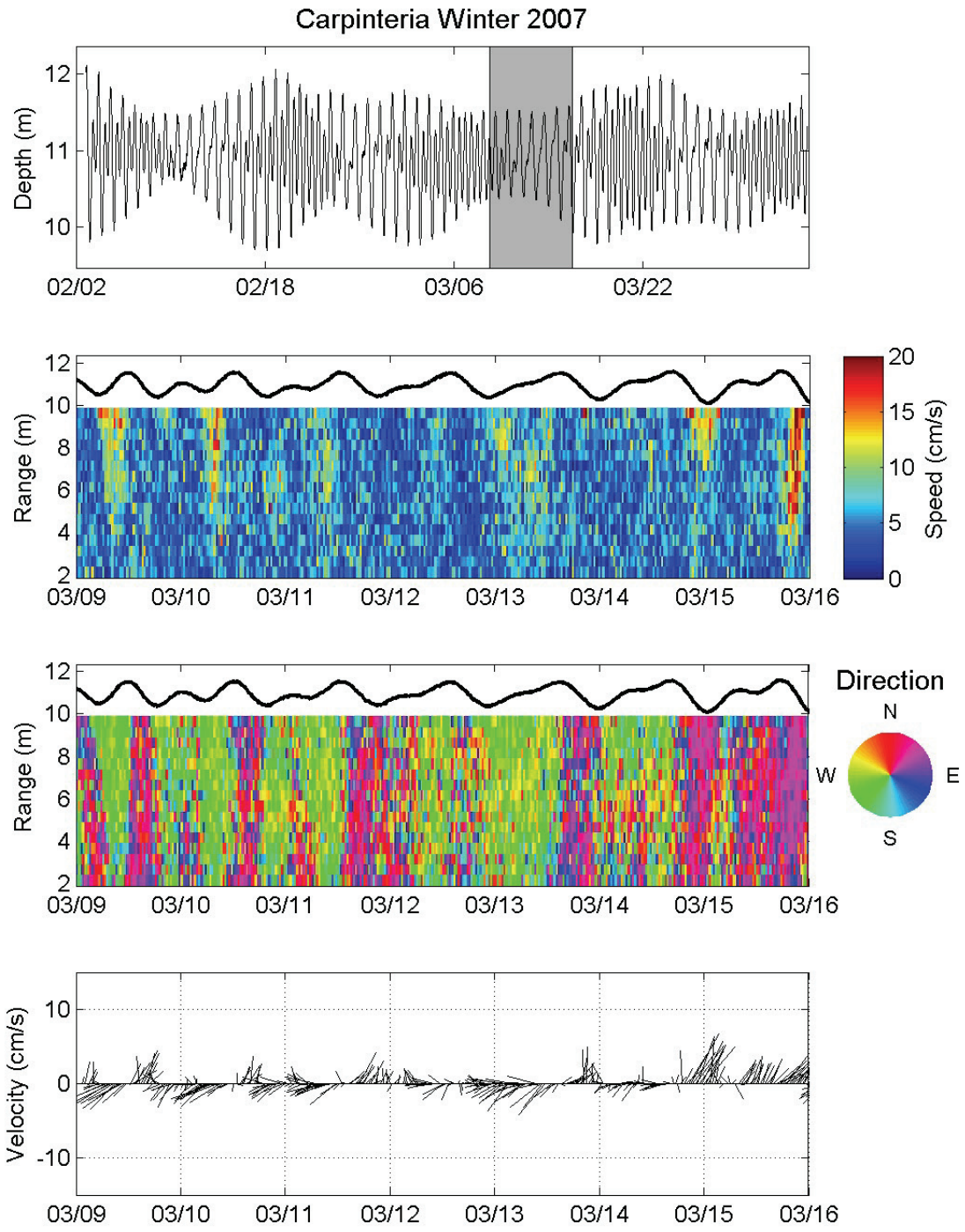

Figure A.16 Measured current data from Nortek AWAC for the week of March 9-16, 2007.

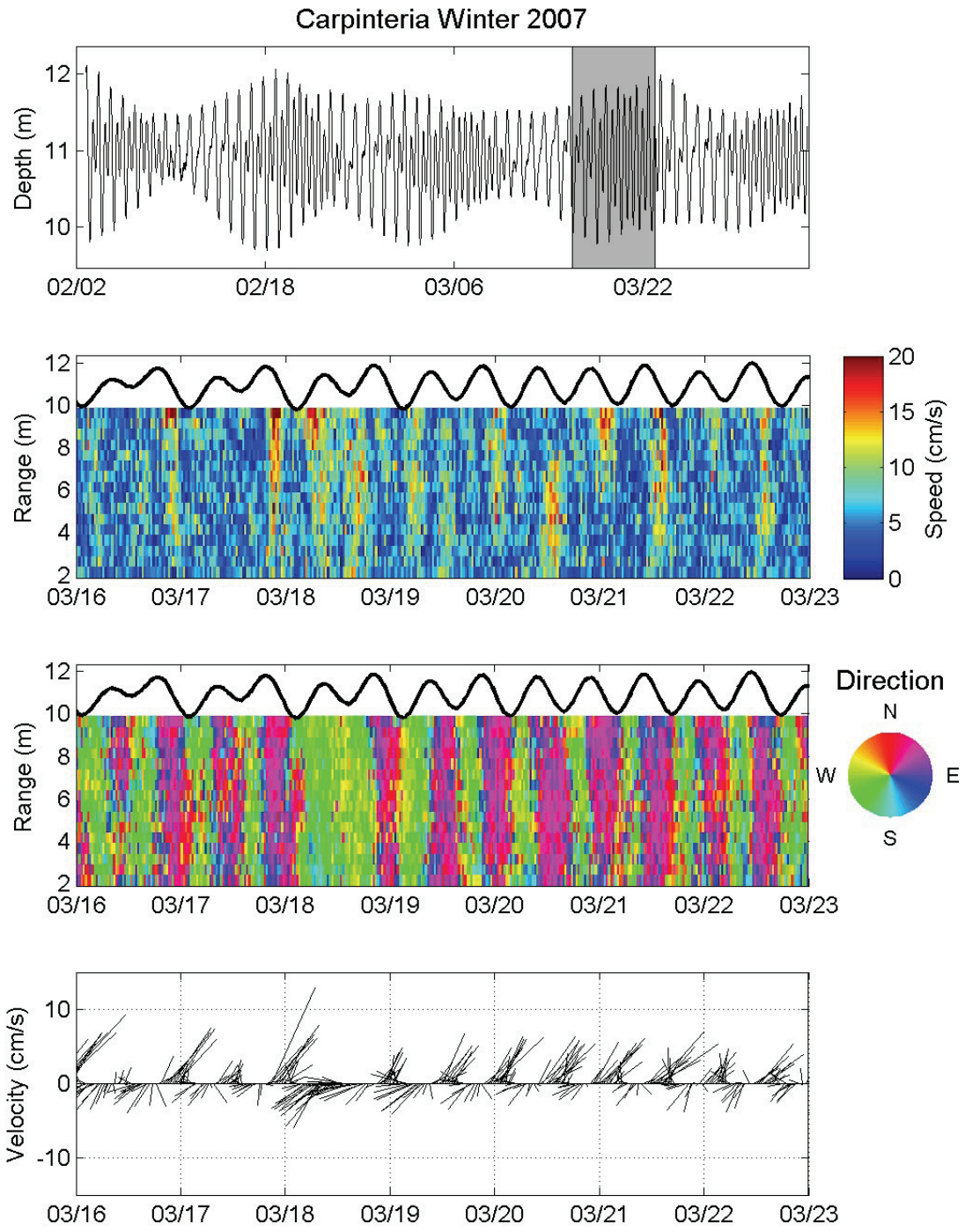

Figure A.17 Measured current data from Nortek AWAC for the week of March 16-23, 2007.

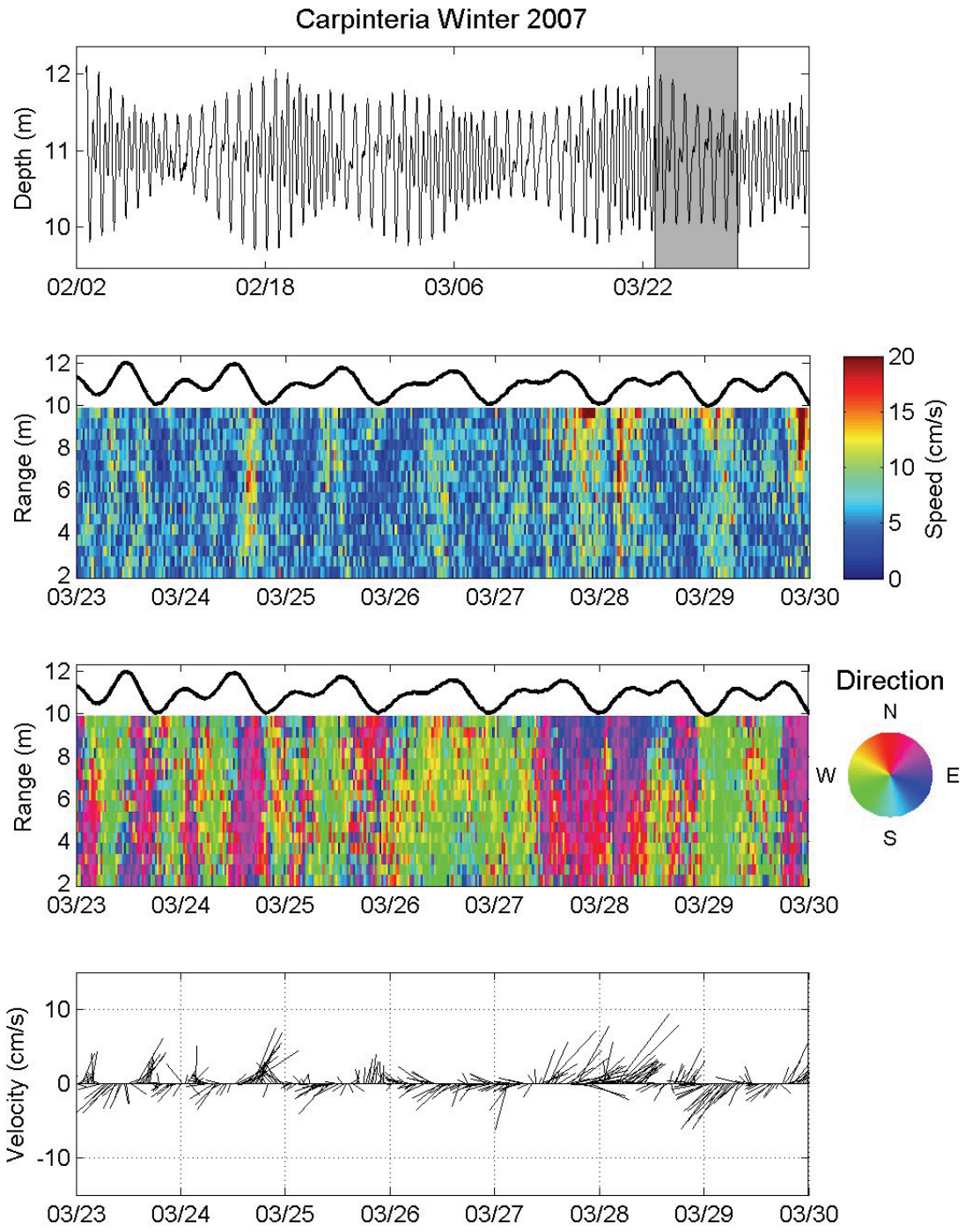

Figure A.18 Measured current data from Nortek AWAC for the week of March 23-30, 2007.

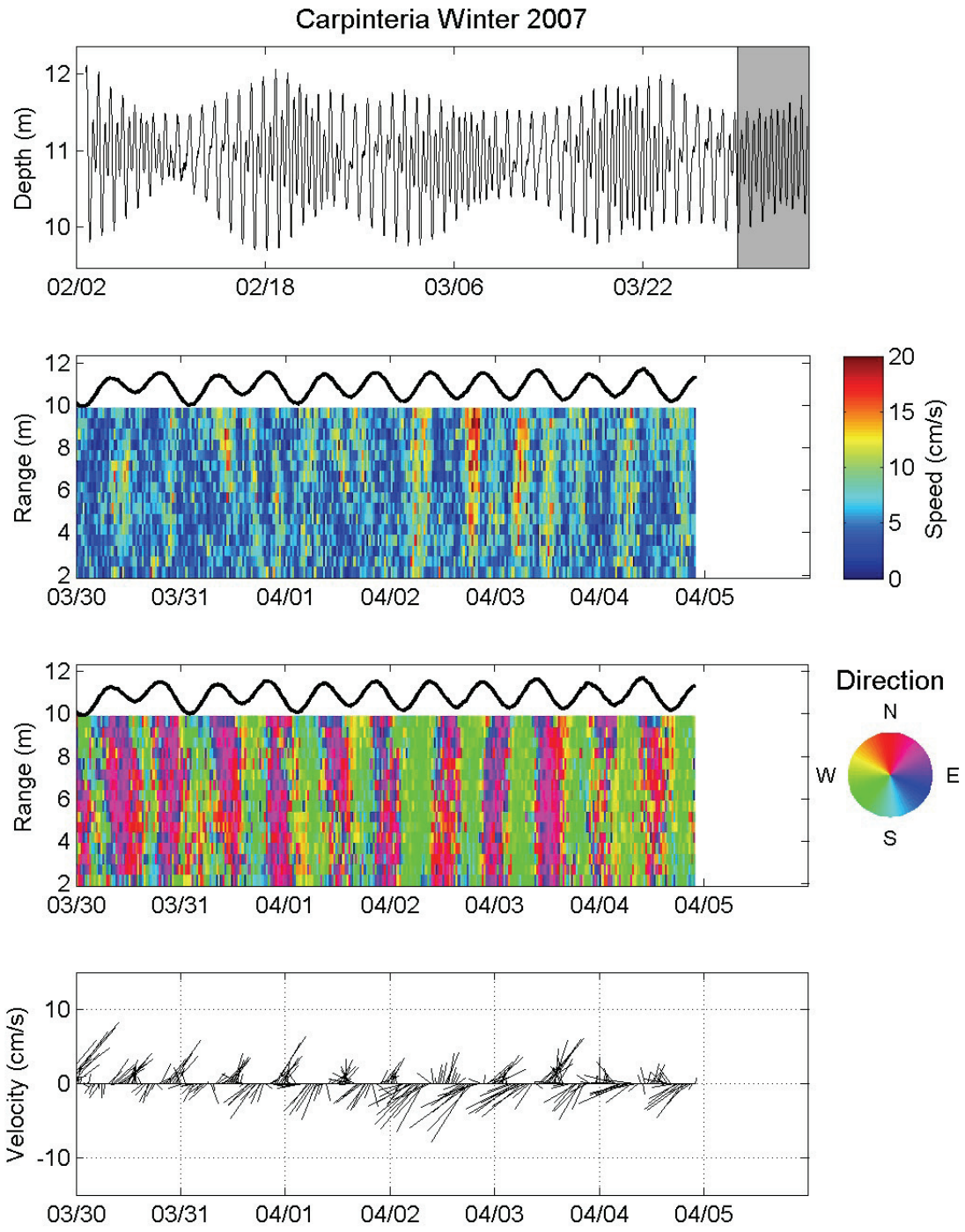

Figure A.19 Measured current data from Nortek AWAC for the week of March 30- April 5, 2007.